**Coastal Systems Station, Dahlgren Division**
**Naval Surface Warfare Center**
Panama City, Florida 32407-7001



**CONTRACTOR REPORT**
**CSS CR 1210-92-1**

**OCTOBER 1992**

# DETAILED NEAR SURFACE FLOW ABOUT YAWED, STRANDED CABLES

**S. M. BATILL**

**J. V. NEBRES**

# REPORT DOCUMENTATION PAGE

*Form Approved*
*OMB No. 0704-0188*



| 1. AGENCY USE ONLY *(Leave blank)* | 2. REPORT DATE | 3. REPORT TYPE AND DATES COVERED |
|---|---|---|
| | October 1992 | Contractor Report 5/89 - 6/90 |

**4. TITLE AND SUBTITLE**

Detailed Near Surface Flow About Yawed, Stranded Cables

**5. FUNDING NUMBERS**

Program Element No. 62315N
Project No. RN15W33

**6. AUTHOR(S)**

S. M. Batill and J. V. Nebres

**7. PERFORMING ORGANIZATION NAME(S) AND ADDRESS(ES)**

Department of Aerospace and Mechanical Engineering
University of Notre Dame
Notre Dame, IN 46556

**8. PERFORMING ORGANIZATION REPORT NUMBER**

**9. SPONSORING/MONITORING AGENCY NAME(S) AND ADDRESS(ES)**

Coastal Systems Station
Dahlgren Division
Naval Surface Warfare Center
Code 1210
Panama City, FL 32407-7001

**10. SPONSORING/MONITORING AGENCY REPORT NUMBER**

CSS CR 1210-92-1

**11. SUPPLEMENTARY NOTES**

**12a. DISTRIBUTION/AVAILABILITY STATEMENT**

Approved for public release; distribution is unlimited.

**12b. DISTRIBUTION CODE**

**13. ABSTRACT** *(Maximum 200 words)*

This report describes the results of the second phase of an experimental investigation of the flow about stranded cables or wire ropes. The purpose of the study was to consider, in some detail, the flow field near the cable and to provide additional experimental information related to the mechanisms associated with the generation of fluid forces on the cables. The development of a steady lift or side force on a stranded cable, yawed with respect to a flow, is a unique characteristic of a cable when compared to a circular cylinder. Experiments were conducted to measure the surface pressure distributions and near wake characteristics for a variety of stranded cable geometries and a circular cylinder. Rigid cable models and cylinders were tested in a low-speed wind tunnel. The models were yawed to four different yaw angles and tested within the Reynolds number range of 5,000 and 50,000. Surface pressure distributions on the yawed cables indicated that the lift force is the result of asymmetric boundary layer separation. Unsteady surface pressures on stationary cables were shown to correlate with earlier hot-wire measurements. Detailed flow visualization illustrated the complexity of the flow about the stranded cables. The influence of test support conditions were examined in order to provide a better understanding of end-effects in testing these long, slender models.

**14. SUBJECT TERMS**

Hydrodynamic forces; flow visualization; stranded cables; cables; vortex shedding; wire ropes; towed cables

**15. NUMBER OF PAGES**

131

**16. PRICE CODE**

| 17. SECURITY CLASSIFICATION OF REPORT | 18. SECURITY CLASSIFICATION OF THIS PAGE | 19. SECURITY CLASSIFICATION OF ABSTRACT | 20. LIMITATION OF ABSTRACT |
|---|---|---|---|
| UNCLASSIFIED | UNCLASSIFIED | UNCLASSIFIED | UNLIMITED |

## FOREWORD

The experimental study described in this report was conducted during the period from May 1989 to June 1990 under an extension to contract N00014-83-K-0239. The research program was entitled "Flow Field Measurements on Stranded Cables" and was conducted by the Department of Aerospace and Mechanical Engineering at the University of Notre Dame, Notre Dame, Indiana for the Naval Coastal Systems Center, Panama City Florida. The Principal Investigator for the contract was Dr. Stephen M. Batill. Mr. Jose V. Nebres was a Graduate Research Assistant in the Department of Aerospace and Mechanical Engineering. The Project Engineer for the contract was Mr. Kennard Watson. The authors wish to acknowledge the contributions of the Project Engineer during the program. They would also like to acknowledge the support of the Department of Aerospace and Mechanical Engineering by providing the graduate student support and research facilities necessary for the successful completion of this project.

## TABLE OF CONTENTS

## LIST OF TABLES

## LIST OF FIGURES

## NOMENCLATURE

| | |
|---|---|
| $A$ | Frontal area = cable length x cable diameter |
| $c_f$ | Mean force coefficient |
| $C_{p_i}$ | tap pressure coefficient |
| $D$ | Cable diameter |
| $F$ | Aerodynamic force component |
| $f_v$ | Vortex shedding frequency |
| $i$ | pressure tap index |
| $n$ | number of pressure taps |
| $q_\infty$ | free stream dynamic pressure |
| $p_i$ | tap pressure |
| $p_\infty$ | free stream static pressure |
| $q$ | Dynamic pressure =( $\rho V^2$) / 2 |
| $V$ | Free stream fluid velocity |
| $\Delta x_i, \Delta y_i$ | panel projections on the x and y axes respectively |
| $\beta$ | Cable angle |
| $\rho$ | Fluid density |

## SUMMARY

This report describes the results of the second phase of an experimental investigation of the flow about stranded cables or wire ropes. The purpose of the study was to consider in some detail the flow field near the cable and to provide additional experimental information related to the mechanisms associated with the generation of fluid forces on the cables. The development of a steady lift or side force on a stranded cable, yawed with respect to a flow, is a unique characteristic of a cable when compared to a circular cylinder. Experiments were conducted to measure the surface pressure distributions and near wake characteristics for a variety of stranded cable geometries and a circular cylinder. Rigid cable models and cylinders were tested in a low speed wind tunnel. The models were yawed to four different yaw angles and tested within the Reynolds number range of 5,000 and 50,000. Surface pressure distributions on the yawed cables indicated that the lift force is the result of asymmetric boundary layer separation. Unsteady surface pressures on stationary cables were shown to correlate with earlier hot-wire measurements. Detailed flow visualization illustrated the complexity of the flow about the stranded cables. The influence of test support conditions were examined in order to provide a better understanding of end-effects in testing these long, slender models.

# 1. INTRODUCTION

## 1.1 Statement of the Problem

The prediction of steady and unsteady forces developed by the flow around yawed cables is of great importance in a number of applications. Stranded cables are used for suspension bridges, transmission lines, guy supports, mooring of offshore structures and airborne or underwater towing. These applications require reliable prediction methods for fatigue and other functional considerations. Understanding the flow field characteristics, together with their dependence on the geometry of the body and the flow environment, is a prerequisite to the development of an efficacious prediction method.

## 1.2 Background

The production of a steady side or lift force and other differences between the flow characteristics on cables and a circular cylinder are issues addressed in this report. The initial phases of this experimental program were documented by Batill, Nelson and Nebres[1988] and illustrated the complexity of the flowfield about the yawed cable. Numerous questions were raised regarding the generation of the steady lift force and the tests documented in this report were intended to address some of these issues.

The lift or side force is directed normal to both the cable's longitudinal axis and the free-stream flow. It is primarily the result of an asymmetric surface pressure distribution. There is also a force component which is in the plane formed by the free stream velocity and the cable's longitudinal axis. This component is often resolved into two components, one parallel to the longitudinal axis of the cable, the tangential drag, and one normal to the cable, the normal drag. The normal and tangential drag components are also primarily the result of a complex surface pressure distribution although surface shear stresses also contribute. Unsteady drag and lift forces, which may cause fatigue due to streamwise and transverse vibrations, are induced by the fluctuations in the flow which alter the instantaneous surface pressure distribution.

Steady and unsteady forces are similarly observed on yawed circular cylinders with the exception of the steady lift (in most cases as is discussed later in the report). The flow around yawed circular cylinders has been a topic of numerous previous investigations and a good overview can be found in Ramberg[1978] and Smith, Moon and Kao[1972]. Unfortunately, the extensive amount of information

which is available on the circular cylinder is not often directly applicable to the yawed, stranded cable.

A cable or wire rope is constructed by twisting wires together according to some pattern. The overall cable geometry is then determined by the number and relative sizes of the wires and strands and the pattern in which they are assembled. (Cable geometry notation is defined in the next Section.) The wires introduce relatively small scale surface irregularities and the strands, or groups of wires, present relatively large scale irregularities, with the scale based upon the wire diameter. It is the irregular surface geometry caused by the strands and wires which alters the development of the surface boundary layer, the free shear layer and wake.

Most of the previous work conducted on yawed cables has been on underwater towing cables or transmission line cables. Much of the work on towing cables was performed at the David W. Taylor Naval Ship Research and Development Center (DTNSRDC), by an unknown author[1949], Schultz[1962], and Horton, Ferrer, Watson and Charvoz[1987]. Studies of transmission line cables were undertaken by Sewell and Taylor[1961] and Counihan[1963]. The DTNSRDC investigators tested geometrically different cables which were free to vibrate at the Reynolds number range of around 15,000 to 100,000. These cables represented a wide variety of geometries and contained from 3 to 12 outer strands. Sewell and Taylor, and Counihan reported tests at Reynolds numbers of 10,000 to 200,000 for rigid cables with 18 to 42 outer strands.

For the unyawed case, Counihan[1963] observed a much lower critical Reynolds number, approximately 35,000, for cables compared to 300,000 for the cylinder. This was based on the characteristic reduction in the drag coefficient at the critical Reynolds number. This was attributed to the influence of the wires on the boundary layer, altering the transition and subsequent separation.

Stranding of the unyawed vibrating cable, has been shown to have a relatively small effect on vortex shedding frequency when compared to the cylinder. Strouhal numbers, which are related to vortex formation frequency in the wake, as measured by Horton, et. al. [1987] were observed to be lower than the nominal cylinder value for the 1x19 cable and somewhat higher than the cylinder for the 4x7 serrated cable. It should be noted that this was also sensitive to Reynolds number. Similarly, Votaw and Griffin [1971] measured the Strouhal numbers for the unyawed vibrating cables and observed slightly elevated values for cables with three and four strands as compared to values for cables with five and six strands.

Though the differences were not large, the values were still within 10% of the unyawed circular cylinder values.

One characteristic of the yawed cable geometry is the asymmetry in the cross-section as illustrated schematically in Figure 1. It would appear that this asymmetric cross section geometry contributes to the asymmetric surface pressure distribution and thus the lift force. Sewell and Taylor[1961] and Counihan[1963] observed lift forces near the critical Reynolds number range for yawed, transmission line cables with 18 to 42 outer strands. Surface pressure measurements indicated that early transition to turbulence and subsequent delayed separation occurred on one side. On the other side, the boundary layer remained laminar and no change or even slightly earlier separation occurred. The resulting asymmetry in separation point location resulted in the steady lift. The measurements further indicated that as the Reynolds number was increased, the boundary layers on both sides become turbulent causing a reduction in lift. As the Reynolds number was increased even further, the side which originally had the laminar boundary layer has a turbulent boundary layer with a separation that moves even farther aft when compared to the other side. This results in a change in the direction of the lift force.

Horton, et. al.[1987] on the other hand suggests that steady lift could be produced on yawed cables whether or not asymmetric transition to turbulence is present. It was proposed that the mere asymmetry in the cross-section would produce an effective camber as in an airfoil. The cables tested by Horton, et. al. had a much lower number of outer strands (3 to 12). In such a case, a large scale cross section asymmetry would result which could produce a lift. As the number of outer strands is increased, the effective camber of the yawed cable would become smaller and at some point become negligible. Transmission line cables with many outer strands can be considered to have negligible effective camber. This may result in the asymmetric orientation of the outer strands becoming important only in the critical regime.

The generation of the lift force on yawed cables was first confirmed experimentally at DTNSRDC in 1949. The tests were conducted on 4x7 serrated cables. Schultz[1962] followed up the tests using models with 12 outer strands and he observed lift at critical and subcritical Reynolds numbers. Schultz conjectured that the side of the cable with grooves caused by the stranding which presented a relatively smaller angle to the flow resulted in less disturbance to the flow. On the other side, the grooves created by the stranding which presented a greater angle to

the flow acted as spoilers, thus prompting separation. Although Schultz's postulation suggested asymmetric separation, no substantiation was presented. Following Counihan[1963], it can be presumed that the lift observed at the critical Reynolds number was due to asymmetric transition. However, Schultz's also observed lift at subcritical Reynolds numbers, suggesting that there was more to the lift mechanism besides asymmetric transition especially for cables with few outer strands.

The mechanics by which lift is developed on towing cables has never had a substantiated explanation. Horton, et. al.[1987] and Schultz[1962] could only provide hypotheses since their experiments were not intended to provide detailed information on the lift force development. The present experiments were performed to investigate the lift development, its direction and mechanism. This has been accomplished using detailed surface pressure surveys and the results are correlated with flow visualization data.

An additional issue which is also addressed in this report is the influence of finite length models and boundary conditions. The behavior of vortex filaments along the cylinder axis for an infinite unyawed cylinder is an unresolved issue. Various investigators have identified an angle between the finite length cylinder and the vortex filaments in the wake of up to ±30°, Gerrard[1966]. This implies that the vortex formation in the wake is occurring at different "times" along the span of the cylinder. This issue is unresolved because of the wide scatter in the results and the uncertainty as to whether this spanwise variation is caused by non-uniformities in the flow or is the result of three-dimensional character of the vortex wake formation process. Being able to model an infinitely long cylinder in a "finite" water channel or wind tunnel, with the intention of understanding the actual behavior of vortex filaments, has been complicated by end effects. One of the primary end effects is related to the presence of the wall boundary layer. Stansby[1974] demonstrated that the wall boundary layer distorts and/or increases the base pressure along the span of the cylinder. He suggests the necessity of placing endplates with a leading edge of at least 2.5 times the cylinder diameter forward of the cylinder axis in order to simulate two-dimensional flow. Fox and West[1990] recommend that L/D should be greater than 7 if the endplate dimensions recommended by Stansby are used.

Boundary layer development at the wall is not the only problem associated with the finite length of the model. The behavior of the vortex filament which is terminated at a solid wall is another complexity that is still unresolved. In

King's[1973] review it was stated that Gowda has suggested that the aspect ratio (length to diameter ratio) be greater than 45 and the endplates could be eliminated. The middle portion of the model could then be deemed free of end effects. Gowda observed that when the aspect ratio is decreased from the suggested 45, the Strouhal number drops. Exactly how much the region of significant end effects varies downstream in the wake is still not clear. In the midst of these finite modeling problems, studies show that there exist spanwise phase shifts in the vortex wake formation process, i.e., the vortex filament is actually broken down into small cells or coherent lengths, Keefe[1961]. This was determined from tests of a cylinder with endplates, and where the endplate spacing was varied. Vibration amplitudes of the cylinder were observed to decrease as the endplate spacing was increased. The conclusion was that the greater endplate spacing resulted in coherent lengths which were smaller. This resulted in lower amplitude vibrations. Alternatively, a long coherent length results in high amplitude fluctuating forces, Toebes[1969]. It is noted that free vibrating structures during lock-in (synchronization of vortex shedding and cylinder vibration) have greatly increased coherent lengths which aggravate vortex induced vibrations by one to two orders of magnitude.

As the flow approaches the leading edge of a yawed cylinder or cable, it attempts to align itself with the cable. This results in a significant component of velocity along the leading edge and thus a highly three dimensional flow. Ramberg[1978] performed a detailed investigation on the effect of endplates on yawed cylinders. He varied the angle of incidence of the endplates, and observed the behavior of the Strouhal number, the shedding angle of vortex filaments, and the base pressure. At a certain endplate angle, one in which the endplate is tipped towards the flow, the vortex filaments were observed to be parallel to the cylinder axis. He found that this endplate angle is dependent on yaw angle and Reynolds number. Furthermore, at this particular endplate angle, the behavior of the Strouhal number was in accordance with the independence principle. Ramberg also indicated that for an infinite, yawed cylinder, the angle between the vortex filaments and the normal to the free stream should be less than the yaw angle, this implies that the endplate should be tipped somewhat less than that required in order for the filaments to be parallel to the cylinder. He suggests that tipping the endplate is necessary to create just about the same spanwise flow as in an infinite yawed cylinder. For the case of the unyawed cylinder, tipping the endplate into the flow is also necessary to compensate for the low base pressure and to eliminate spanwise flow.

## 1.3 Scope of Current Work

A series of wind tunnel models were developed in order to perform the tests described in this report. The baseline models which were considered in this study were the circular cylinder, a 7x7 cable and 4x7 serrated cable. There were three primary goals in this study. First, detailed surface pressure measurements were conducted in order to improve the understanding of the development of the steady lift or side force on the yawed cable. Secondly, flow visualization methods were developed and data collected which allowed for a more detailed, qualitative evaluation of the flow near the surface of the models. This data was then correlated with the detailed pressure measurements. Lastly an assessment of the influence of the wall boundaries was performed. This was accomplished by attempting to isolate the ends of the models from the wind tunnel walls using endplates.

These studies were performed for a variety of cable angles ranging from 90° to 20°. A relatively wide range of Reynolds number was considered and the Reynolds number for each series of tests was often dictated by the type of test and instrumentation. The detailed flow visualization tests were performed for a Reynolds number of 6,000 and the pressure measurements range from 10,000 to 46,000.

The results of the study were correlated with other measurements when possible. Since a wide range of test conditions and models were considered, a large amount of experimental information has been collected. A discussion of the results is presented but a detailed evaluation is beyond the scope of the current effort.

## 2. CABLE MODELS

### 2.1 Wind Tunnel Models

The series of experiments described in this report were conducted using a number of stranded cable configurations. A stranded cable or wire rope is actually a complex three dimensional slender body. The baseline model used for comparison purposes was the circular cylinder. Two of the cable models were the same cables tested by Batill, Nelson and Nebres [1988], these were the 7x7 and 4x7 (serrated). Two additional cable models were also tested. These are designated as 7x1 and 4x1. Each had a single large diameter "wire" per strand and approximately the same pitch as the 7x7 and 4x7 cables. These additional models were developed in order to evaluate the influence of the small scale surface perturbation associated with the individual wires within a strand in contrast to the influence of the large scale irregularity associated with the primary cable stranding. The length of the cable models varied depending upon the cable angle since the size of the wind tunnel test section was fixed.

In order to provide information over the range of Reynolds numbers of interest, cable models with two different diameters were fabricated. The smaller series of models were used for testing at the lower Reynolds numbers and for most of the flow visualization and end effects study. They were fabricated from epoxy castings as described below and had an effective outer diameter of 0.625 inches. They were the same size as the original models tested by Horton, Ferrer, Watson and Charvoz [1987]. The smaller diameter models were fabricated for the cylinder, 7x7 and 4x7 geometries. The small outer diameter of these models limited the number of surface pressure locations and therefore another series of larger diameter models were constructed. These were fabricated using braided strands of neoprene tubing. These larger models were approximately 1.85 inches in diameter and allowed for the positioning of up to 36 circumferential pressure taps. The larger models were developed for the cylinder, 7x1, 4x1, 7x7 and 4x7 geometries. The following sections provide additional details on each of the models.

### 2.2 Pressure Models

One of the goals of Phase I of this test program was to establish a procedure for wind tunnel model fabrication. A procedure was developed with which models with excellent surface detail definition were assembled from epoxy castings. Sample cable specimens provided by NCSC were used as the masters to develop

the molds for each model so integrity of the surface geometry was maintained with the castings. Table 1 is a summary of the models used for this test program and indicates both pressure and flow visualization models. The nominal and actual diameters for the smaller, cast models were taken from Horton et.al.[1987] and since the models tested were cast directly from their original steel cables these values were used to describe the cable size. The diameters for the larger models were estimated as nominal diameters.

The basic 0.625 inch diameter cable replicas of the 7x7, 4x7 and the circular cylinder were used for both the pressure and flow visualization studies. Fabrication of the two cable models made use of the casting procedure developed during the Phase I tests. Hollow epoxy cable pieces of the actual metal cables were produced. These were positioned and glued to a hollow metal shaft and also to four solid steel shafts of different lengths as shown in Figure 2. Alignment of the epoxy cable model pieces on the shaft was accomplished using the same techniques developed in Phase I. The hollow shaft cable piece could then be assembled with either of the four solid shaft cable pieces, each of which corresponded to the cable angles of 90°, 60°, 40° and 20°. The solid shaft fit snugly into the hollow shaft and two set screws were used to secure the rigid assembly, Figure 3.

The hollow cable model piece, i.e., the epoxy/metal tube assembly was drilled for two pressure taps; one on a "peak"(i.e. the top of a strand) and one in a "valley"(i.e. between strands). The taps were connected by short pieces (0.05 in. ID, 0.09 in. OD) of tygon tubing, flush with the cable surface, into (0.044 in ID, 0.054 in OD) stainless steel tubes. The stainless steel tubes then passed out of the downstream end of the model. It was the downstream end of the cable model which protruded out of the tunnel wall during the testing. The stainless steel tubes were then connected to a scanivalve and in turn to an electronic manometer for the pressure measurement. Due to the small size of the models only two pressure taps could be mounted on the surface of the small models. Attempts were made to place additional taps on the cable surface in order to achieve better pressure profile resolution but these were unsuccessful.

The locations of the pressure taps on the cast epoxy models were selected in order to allow for as much detail in the surface pressure distribution as possible. Due to the symmetry of the cross section and the placement of the pressure taps, 8 unique pressure measurements were possible for the 4x7 cable and 12 unique pressure measurement locations were possible for the 7x7 cable. This is illustrated

schematically in Figure 4. Rotation of the models through angles of 45° and 30° respectively, allowed measurement at additional locations for a given cable orientation even though there were only two surface pressure taps. This implies that the pressure measurements were not simultaneous and required rotation of the model between measurements.

The small diameter circular cylinder model was fabricated from a solid 0.625 in. steel rod. A 0.125 in. groove was milled in the surface of the model to accommodate a 0.044 in ID, 0.054 in. OD stainless steel tubing as shown in Figure 5. With the steel tubing positioned in the groove, the groove was filled with epoxy and the surface refinished by fine sanding. Four pressure taps were then drilled into the stainless steel tubing. The four taps correspond to the center of the wind tunnel for each of the four cable angles that were considered. Three of the taps were sealed during a particular test so that only the desired tap monitored the pressure.

The 1.875 in. cable and cylinder models were fabricated using a different technique. For a model of the 7x1 cable, 6 neoprene tubes were twisted and wrapped around a solid steel rod at the proper lay angle and fastened at the ends. Each of the six external neoprene tubes were fit with a surface pressure tap. Again taking advantage of the symmetry of the models and location of the pressure taps, 36 unique surface pressure measurement locations could be established. A schematic of the cross section and tabular positions for the pressure taps are shown in Figure 6. The points indicated by the "letters" represent information used in the integration of the pressure distributions as will be discussed later in the report. Since there are only six surface pressure taps, the 36 measurement locations are the result of 6 - 60° rotations of the model relative to a selected starting position.

The 4x1 model was constructed in a similar fashion. Due to the diameter of the primary strands, there was a region at the center of the cable which allowed for a solid metal rod (OD = 0.312 in) which provided the stiffness for the model. Figure 7 is a schematic for this model and also indicates the positions of the pressure measurements. Each strand was fit with a single pressure tap, so four 90° rotations would permit measurements at 16 unique pressure tap locations.

These larger models, the 7x1 and 4x1, have the same primary surface features of the actual cable but do not have the small scale surface irregularities associated with the wires within a particular strand. Because of the larger model perimeter, a larger number of pressure taps, as well as more accurate placement of

the pressure taps, was also possible. It should still be noted that the resolution of the significant pressure gradients that can occur on these complex shapes was still rather crude.

Fabrication of the larger diameter 7x7 and 4x7 serrated was somewhat more complicated. Actual cables were woven using "neoprene wires". For the 7x7 model, 3/16 in OD / 1/16 in ID neoprene tubes were twisted and wrapped to form a single strand. Then six strands were twisted and wrapped about a solid center-strand to form the model. The lay and pitch was matched to the cast model. Figure 8 presents a schematic of a cross section for this model. A pressure tap was installed on each strand on the perimeter of the model as indicated in Figure 8. The azimuthal orientations of the pressure taps relative to the center of the model are indicated on the figure.

The 4x7 model was constructed in a similar fashion and a schematic of a cross section is shown in Figure 9. Six of the wires in each strand were 3/16 in. OD / 1/16 in. ID neoprene tubing. The center "wire" in each strand was a 0.221 in. OD electrical wire. The somewhat larger diameter electrical wire was used as the center-wire in each strand to provide additional structural rigidity to the model. Two of the neoprene "wires" in each strand were twisted to provide the serrated elements within the strand. The entire cable used a 3/8 in OD steel rod as a central element. The resulting model, which had a 1.68 in nominal diameter, appeared to represent the surface detail of the 4x7 serrated cable. Due to the serrated elements, this model did not possess the same symmetry as the other models. The non-uniform distribution of the pressure taps was the result of the non-uniformity in the cross section geometry. Figure 9 illustrates the location of the serrated elements on the section where the pressure taps were installed as well as the location of the pressure taps. There were 26 pressure taps located on the perimeter of this cross section.

The stiffness characteristics of the cable models was investigated in some detail as part of the Phase I study. The models used in the current effort were of comparable stiffness and no detailed assessment of the stiffness properties was made. Each model was monitored for vibration during the testing and no appreciable vibration was observed.

## 2.3 Flow Visualization Models

The initial flow visualization studies were performed using a $TiCl_4$ tracer injection system developed by Visser, Nelson and Ng (1988). These were conducted using the large diameter 7x1 neoprene model. The details of the method are described below, but the smoke was introduced into the neoprene tubing from outside of the test section and injected into the flow at an orifice similar to the pressure taps described above. This was also attempted on preliminary versions of the smaller epoxy cast cable models, again using the surface pressure taps as smoke injection ports. This method proved unsatisfactory since in order to introduce an adequate amount of the tracer into the flow, a rather large "injection" velocity was required. This small "jet" of tracer perturbed the flow in the region of interest and appeared to significantly alter the flow characteristics. After these preliminary tests no additional models were used with the $TiCl_4$ smoke visualization and alternative methods were considered.

Smoke wire flow visualization was used for the majority of the flow visualization tasks in this study. Tests were conducted for the cylinder and the 7x7 and 4x7 cable replica models. All these models were 5/8" in diameter. These were the same models used for the surface pressure distribution measurements and they were modified in order to mount the smoke wire to the model surface.

A preliminary surface oil flow visualization study was performed using the 7x1 large diameter model. This was the same model used in the surface pressure measurement studies except the pressure taps were removed. This test was useful in identifying regions of separation and reattachment but recording the data was very difficult and this test was only used for a qualitative assessment of the flow at the surface of the model.

## 2.4 Model Endplates

As in the case of the flow visualization tests, all of the endplate studies were conducted using the 5/8 in diameter models. There were a large number of potential endplate geometries which were considered. The design that was selected was composed of circular plates, 5.75 inches in diameter and 0.125 inches thick, which were mounted directly to the 5/8" cable models and provided an endplate to model diameter ratio of 9.2. The endplates were fabricated from plexiglass in order to minimize the interference with the strobe lighting of the smoke tracers close to the model. The edges of the plates were bevelled with a 30° bevel

with the "flat" face on the side closest to the cable. The gap between the model and the endplate was sealed to prevent flow leakage through the endplate.

# 3. EXPERIMENTAL FACILITIES, INSTRUMENTATION and TEST PROCEDURES

The series of experiments described in this test report were conducted at the University of Notre Dame Aerospace Engineering Laboratory. The wind tunnels used for the tests are specifically designed for smoke flow visualization and have been used extensively for basic flow physics studies. Separate test sections were used for the surface pressure measurements and the detailed flow visualization studies. Accurate positioning of the models was the critical issue in the pressure study and proper lighting and tracer placement were the primary factors in the design of the flow visualization facility.

## 3.1 Wind Tunnels

The wind tunnel used in the experiments was a low turbulence, subsonic wind tunnel located at the University of Notre Dame Aerospace Laboratory. The tunnel is an indraft, open circuit type which exhausts to the atmosphere as illustrated in Figure 10. The inlet of the tunnel consists of a 20.6:1 area contraction with 12 anti-turbulence screens located just upstream of the inlet. This provides a near uniform freestream velocity profile in the test section with a turbulence intensity of less than 0.1%. A test section with a 2 ft by 2 ft cross section was used. The flow is then expanded through a diffuser to the fan. The diffuser has a 4.2° angle of divergence and is 13.78 ft long. The tunnel is powered by an eight-bladed 3.94 ft diameter fan directly coupled to an 18.6 kW AC induction motor located at the end of the diffuser section. The flow velocity is monitored through a digital differential manometer which displays the dynamic pressure in the test section as measured by the pitot-static tube placed in the flow.

The two basic tests described in this report required the development of two wind tunnel test sections. One section was used for the flow visualization tests and included the capabilities for smoke sheet generation and windows for lighting and photography. The other was used for the surface pressure measurements. The cables were mounted from either the side wall or the floor of the test section depending upon the requirements of the particular test.

The visualization section is described in detail in Batill, Nelson and Nebres[1988]. For these tests the models were in the inclined configuration so they were supported from a pivot on the bottom of the section and were set to the

required orientation relative to the free stream and then passed out of the top of the test section at an appropriately positioned port.

For the surface pressure measurements, the model was supported in a yoke on the front wall of the section and was free to rotate about its longitudinal axis to the required orientation. The orientation was manually controlled with a metered gear train from outside of the test section.

## 3.2 Pressure Measurements

The pressure profile measurements entailed positioning the model at a specified cable angle, while keeping the pressure taps located at approximately the center of the test section. The pressure taps were initially positioned at a specified orientation about the longitudinal axis. Pressure values corresponding to the other points on the profile were obtained by rotating the model about its longitudinal axis through some predetermined angle. This rotation angle was determined by the symmetry of a given model and the number of surface pressure taps. This required the ability to accurately position the model and this was accomplished using crank operated, gear mechanism. A revolution counter which served as the position indicator had a resolution 0.01°. It was operated manually by a crank that turned the cable through the gear train. Considering backlash, the apparatus was accurate to within ± 0.5°. Considering errors in setting the initial reference angle and the positioning of the taps on the model surface, it is estimated that the overall uncertainty in the location of the pressure measurement is about ±2°.

The determination of the angle settings for the positioning apparatus which would correspond to the pressure taps distribution on a cross section normal to the longitudinal axis of the cable was straightforward. This involved a series of rotations of the models to account for the symmetry in the model cross section and the placement of the pressure taps. This approach was used for both yawed and unyawed models.

In the case of yawed models, two options existed for measuring and presenting the surface pressure distributions. Either streamwise cross sections or cross sections normal to the longitudinal axis of the model could be considered. If streamwise cross sections were considered, it involved the development of numerical models for the streamwise cross section plane, as described in the Phase I report, and each pressure tap was positioned manually to the appropriate

position through a series of model rotations. The use of streamwise cross-section pressure profiles was limited, considering the complexity associated with developing this information and the fact that they provided little additional useful information in comparison with the normal cross-section profiles.

The cable models are three dimensional. Though there is a spanwise periodicity in geometry, every cross section is unique and this results in a three dimensional or spanwise variation in the pressure profiles. By starting each profile measurement at different initial angular orientations of the model, one is able to simulate the variation in the longitudinal direction. Figure 11 illustrates the equivalence between a rotation of the model and a spanwise shift in the measurement location. The spanwise distance between two cross sections with the same geometry is referred to as the "peak-to-peak" (ppd) distance in this report.

The quantities measured in obtaining the pressure profiles were the local static pressure at the surface of the model, the free stream static pressure and the free stream dynamic pressure. These were used to calculate the non-dimensional local static pressure coefficient which is defined as,

$$C_p = ( P_{\text{local static}} - P_{\text{free stream static}}) / Q_{\text{free stream dynamic}} = P_{tap} / P_{pitot}$$

Figure 12 is a schematic of the measurement system. A pitot static tube was located upstream of the model and was used to measure the difference between the free-stream static and total pressure. Since a number of the models were equipped with multiple pressure taps, they were each connected to an automated switching mechanism or scanivalve. The static pressure at the surface of the model was transmitted through the scanivalve to an external, low-range electronic manometer. Adequate settling time was allowed before data was recorded as the scanivalve was switched from one surface pressure tap to the next.

The data acquisition system consisted of two electronic manometers which were pressure transducers with output analog voltage signals, and a Macintosh II equipped with a National Instruments, Inc. board which performed the analog to digital (A/D) conversion. The National Instruments, Inc. board was controlled by the LabView software system, which was programmed for data acquisition and equipment control operations tailored for each particular test.

The program, written with the LabView software, was designed to control the scanivalve to select the appropriate pressure measurement location and to read two channels, i.e., two analog voltages output from the manometers and convert

them into digital voltages with a resolution of 0.00061 volts. For each pressure coefficient computation, 1,000 samples were recorded for each of $P_{tap}$ and $P_{pitot}$ at an interval of 0.004 sec per sample per channel. The 1,000 samples were averaged before $P_{tap}$ was divided by $P_{pitot}$ to obtain the pressure coefficient. This sampling rate could be set to frequencies between 6.25 to 125 Hz. This acquisition rate was adequate for the mean pressure measurements. The data sampling rate for the unsteady surface measurements was dependent upon the dominant frequencies in the unsteady pressure signal. The LabView program was designed to actuate the scanivalve which is a rotary switch which can be programmed to select the desired surface pressure tap to be measured. This arrangement enables the automatic measurement or scanning of a series of pressure inputs while using only a single transducer. The entire pressure measurement system was periodically tested for leaks using a vacuum leak tester.

Unsteady surface pressure measurements were conducted for the three 5/8 in. replica models: the circular cylinder, 7x7 cable and 4x7 serrated cable. These were the same models used for the steady pressure measurements. They were modified in order to minimize the attenuation of the fluctuating pressure signal through the pressure transmission lines. The surface pressure taps were connected by 0.044 in. ID and 3 ft. long stainless steel tubes directly to a pressure transducer (0 to 0.55 in. water range Setra electronic manometer). An adaptor, approximately 3 inches in length was used to connect the stainless steel tubing to the pressure transducer. Analog voltage signals from the pressure transducer was then acquired by a Scientific Atlanta SD380 Spectral Dynamics Signal Analyzer. The SD380 has a 12-bit A/D conversion and built-in anti-aliasing filters. Spectral functions were obtained from 2048 points acquired at a sampling rate of 1024 hz. A total of 50 of these spectral functions were then ensemble averaged to obtain a more representative spectral function, see Weaver [1983] for a description of ensemble averaging. Time domain data were acquired from 1024 points at a sampling rate of 12.5 kHz. The choice of the sampling rate was based upon the dominant frequency of interest which was the shedding frequency. No pressure magnitude calibration or correction for the effect of the conducting tubing was performed since the tests were conducted basically to identify dominant frequencies in the surface pressure and amplitude attenuation was not considered important.

## 3.3 Flow Visualization

Numerous flow visualization techniques were developed during the Phase I effort which were suitable for this complex, three dimensional flow field. These initial tests were conducted using flood, laser sheet and stroboscopic lighting. Data were collected with both 35mm camera records and video tape recording. These tests served as a basis for the flow visualization methods used as part of this research program. During the Phase I tests, rather large scale details of the wake structure were studied. The primary purpose of the tests performed in Phase II was to more closely observe the flow field near the cable. This required more accurate positioning of the smoke or tracer used to visualize the flow.

The initial method considered for smoke generation involved using the titanium tetrachloride $TiCl_4$ smoke vapor as described by Visser, et.al. [1988]. A number of cable models were developed on which a thin stainless steel tube was mounted to the downstream side of one of the cable models and the $TiCl_4$ vapor was introduced into the wake of the cable. These preliminary results indicated potential so a model was then developed similar in design to the surface pressure measurement models. The $TiCl_4$ vapor was carried into the model in $N_2$ gas at room temperature. As the $TiCl_4$-$N_2$ gas/vapor mixture exited the model at the surface, the $TiCl_4$ reacted with the water vapor naturally occurring in the air and formed a dense, white smoke. Flow visualization was initially performed using the $TiCl_4$ on the 7x1 Neoprene model. By keeping the flow at a very low speed, vortical structures in the regions between the large scale surface irregularities were revealed. However, the method was only favorable for tests up to about 3 fps, or about Re=1000 for the 5/8" epoxy models and there were problems in regulating the injection of the vapor without significantly altering the local flow characteristics. This method which has been used very successfully for visualizing the leading edge vortex over delta wings did not seem well suited for this particular application of bluff body flow visualization. Since the method could only be used far below the flow Reynolds number of interest in this study no data were recorded using the $TiCl_4$ method. Limitations of the method led to the consideration of other methods, particularly the smoke wire.

A detailed description of the smoke-wire technique is presented in Batill and Mueller [1981]. The primary benefits of the smoke wire technique are that it produces very fine streaklines that provide excellent detail in the flow field and it can often be placed so that the smoke tracer can be injected into regions of special interest. This method requires a synchronized camera and strobe system because

the smoke only lasts a few seconds. The smoke-wire technique is limited to velocities at the wire of less than 25 ft/sec. The smoke-wire technique requires the introduction of a fine stainless steel wire into the flow upstream of the region which is to be marked with the smoke tracer. For this application a 0.003 inch diameter wire was actually mounted on the cable model. By placing the wire near the surface of the cable model, the orientation of the cable and the smoke sheet position relative to the cable could be accurately controlled. This provided much greater detail on the flow field very near the surface of the cable models.

The wire was coated with mineral oil and the oil was heated by passing a controlled electric current through the wire for a prescribed time interval. The wire was spring-loaded to compensate for the thermal expansion when the wire was heated. Due to the surface tension of the oil, "beads" form on the wire and, when heated, fine filaments of smoke are emitted from each bead and form a sheet of smoke in a flow. The orientation of the wire relative to the model could be varied so that the smoke could be "injected" into various locations in the near field flow. In most cases the wire was placed immediately upstream of the stagnation point approximately 1/8th of an inch from the model. The cable models were rotated from 0° to 45°, 90°, 135° and 180° in both directions so as to change the position of the smoke tracer relative to the models.

By taking two photographs with the cable inclined upstream and downstream, for the yawed cases, visualization of the flow over both "sides" of the cable could be achieved. Tests were conducted for the cylinder, 7x7 and 4x7 cable replica models, all 5/8" in diameter. These were performed at cable angles of 90°, 60°, 40° and 20° at Re=5,500. This series of tests was performed without endplates.

Event timing for use of the smoke wire was critical and a specially designed timing and control system was used for these experiments, see Batill and Mueller [1981]. A controllable DC current was passed through the thin wire for a variable length of time. Simultaneously, a signal was sent to the camera with a variable delay to trigger a photograph. The delay is important because after current application, it takes a fraction of a second for a good quality smoke sheet to appear. The camera then is activated and simultaneously triggers a flash from the strobes.

Proper lighting techniques are necessary to insure good quality flow visualization. The stroboscopic lighting technique proved to be the most suitable for this application. Four GenRad Strobolume Model 1540 strobes, set in a single flash mode, were used to provide lighting for the flow visualization photographs.

The models were illuminated through the bottom of the test section and photographed through the front window of the test section. The camera used for all the still photography was a 35 mm Nikon FM2 with a motor drive and mounted on a tripod. The lens used was a standard 50 mm f/1.4 lens. Kodak TMAX P3200 35mm film was used.

Limited surface oil flow visualization tests were conducted using the 1.875 in. diameter 7x1 cable. A mixture of kerosene, titanium dioxide powder and oleic acid was prepared and this mixture was "painted" uniformly on the surface of the model with no flow passing over the model. The wind tunnel was then started and the surface shear stress redistributed this white "oil" and highlighted regions of attached and separated flows. This provided good qualitative information but was very difficult to record photographically due to the complex, three-dimensional character of the surfaces. Though this approach could provide additional useful information, only limited results are included in this report.

### 3.4 End Effects Study Equipment

A set of endplates were fabricated in order to investigate the influence of end boundary conditions. Circular plates 5.75 inches in diameter and 0.125 inches thick were mounted directly to the cable models. The plates provided an endplate to model diameter ratio of 9.2. The edges of the plates were bevelled with a 30° bevel with the "flat" face adjacent to the cable.

Tests were conducted for the cylinder, 7x7 and 4x7 cable replica models, 5/8 in. in diameter, at cable angles of 90° and 40°. The cables were tested without endplates and with endplates at a fixed spacing such that the ratio of the distance between the plates to the cable diameter was approximately 25. These tests were conducted at a flow velocity which corresponds to a Reynolds number of $6 \times 10^3$. For the tests conducted with the endplates in-place, three plate configurations were used.

a. Both plates aligned with the flow.

b. Both plates canted so that the region between the plates was diverging, the plate angles were 5° to the free stream.

c. Both plates canted so that the region between the plates was converging, the plate angles were 5° to the free stream.

The results of these tests were planform view flow visualization photographs which allowed for a qualitative assessment of the influence of the endplates.

# 4. RESULTS AND DISCUSSION

The following sections document the results of each task in this study. These include the steady and unsteady pressure measurements, the detailed flow visualization study and the end effects study.

## 4.1 Pressure Measurements

Pressure measurements on the yawed cables indicated lift generation and suggest the mechanism by which lift was developed. Significant differences between flows around the cables and the cylinder were also observed. Steady surface pressure profiles showed characteristics which were not present on the cylinder. Test results provided some insight to the details of this complex, three-dimensional flow.

### 4.1.1 Steady Pressure Measurements

Pressure profiles measured for the cables have shown a distinctly different character when compared to the circular cylinder. Pressure coefficients around the cylinder have shown symmetric profiles, while those for the cables have shown strongly asymmetric profiles.

The surface pressure distributions can be measured and presented in two different manners, either around a cross-section normal to the cylinder longitudinal axis or streamwise, i.e., about a cross-section formed by a plane parallel to the free stream velocity vector and normal to a plane formed by the model longitudinal axis and the free stream velocity vector. The azimuthal angle along the cross-section, $\theta$, follows the standard polar coordinate system, with $\theta=0°$ directed into the free stream, and with positive $\theta$ going clockwise. In the following, steady surface pressure data is presented for the circular cylinder, 4x1, 7x1, 4x7 and 7x7 models for a range of cable angles and Reynolds numbers. Both tabular and graphical data are presented. In each case an attempt has been made to correlate the pressure data to the surface geometry.

Figure 13 illustrates the surface pressure coefficient distribution for the 7x1 model at a cable angle of 40° for a streamwise cross section. A schematic of the cross section is included in the Figure and illustrates the asymmetry characteristic of the cables. The asymmetry in the pressure distribution is also quite evident. The "top" or what is referred to as the smooth side of the model has significantly lower

surface pressure ( more negative $C_p$). The "smooth" side of the cable is that side on which the effect of yaw is to more nearly align the free stream velocity with the cable strands. The influence of yaw on the opposite or "rough" side is to orient the strands so they are more nearly normal to the free stream velocity. As illustrated with this Figure, it is rather difficult to correlate the surface pressure distribution to the surface geometry. As shown in the following results, presenting the surface pressure data for cross sections normal to the cable axis allows for better correlation with the surface geometry detail. For that reason the remainder of the pressure data presented in this report are for cross sections normal to the cable axis.

Measurements on the cylinder resulted in symmetric pressure profiles, consistent with published data. Table 2 presents the measured pressure coefficients at 90°, 60°, 40° and 20° cable angles at Reynolds numbers of 10,000, 30,000 and 46,000. Figure 14 shows the profiles from the data in Table 2. The plots show that the pressure distributions are consistently symmetric except for a slight asymmetry in the base region at the 60° cable angle. They also indicate that the locations of the upper and lower points of separation were symmetric. It should be noted that stagnation only occurs at the leading edge for the $\beta = 90°$ case. In the yawed cases, the flow begins to align with the cable and does not stagnate at the leading edge. A dependence upon Reynolds number is indicated particularly in the base pressure. The Re = 10,000 case consistently displays a higher base pressure except for the 20° cable angle case.

Tables 3 - 6 present the pressure coefficient data for the large diameter 4x1 cable model. Along with the pressure coefficients, at the bottom of each Table, are integrated values of the pressure coefficients which provide force coefficients which are discussed later in the report. Figures 15 - 18 are graphical presentations of the same information. These figures illustrate the manner in which much of the surface pressure data will be presented in the remainder of this report. These represent normal cross sections for this model. The geometry of the cross section depends upon the spanwise position of the cross section relative to the helical geometry of the cable. The 0% ppd designation is used to indicate that spanwise position, or cable orientation, in which the plane of symmetry of the model, which bisects two of the strands, is aligned with the free stream velocity. As one moves along the span of the model (or rotates the model) measurements are presented for three other spanwise stations corresponding to the 25%, 50% and 75% ppd positions. Along with the pressure profiles are an illustration of the surface geometry. The "scallops"

on the $C_p$ plots indicate the local surface geometry and can be used to help correlate the surface geometry with the surface pressure distribution.

Tables 7-10 present the pressure coefficient data for the large diameter 7x1 cable model. There is more detail presented for this model since greater resolution could be achieved in the pressure tap locations. Figures 19-22 are graphical presentations of the same information. Again four locations along the span corresponding to the 0%, 25%, 50% and 75% ppd positions are presented.

Table 11 presents the pressure coefficient data for the small diameter 4x7 cable model at a Reynolds number of 10,000. Only a rather crude distribution of the pressure taps could be achieved with this model and the same four %ppd positions are presented. Tables 12-19 present the surface pressure coefficient data for the large diameter 4x7 cable model. The increased resolution allowed by the larger model provides additional detail. Also %ppd positions of 0% to 87.5% with a 12.5% increment are included.There is more detail presented for this model since greater resolution could be achieved in the pressure tap locations. Figures 23-26 are graphical presentations of the same information. Even though greater spanwise detail is available for this case only the same four locations along the span corresponding to the 0%, 25%, 50% and 75% ppd positions are presented since they illustrate the basic characteristics of the pressure distribution.

The last set of pressure data is for the 7x7 cable model. Table 20 presents the pressure coefficient data for the small diameter 7x7 cable model at a Reynolds number of 10,000. This small diameter model also has a rather coarse pressure distribution although more data is available than for the 4x7 model. The same four %ppd positions are presented for this model. Tables 21-28 present the surface pressure coefficient data for the large diameter 7x7 cable model. The increased resolution allowed by the larger model again provides additional detail. Also %ppd positions of 0% to 87.5% with a 12.5% increment are included. Figures 27-30 are graphical presentations of the same information. Even though greater spanwise detail is available for this case only the same four locations along the span corresponding to the 0%, 25%, 50% and 75% ppd positions are presented.

In each case the plots also show higher suction pressures at the smooth side. There are some differences between the pressure coefficient values at the 30,000 and 46,000 Reynolds number but more significant differences with the 10,000 Reynolds number cases. This further illustrates the complexity of these flowfields which are strongly influenced by flow separation. When comparing the 60° and 40° cable angle case for the 7x7 cable, the suction pressures seem to be

relatively lower for the 40° case, which implies a smaller steady lift force at the 40° cable angle. It should be noted that when comparisons are made to the Re = 10,000 case, the difference in surface pressure distribution resolution can also influence the comparison.

Steady pressure measurements on each of the cable models showed very significant effects of the cable stranding. Even for the unyawed case, the cable models showed very different pressure profiles compared to the cylinder. First, the helical stranding of the cable created spanwise differences in pressure profiles corresponding to spanwise differences of the cross-section. Three dimensional effects were very prominent. Also, there was no circumferential symmetry in the pressure profiles even when the cross section was symmetric. This asymmetry indicates a local lift or side force for a particular cross-section even in the unyawed case. However, the four cross-sections do not appear to have an average skewness. Second, the strands appeared to develop local, strong adverse pressure gradients which promote separation. This caused the separation points to vary from 60° to 120° depending on the cross-section and cable angle. For a cylinder, the separation point occurs approximately at 80°. It should be emphasized that the separation points mentioned here are approximate locations.

Steady pressure profile measurements on the yawed cable indicated definite lift development in the direction of the "smooth" side. As an example consider Figure 21, the 7x1 cable at 40° cable angle. Relatively lower pressure coefficients on the smooth side, i.e., from 180° to 360° on this 7x1 cable which was left lay were observed compared to the opposite side, 0° to 180°. It is evident in the yawed cases that separation is delayed on the smooth side. In Figure 21, separation on the smooth side occurred from -100° to -130°, while on the rough side, separation occurred from 50° to 100°. Some separation points cannot be well defined simply using the surface pressure data. This case also illustrates the significant spanwise variation in the pressure distribution, which implies significant spanwise flow components. This observation is supported with the flow visualization results.

The asymmetry in the pressure distribution appears to be the result of the strands on the smooth side of the yawed cable presenting less abrupt surface geometry variations to the flow. The adverse pressure gradient for the flow over the strand is altered and influences the separation point. The opposite side or "rough" side presents basically a different geometry to the oncoming flow again altering the pressure distribution and influencing separation. The conclusion that the lift force is

separation-induced is similar to the findings of Sewell and Taylor[1961] and Counihan[1963]. However, the lift force they observed was generally towards the rough side and opposite to the direction observed in the present study. Delayed separation on their transmission line cables occurred on the rough side and was due to the early transition to turbulence which then influences separation. Furthermore, they observed lift only in the critical Reynolds number regime where asymmetric transition to turbulence in the boundary layer occurs. It is important to note that although the lift force observed in the present study was separation-induced, the direction of the lift force as well as the Reynolds number where lift was observed were different from that observed by Sewell and Taylor[1961] and Counihan[1963].

Interestingly, the mechanism of lift development indicated by the present measurements substantiates the conjecture made by Schultz[1962]. Schultz lacked the supporting measurements which are provided by this study. Also, Schultz did not differentiate whether the asymmetry in separation may have been caused indirectly by asymmetric transition or directly by the adverse pressure gradient.

The cables used in the steady pressure tests, i.e., the 7x1 and the 4x1, are in fact simplified models of the actual 7x7, or 4x7 serrated cables and neglected small scale surface irregularities. For the 7x7, or 4x7 serrated cables, the wires in the strands could promote transition as well as the strand themselves directly promoting separation. It is reasonable to assume that a combined effect of the small scale wire irregularities and the large scale strand irregularities is possible in critical regime. It could also be expected that transition to turbulence would be earlier for the 7x7, or 4x7 serrated cables than for the 7x1 and 4x1 cable. This may mean lower critical Reynolds numbers. The orientation of the wires in the strand, i.e., whether the cable is regular or lang lay and the wire lay angle may then have significance. It should however be noted that the strands create the larger scale surface irregularity and probably the greater influence. It would be more likely that separation induced by the adverse pressure gradient over the strand would be the more dominant factor in lift development, even in the critical regime.

### 4.1.2 Integrated Pressure Forces

Force coefficients were estimated by integrating the mean surface pressures measured around the cables. Local or sectional values of $C_l$ and $C_d$ were calculated for different cross-sections normal to the cable axis. The side or lift force

coefficient $C_l$ is related to the force acting normal to the plane formed by the free stream velocity and the longitudinal axis of the model. The "drag" force coefficient was related to that component of the total drag force acting normal to the model's longitudinal axis and in the plane formed by the free stream velocity and the longitudinal axis of the model. The drag coefficient is not defined in the traditional sense and can only be compared with total pressure drag for the $\beta = 90°$ cases. It should also be noted that these integrated force coefficients are approximations based upon surface pressures and do not include shear stress components.

Each cross-section was subdivided into a series of panels upon which it was assumed that a uniform normal, surface pressure acted. This is the pressure measured at the surface pressure tap. The schematics of the individual cable models, shown in Figures 6 - 9, illustrate the individual panels and define the panel positions in terms of their endpoints. Lift and drag components of the incremental forces on each panel were summed to obtain the coefficients. Local values of $C_l$ and $C_d$ within a peak to peak distance were then averaged to obtain the mean lift and drag coefficients for a particular cable geometry.

The generalized formulas for obtaining the local lift and drag coefficients are as follows:

$$C_l = \frac{\text{lift force}}{q_\infty D} = \frac{\Sigma\,(p_i - p_\infty)\,\Delta x_i}{q_\infty D} = \sum \frac{p_i - p_\infty}{q_\infty}\frac{\Delta x_i}{D} = \sum C_{p_i}\frac{\Delta x_i}{D}$$

$$C_d = \frac{\text{drag force}}{q_\infty D} = \frac{\Sigma\,(p_i - p_\infty)\,\Delta y_i}{q_\infty D} = \sum \frac{p_i - p_\infty}{q_\infty}\frac{\Delta y_i}{D} = \sum C_{p_i}\frac{\Delta y_i}{D}$$

The unit length considered is spanwise regardless of yaw angle. Horton, et. al.[1987] however defined the lift and drag coefficients in this manner, and for comparison purposes, their definition was adopted in this report. In the above formulas, $\Delta x$ and $\Delta y$ for a particular panel must possess the correct sign. Following the direction for the discretized line of integration around the body, $\Delta x$ and $\Delta y$ must be positive when increasing and negative when decreasing. The method can be illustrated on a circular cylinder as follows:

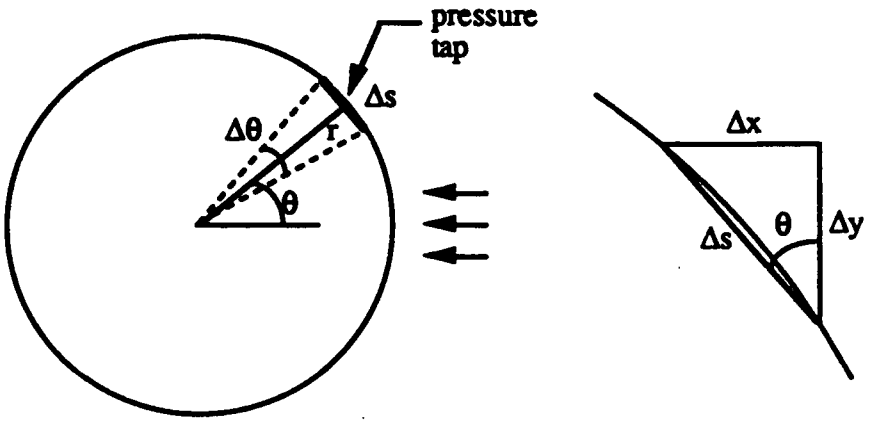


$\Delta x = -\Delta s \sin\theta = -r\,\Delta\theta \sin\theta$

$\Delta y = \Delta s \cos\theta = r\,\Delta\theta \cos\theta$

$$C_l = \sum C_{p_i} \frac{\Delta x_i}{D} = \sum C_{p_i} \frac{-r\,\Delta\theta \sin\theta_i}{2r} = -\frac{\Delta\theta}{2} \sum C_{p_i} \sin\theta_i$$

$$C_d = \sum C_{p_i} \frac{\Delta y_i}{D} = \sum C_{p_i} \frac{r\,\Delta\theta \cos\theta_i}{2r} = \frac{\Delta\theta}{2} \sum C_{p_i} \cos\theta_i$$

For the case of the cylinder from Table 2, the $C_p$ values are given for each $\theta$ location, and $\Delta\theta$ is 10°. The lift and drag coefficients are obtained from the summation. For the 7x1, 4x1, 7x7 and 4x7 cables used for the high Reynolds number tests (Re ≥ 30,000), the endpoints of the line segment representing the panel were the midpoints of either the arc or the line segment between the taps. The taps were identified by the numbers and the endpoints were identified by the letters. The coordinates of the panel endpoints are given in the tables on Figures 6-9 in polar form, i.e., the non-dimensional distance, r/D of the endpoint from the cable axis and the angular position, $\theta$ of the endpoint from the reference axis shown. From these polar coordinates, $\frac{\Delta x_i}{D}$ and $\frac{\Delta y_i}{D}$ were easily obtained and applied in the formula for $C_l$ and $C_d$.

The 4x7 and 7x7 cables for the low Reynolds number tests, (Re=10,000) were assumed to be "circular cylinders" in order to estimate the $C_l$ and $C_d$. Figure 4 shows idealized cross-sections of the cables and indicates the pressure tap locations. In both cases, and in particular for the 4x7 model, integrated pressures will only provide a gross approximation to the resultant force. In the case of the 4x7

cable, the serration was considered to be randomly located as can be expected for a real serrated cable.

Tables 2 - 28 provide the sectional lift and drag coefficients for each of the models and test conditions described above. This data has been summarized by developing average values for each model, at each cable angle and at each Reynolds number. The drag data are summarized in Figures 31 - 34 and the lift data in Figures 35 - 38 and is included in tabular form in Tables 29 and 30. The data is compared with the results of Horton, et.al. (1987). The drag data for the circular cylinder is shown in Figure 39.

The integrated drag coefficients agree very well with the force transducer measurements of Horton, et. al.[1987]. This is despite the fact that the cables tested in the current study were rigid unlike the vibrating cables in the earlier study. The data presented from Horton is the loading function which is a curve fit to the experimental drag data which had a fair amount of scatter. The agreement between Horton's drag loading function and the Re=10,000 data for the 4x7 and 7x7 and that of the 4x1 and 7x1 is actually very good.

For the Re=30,000 and 45,000 for the 4x7 and 7x7 cables, the drag coefficients showed a significant drop when compared to the lower Reynolds number or the Horton data. This could be due to the fact that the flow had exceeded the critical Reynolds number. It is known that the drag for these types of bluff bodies, the plain cylinder for example, drops once the flow is in the critical regime. For cables, Counihan [1963] observed that the critical Reynolds number could be as low as 30,000. It is possible that the the critical Reynolds numbers for the 4x7 serrated and 7x7 cables are lower than 30,000 due to their irregular geometry and the presence of the small scale surface perturbations.

It can be seen that for the 7x1 and the 4x1, the flow appears to be subcritical, since the drag coefficients compare quite well with Horton's loading function and with the Re=10,000 result for the 4x7 and 7x7 cases. The absence of the small scale surface perturbations may have raised the critical Reynolds number for these cases.

The integrated lift coefficient data was more difficult to interpret. There was considerable scatter in the data and comparison with the earlier Horton results was less conclusive. The lift results appeared to be highly Reynolds number dependent. The integrated lift coefficients for the yawed 7x7 and 7x1 cable were negative since the 7x7 cable was a left lay cable and thus presents a smooth side to the flow on the "bottom" side for the convention used in this study. For the yawed 4x7 and 4x1,

the lift is positive except for a few cases. The lift coefficients for the unyawed case, cable angle=90°, are expected to be zero. Data for the 7x7, 7x1 and the 4x7 can be considered close to this expected value. The values for the 4x1 are quite anomalous and the reason for this is not known. The lift coefficient data for the 7x7 from Horton, et. al.[1987] were assumed to be negative. Horton did not specify the direction of the lift force. But in a private communication with Watson, he stated that the lift force was toward the smooth side which implies a negative lift for the 7x7 based on the present sign convention. For the 4x7 serrated cable, the lift in all cases seems to be insignificant, within a range of about ±0.05 about a zero mean. This may be due to the critical nature of the flow. In general, the maximum lift coefficient occurs at a cable angle of 60° at a value of roughly 0.2. It is lower at 40° and is lowest at 20°.

### 4.1.3 Unsteady Surface Pressures

The small diameter epoxy models were used for these tests at cable angles of 90° and 60° at a Reynolds number of 10,000. A single pressure tap was located at the model mid-span and the circumferential location of the tap was varied. The tap was connected using a stainless steel tube to a pressure transducer located outside of the tunnel. Both time and frequency domain data were collected for each of the cable models and processed on-line using a dynamic signal analyzer. Figure 40 is an illustration of the variation with time of the surface pressure on the cylinder and 7x7 and demonstrates the marked periodicity in the flow. Figures 41 - 46 are the frequency spectrum of the pressure signal in the range of 0-400 Hz at each cable angle considered for the cylinder and both cable models. In most cases the azimuthal orientation of the pressure tap was varied from 30° to 80°(near separation) and then to 180° (in the wake.) In each case there was a frequency "peak" near 60 Hz. This may have been due to a combination of electronic noise wind tunnel disturbances. This peak appeared to be independent of the model or its orientation.

Both the cylinder and the 7x7 cable provided similar results. A dominant peak at approximately 125Hz which corresponds to a Strouhal number consistent with earlier hot-wire measurements. Spectra of surface pressure fluctuations showed peaks at the shedding frequency even at surface pressure tap angular positions upstream of separation. Peaks at the shedding frequency were observed at tap locations as small as $\theta$=5°. Shedding frequencies are apparent for the

cylinder (127 Hz) and the 7x7 cable model (124 Hz). The first harmonic of the shedding frequency was also present, and it was particularly evident at the pressure tap located in the base pressure region. These shedding frequencies correspond to Strouhal numbers of 0.207 and 0.202 respectively.

Interestingly, a peak at the primary shedding frequency did not show up for the 4x7 cable for the 90° cable angle. This appears to indicate that surface pressure fluctuations due to the shedding frequency for this cable are at a low level and that they are masked by the measurement "noise" or more random pressure fluctuations. This does not imply however that the vortex shedding process has been eliminated since earlier hotwire and flow visualization measurements showed a definite shedding frequency for this cable configuration. It however implies a delayed formation or relatively longer formation length compared to the cylinder or 7x7. This also agrees with the earlier flow visualization results. The fluctuating pressure field due to the alternate vortex formation which takes place farther downstream then has less influence on the surface pressure distribution, which could then suggest lower vortex induced vibrations. One should however be careful to note that the model here is rigid and stationary, and that vibrating cables may behave differently.

At the 60° cable angle, Figures 44-46, the frequency spectrum for the fluctuating surface pressure on the cylinder indicated a relatively wide peak at the known shedding frequency for pressure tap orientation of both $\theta = 30°$ and 80°. For the cylinder, the rather wide "peak" occurred at 108 Hz corresponding to a Strouhal number of S=0.176, and for the 7x7 cable it was 112.5 Hz corresponding to S=0.183. The values for the Strouhal numbers from these unsteady surface pressure measurements agree with those obtained from the earlier hot wire tests. The 4x7 serrated cable, again did not show any peak at the shedding frequency for the cable angle of 60°.

There was a similar series of tests conducted at a 40° cable angle. Spectra observed at the cable angle of 40° showed very wide band peaks at the shedding frequency and the data was inconclusive so it has not been included.

In all cases considered, the unsteady surface pressure measurements were conducted using pressure sensors which were not located at the model surface. Small diameter tubing was used to transmit the pressure signal from the model surface to the transducer which is located outside of the wind tunnel. It is well known that this type of tubing will attenuate the fluctuating pressure signal and shift the phase of the dynamic signal. A recent study by Batill and Nebres (1991) has

considered this problem in some detail. They developed a time domain approach for correcting unsteady pressure measurements. Their results indicate that the tubing used in this study would alter the amplitude and phase in the time domain for the unsteady pressure signals but since only frequency domain data was of interest in this study, there was no need to correct the unsteady pressure data.

## 4.2 Detailed Near Field Flow Visualization

The purpose of the detailed flow visualization study was to provide additional insight to the flow near the surface of the models. Of primary concern were results which indicated regions of flow separation and highlighted the three dimensional character of this complex flow.

### 4.2.1 Smoke Wire Visualization

All of the qualitative flow visualization results presented in this section were developed using the smoke wire technique. In each case views of relatively small sections near the center of the models are provided. The flow on "both" sides of the yawed models are shown to illustrate the asymmetry in the flow field. The tests were all conducted at Re = 6,000 for each cable angle. The smaller diameter, epoxy casting models were used and provided excellent surface definition.

Figures 47 and 48 provide a comparison between the circular cylinder and the two cable models. The smoke wire was placed at the $\theta = 0°$ position which is immediately upstream of the stagnation point. It was slightly biased toward the viewer so that all of the smoke traces passed to the camera side of the model. The transition in the near wake, free shear layer is evident for the cylinder and the two-dimensional character of the flow is illustrated. In contrast the cable flow fields are very complex and three dimensional. Curvature of the streaklines is shown upstream of the models and transition of the shear layer appears to occur shortly after separation.

Figures 49 - 57 provide the remaining detailed flow visualization data. For each cable angle, except Figure 50, a close-up view is provided of both sides of the model. The smokewire was placed at approximately the $\theta = 0°$ location but biased toward the side closest to the camera. In the photograph on the left, the flow is moving from right to left and in the photograph on the right, the flow is moving from left to right. In Figure 50, a wider view is provided to illustrate the general two-dimensional character of the flow field across the span of the model. In each case the cylinder model displayed symmetry in both views, while the flow about the

cable models was highly three dimensional. The complex cellular structures seen in each of the photographs, often were well correlated to the geometry of the cables. The significant difference between the flow over the "smooth" and "rough" sides of the cable is readily apparent.

Figure 58 - 61 present a study in which the location of the smokewire relative to the model was varied. Figure 58 has the smoke wire positioned 45° about the cable longitudinal axis from the front of the cable. Since the wire is approximately $\frac{1}{8}$ in. from the surface, the streaklines in Figure 58(b) do not appear to be significantly influenced by the detailed surface geometry. However, the streaklines still break-up upon reaching the near wake due to instability of the free shear layer. In Figure 59 the smoke wire is positioned at the 90° orientation with respect to the longitudinal cable axis. The streaklines show similar characteristics to that of Figure 58. Figure 60 has the smoke wire positioned 135° from the front of the cable. It appears that the smoke wire is in the separated wake region. Some diffused smoke is observed to be entrained upstream toward the separation point. Figure 60 (b) indicates rapid mixing in the region where the smoke wire is located. There do not seem to be definite structures formed. But because the smoke is highly illuminated in this particular picture, other structures may have been obscured. In Figure 60 (a), some spanwise periodic structures do appear. In Figure 61, the smoke wire is directly at the back of the model. Back flow is very evident in both photographs. There appears to be no cellular structures formed except for the expected tendency of the back flow to move into the valleys indicating spanwise periodic variation in the separation location as indicated in the earlier surface pressure measurements.

### 4.2.2 Oil Surface Flow Visualization

Figure 62 shows the large diameter 7x1 cable, $\beta$ =60°, with surface oil flow visualization to illustrate the type of results achieved with the surface oil method. The light colored surfaces are indicative of separated flow regions (low surface stress and thus the pigmented oil remains in these regions). The dark colored surfaces indicate attached flow ( high surface shear stresses and therefore the oil flows from these regions). The surface flow patterns are very definite on each strand. Figure 62 indicates that the flow may separate at one strand and may reattach to the next strand when viewed in a normal cross section plane. Final separation may occur as early as approximately 60° and at the latest, around 135°.

Care must be taken in the evaluation of these photographs in order to differentiate between the surface flow patterns caused by the air passing over the body from those caused by movement of the oil due to gravity. Since this method did not appear to provide significant additional information, only limited tests were conducted. For the current models, quantitative information on the boundary layer separation was not available but this method does hold promise if methods could be developed to provide quantitative results from the photographs.

### 4.2.3 Summary of Visualization Results

Both the smoke wire and oil surface flow visualization show the distinct differences in the flow associated with the stranded cables when compared with the circular cylinder. The smooth side of the cable models have a surface geometry that tends to define specific flow separation characteristics and appears to result in the formation of streamwise vorticity that convects down the "valleys". These regions tend to dominate the cellular patterns associated with the detailed cable surface geometry. These, however, eventually dissipate as they get entrained in the larger scale wake vortex formation. Whether this streamwise vorticity is associated with the mechanism for lift development is a topic for further study.

Both the smoke wire and surface oil flow visualization seem to show that depending on location, flow may separate and reattach from strand to strand. The photographs indicate that the separated flow region on the rough side is larger when compared to the smooth side. Preliminary estimates of final separation points are from 60° to 100° for the "rough" side and 80° to 135° for the "smooth" side depending on longitudinal location for a particular cable and orientation.

There was a marked difference in the flow around the opposing sides of the yawed cables. There are spanwise, cellular flow structures that follow the "peaks" and "valleys" in the cable geometry. The cellular flow patterns show streamwise structures emanating from the valleys. It can be supposed that these structures result from the roll-up of separated shear layers over the strands, which are then convected towards the low pressure region in the valleys. The opposite side has the cellular flow patterns indicating complicated separations and possibly some reattachments. Obviously, the difference in flow is due to the difference in orientation of the strands with respect to the flow. This difference in flow around opposite sides of the yawed cables highlights the asymmetry associated with lift development.

## 4.3 End Effects Study

The end effects study was limited to two cable angles, three models and four endplate configurations which represented twenty-four different test conditions. Multiple photographs at each test condition again provide a large amount of visualization data. Figures 63-68 illustrate representative results from these tests. Figure 63 shows the four different endplate conditions for the cylinder model at a cable angle of 90°. The top-left photograph is without endplates, in the lower-left photograph the endplates are in position and aligned with the freestream flow direction. In the photograph on the upper-right the endplates are canted 5° to the oncoming flow such that the distance between the plates is decreasing in the streamwise direction. In the lower-right photograph, the same 5° cant angle is used but now the distance between the plates is increasing as you move downstream. The sensitivity of the near wake to the endplates is evident from the photographs.

For the cable angle = 90° case, the photographs without endplates indicate that the vortex filaments tend to be curved ; i.e., they show a character of being concave relative to the incoming flow. Since the mean flow appears to be more uniform than is suggested by the filament curvature, the wake formation may be influenced by the wall. The parallel endplates tend to show filaments with a somewhat reduced curvature, though somewhat convex relative to the incoming flow. The endplates obviously influence the boundary conditions and alter the wake formation. The converging endplates show filaments with curvature convex to the incoming flow similar to the case of parallel endplates. The curvature, however, seems to be greater than that for parallel endplates. Diverging endplates show nearly straight filaments, a condition that may be more like the flow field of an infinitely long cylinder or cable.

There was no significant difference between visualization data for the cylinder and the 7x7 cable. The 4x7 serrated cable photographs, due to the more diffused wake, did not show consistent endplate effects on the filament curvature. This is unlike the cylinder and the 7x7 cable but the earlier studies with the 4x7 indicated a very diffuse near wake. Just because the smoke is diffused does not mean that significant structure is not present in the wake. A spanwise structure was evident in the results for the 4x7 cable which appears to correlate with the cable geometry.

The second case considered was for $\beta = 40°$. The character of the wake formation is notably different for the yawed cables. For all three models, Figures 66-68, the cases without endplates are similar. Breakdown of the shear layer precedes

the formation of what appears to be coherent, spanwise wake structures. The primary wake structure is not necessarily aligned with the model axis and does not appear to be "two-dimensional". For all models, modification of the wake formation region appears to occur more near the lower wall (upstream section of the model). There is no apparently consistent effect near the upper wall.

For cases of parallel plates (the lower-left photograph in each Figure), the influence of the upstream endplate appears to dominate. For each model, there appears to be a significant, longitudinal velocity component along the model and away from the upstream endplate. The smoke tracer is convected along the model and resulting in a region free of smoke near the endplate. In the case of the 7x7 model there also appears to be coherent streamwise structures and a noticeable qualitative difference between the case without endplates. These "streamwise" structures which are inclined at an angle less than the cable angle are more apparent near the lower endplate. One cannot determine how these streamwise structures interact with the "normal" spanwise vortex wake formation from these limited vizualization photographs. Ramberg[1978] also observed these two patterns which he called "modes" in his flow visualization tests. The source of these modified structures is still unknown. In the case of the yawed, 4x7 cable there are streamwise structures present but these appear to be correlated with the cable stranding similar to the case without endplates.

For cases with converging and diverging endplates, again the most obvious influence appears to be in the region near the upstream endplate. In the case of converging endplates the streamwise structure observed for the parallel endplates and the 7x7 model is present for the circular cylinder. Conversely for the 7x7 cable model, the inclination of the endplates alters the apparent streamwise structures.

It is particularly difficult to draw definite conclusions from this type of study. The most effective use of flow visualization is when it is employed in conjunction with quantitative measurements. It is obvious that the endplates do alter the wake though their influence on the cable itself is less obvious. No attempts to systematically evaluate the influence of the endplates on the qualitative measurements were made. Other experiments have indicated that the presence of endplates influences the base pressure even for the case of the unyawed cylinder. This will influence the drag for the cylinder and one would expect a similar influence for the cable, particularly in the yawed case.

# 5. CONCLUSIONS AND RECOMMENDATIONS

The results of an experimental investigation of the flow about stranded cables or wire ropes have been presented. The goal of the study was to improve the understanding of the flow field near the stranded cable and to develop additional insight into the mechanisms associated with the generation of fluid forces on the cables.

Pressure measurements have shown that a steady lift force can be developed on certain stranded cables yawed to the flow even in the subcritical regime. For the class of cable considered in this study, the steady lift force was directed towards the "smooth" side and appears to be the result of asymmetric separation between opposite sides. The surface pressure distributions measured for the stranded cables indicate a strong correlation between the local surface pressure and the detailed surface geometry. In all cases considered, there was a higher suction pressure on the smooth side. There were some differences between the pressure coefficient values at the 30,000 and 46,000 Reynolds number but more significant differences with the 10,000 Reynolds number cases. When comparing the 60° and 40° cable angle case for the 7x7 cable, the suction pressures seem to be relatively lower for the 40° case, which implies a smaller steady lift force at the 40° cable angle.

Steady pressure measurements on each of the cable models showed very significant effects of the cable stranding. The helical stranding of the cable created spanwise differences in pressure profiles corresponding to spanwise differences of the cross-section. Three dimensional effects were very prominent. Also, there was no circumferential symmetry in the pressure profiles even when the cross section was symmetric. This asymmetry indicates a local lift or side force for a particular cross-section even in the unyawed case. This implies considerable variation in the location of boundary layer separation.

The asymmetry in the pressure distribution appears to be the result of the strands on the smooth side of the yawed cable presenting less abrupt surface geometry variations to the flow. The adverse pressure gradient for the flow over the strand is altered and influences the separation point. The opposite side or "rough" side presents basically a different geometry to the oncoming flow again altering the pressure distribution and influencing separation. For the 7x7, or 4x7 serrated cables, the wires in the strands could promote transition as well as the strand themselves directly promoting separation. It is reasonable to assume that a

combined effect of the small scale wire irregularities and the large scale strand irregularities is possible in the critical regime. The orientation of the wires in the strand, i.e., whether the cable is regular or lang lay and the wire lay angle may then have significance. It should however be noted that the strands create the larger scale surface irregularity and probably the greater influence. It would be more likely that separation induced by the adverse pressure gradient over the strand would be the more dominant factor in lift development, even in the critical regime.

Flow visualization photographs which illustrated the complex cellular flow patterns on opposite sides of the yawed cable, supported these observations. Visualization results also show that stranded cables have significantly different shedding characteristics and wake structure when compared to the plain cylinder. Cable models which presented highly irregular geometries to the flow showed more diffused and less coherent wake structures. Both the smoke wire and oil surface flow visualization show the distinct differences in the flow associated with the stranded cables when compared with the circular cylinder. The "smooth" side of the cable models have a surface geometry that appears to result in the formation of streamwise vorticity that convects down the "valleys" for certain yaw angles. This results in cellular patterns associated with the detailed cable surface geometry. These, however, eventually dissipate as they get entrained in the larger scale wake vortex formation. Whether this streamwise vorticity is associated with the mechanism for lift development is a topic for further study.

Both the smoke wire and surface oil flow visualization seem to show that depending on location, flow may separate and reattach from strand to strand. The photographs indicate that the separated flow region on the rough side is larger when compared to the smooth side. Obviously, the difference in flow is due to the difference in orientation of the strands with respect to the flow. This difference in flow around opposite sides of the yawed cables highlights the asymmetry associated with lift development.

A limited number of tests were conducted to evaluate the influence of the end conditions on the flow field for the yawed and unyawed cables. These flow visualization tests did indicate that the use of endplates did alter the wake development for the cylinder and cable models. The orientation of the "upstream" endplate appeared to have the greatest influence on the flow field. For a number of the yawed cases, there appeared to be a very definite streamwise structure in the wake which was not apparent for other conditions. The influence of the endplates on the quantitative measurements of the lift and drag was not determined.

The existence of a steady lift force on the yawed cable, although quite interesting, may be undesirable for some applications. For example, the galloping of transmission lines have been partly attributed to the steady lift force, Richards[1965]. To minimize the steady lift, methods of lessening the stranding effect have actually been implemented, e.g., the wrapping of tape on the cable. Cable applications like towing cables however may be amenable to similar modifications. Replacement of cables with circular cross-sections is an option but may prove to be costly. Precise placement of towed bodies will therefore require accurate prediction of the fluid dynamic forces.

The development of prediction methods must come from an improved understanding of the basic flow physics involved in cable fluid dynamics. This requires the separation of the effects of strand size, wire size, strand helix angle, wire helix angle, the lay of the wires in the strand and the number of wires. Not only improved understanding of flow around cables may be achieved but also better understanding of basic flow physics of bluff bodies in general may be gained.

## 6. REFERENCES


Batill, S.M., Mueller, T.J., 1981, "Visualization of Transition in the Flow over an Airfoil Using the Smoke-Wire Technique", AIAA Journal, Vol.19, No.3.

Batill, and Nebres, 1991, "Application of Digital Filtering Techniques to Unsteady Pressure Measurements," AIAA Paper-91-0061, 29th Aerospace Sciences Meeting, Reno, Nevada, January.

Batill, S. M., Nelson, R. C., and Nebres, J. V., 1988: "An Experimental Investigation of the Flow Field Around Yawed, Stranded Cables", Naval Coastal Systems Center Contractor Report 2201-89-1, Contract No. N00014-83K-0239.

Counihan, J., 1963, "Lift and drag measurements on stranded cables", Imperial College of Science and Technology, Aeronautics Department, Report No. 117, London.

David Taylor Model Basin, Author Unknown, 1949, "Wind-tunnel tests of mine sweeper cables", David W. Taylor Model Basin Report R-312, Aero Report 705.

Gerrard, J. H., 1966, "The Mechanics of the Formation Region of Vortices Behind Bluff Bodies," Journal of Fluid Mechanics, Vol. 25, p. 401-413.

Horton, K., Ferrer, C., Watson, K. and Charvoz, D., 1987: "Measurement of the hydrodynamic force and strum characteristics of stranded cables", Naval Coastal Systems Center Technical Memorandum 471-87.

Keefe, R.T. , 1961, "An Investigation of the Fluctuating Forces Acting on a Stationary Circular Cylinder in a Subsonic Stream and of the Associated Sound Field", UTIAS Report 76.

King, R., 1977, " A Review of Vortex Shedding Research and Its Applications", Ocean Engineering, Vol. 4, Pergamon Press, Great Britain, pp. 141-171.

Ramberg, S., 1978: "The influence of yaw angle upon the vortex wakes of stationary and vibrating cylinders", Naval Research Laboratory Memo. Report No. 3822; see also J. Fluid Mech., 1983, Vol. 128, pp. 81-107.

Richards, D., 1963: " Aerodynamic properties of the Severn Crossing conductor" Proceedings of the National Physical Laboratory Symposium No. 16, Teddington 1963, Wind Effects on Buildings and Structures, C. Scruton (Ed.), London: Her Majesty's Stationary Office, 1965, pp. 688-771.

Schultz, M. P., 1962: "Wind-tunnel determination of the aerodynamic characteristics of several twisted wire ropes", David W. Taylor Model Basin Aerodynamics Laboratory, Report 1645, Aero Report 1028.

Sewell P. and Taylor, P. N., 1961, "The aerodynamic effects of wind on stranded cables", University of Bristol, Department of Aeronautical Engineering, B. Sc. thesis. Also Report no. 58, Original paper not available, see Richards[1963] and Simpson[1979].

Smith, R., Moon, W. and Kao, T., 1972: "Experiments on flow about a yawed circular cylinder", Trans. ASME, Journal of Basic Engineering, December, pp. 771-776.

Stansby, P.K., 1974, "The Effects of Endplates on the Base Pressure Coefficient of a Circular Cylinder", Aeronautical Journal, January.

Toebes G.H., 1969," The Unsteady Flow and Wake Near an Oscillating Cylinder," Journal of Basic Engineering, Vol. 91, p. 493.

Visser, K. D., Nelson, R. C. and Ng, T. T., 1988, "Method of Cold Smoke Generation for Vortex Core Tagging", AIAA Journal of Aircraft, Vol. 25, No. 11, pp.1069-1071.

Votaw, C. W., and Griffin, O. M., 1971, "Vortex Shedding From Smooth Cylinders and Stranded Cables," Trans. ASME, J. Basic Engineering, Vol. 93, pp. 457-460.

Weaver, H. J., 1983, Application of Discrete and Continuous Fourier Analysis, John Wiley & Sons Publ., New York, NY, pp. 360-362.

Table 1

Summary of Models

| Model | Lay | Actual Dia.(in.) | Material | Tests Performed | | | | |
|---|---|---|---|---|---|---|---|---|
| | | | | Mean Pressure | Detailed Flow Vis. | Flow Vis. w/ End Plates | Unsteady Pressure | Surface Oil Flow Vis. |
| Cylinder | - | 1.875 | steel pipe | √ | | | | |
| 7x1 Cable | left | 1.87 | neoprene | √ | | | | √ |
| 4x1 Cable | right | 1.81 | neoprene | √ | | | | |
| 7x7 Cable | left | 1.69 | neoprene | √ | | | | |
| 4x7 Serrated Cable | right | 1.68 | neoprene | √ | | | | |
| Cylinder | - | 0.625 | steel rod | √ | √ | √ | √ | |
| 7x7 Cable | left | 0.625 | epoxy | √ | √ | √ | √ | |
| 4x7 Serrated Cable | right | 0.625 | epoxy | √ | √ | √ | √ | |

Table 2

Pressure Coefficients for the Circular Cylinder

| θ,° | β=90° | | | β=60° | | | β=40° | | | β=20° | | |
|---|---|---|---|---|---|---|---|---|---|---|---|---|
| | Re= 10k | Re= 30k | Re= 46k | Re= 10k | Re= 30k | Re= 46k | Re= 10k | Re= 30k | Re= 46k | Re= 10k | Re= 30k | Re= 46k |
| 0 | 0.98 | 0.98 | 0.97 | 0.73 | 0.72 | 0.73 | 0.42 | 0.38 | 0.38 | 0.10 | 0.09 | 0.09 |
| 10 | 0.93 | 0.82 | 0.85 | 0.67 | 0.62 | 0.62 | 0.39 | 0.32 | 0.32 | 0.09 | 0.07 | 0.07 |
| 20 | 0.70 | 0.47 | 0.55 | 0.48 | 0.38 | 0.37 | 0.29 | 0.18 | 0.18 | 0.06 | 0.03 | 0.03 |
| 30 | 0.34 | 0.01 | 0.09 | 0.19 | 0.02 | 0.02 | 0.14 | -0.01 | 0.00 | 0.01 | -0.02 | -0.03 |
| 40 | -0.11 | -0.51 | -0.43 | -0.17 | -0.35 | -0.34 | -0.06 | -0.22 | -0.23 | -0.05 | -0.08 | -0.09 |
| 50 | -0.58 | -1.00 | -0.91 | -0.50 | -0.72 | -0.66 | -0.25 | -0.45 | -0.44 | -0.11 | -0.14 | -0.15 |
| 60 | -0.96 | -1.31 | -1.27 | -0.77 | -0.99 | -1.02 | -0.41 | -0.59 | -0.59 | -0.16 | -0.18 | -0.19 |
| 70 | -1.19 | -1.33 | -1.33 | -0.93 | -1.05 | -1.16 | -0.49 | -0.64 | -0.64 | -0.19 | -0.20 | -0.20 |
| 80 | -1.10 | -1.14 | -1.12 | -0.83 | -0.91 | -0.98 | -0.48 | -0.57 | -0.57 | -0.20 | -0.18 | -0.17 |
| 90 | -0.97 | -1.11 | -1.07 | -0.75 | -0.88 | -0.98 | -0.43 | -0.54 | -0.53 | -0.18 | -0.1[illegible] | -0.17 |
| 100 | -0.93 | -1.12 | -1.08 | -0.75 | -0.89 | -0.92 | -0.40 | -0.54 | -0.55 | -0.18 | -0.17 | -0.18 |
| 110 | -0.95 | -1.14 | -1.09 | -0.74 | -0.89 | -0.86 | -0.40 | -0.54 | -0.53 | -0.16 | -0.17 | -0.19 |
| 120 | -0.95 | -1.15 | -1.09 | -0.75 | -0.88 | -0.86 | -0.40 | -0.55 | -0.53 | -0.17 | -0.17 | -0.18 |
| 130 | -0.95 | -1.16 | -1.08 | -0.75 | -0.91 | -0.90 | -0.41 | -0.54 | -0.56 | -0.17 | -0.19 | -0.18 |
| 140 | -1.00 | -1.17 | -1.08 | -0.75 | -0.91 | -0.91 | -0.41 | -0.56 | -0.56 | -0.17 | -0.17 | -0.18 |
| 150 | -0.94 | -1.19 | -1.08 | -0.76 | -0.91 | -0.87 | -0.41 | -0.57 | -0.58 | -0.18 | -0.18 | -0.17 |
| 160 | -0.93 | -1.20 | -1.09 | -0.76 | -0.90 | -0.77 | -0.41 | -0.57 | -0.60 | -0.18 | -0.18 | -0.18 |
| 170 | -1.00 | -1.20 | -1.10 | -0.76 | -0.91 | -0.77 | -0.42 | -0.58 | -0.61 | -0.18 | -0.18 | -0.18 |
| 180 | -0.93 | -1.19 | -1.09 | -0.76 | -0.93 | -0.97 | -0.41 | -0.59 | -0.62 | -0.18 | -0.19 | -0.18 |
| 190 | -1.00 | -1.19 | -1.09 | -0.76 | -0.95 | -0.99 | -0.42 | -0.59 | -0.62 | -0.17 | -0.19 | -0.18 |
| 200 | -0.96 | -1.20 | -1.08 | -0.75 | -0.94 | -0.98 | -0.41 | -0.56 | -0.59 | -0.16 | -0.20 | -0.19 |
| 210 | -0.95 | -1.18 | -1.09 | -0.76 | -0.93 | -0.89 | -0.41 | -0.56 | -0.59 | -0.15 | -0.20 | -0.19 |
| 220 | -0.97 | -1.17 | -1.10 | -0.74 | -0.92 | -0.92 | -0.41 | -0.54 | -0.57 | -0.16 | -0.19 | -0.18 |
| 230 | -0.94 | -1.17 | -1.10 | -0.75 | -0.92 | -0.91 | -0.41 | -0.54 | -0.56 | -0.16 | -0.20 | -0.18 |
| 240 | -0.95 | -1.15 | -1.10 | -0.73 | -0.92 | -0.91 | -0.39 | -0.52 | -0.54 | -0.15 | -0.20 | -0.18 |
| 250 | -0.95 | -1.13 | -1.09 | -0.73 | -0.89 | -0.89 | -0.40 | -0.51 | -0.55 | -0.15 | -0.18 | -0.18 |
| 260 | -0.98 | -1.10 | -1.06 | -0.73 | -0.87 | -0.87 | -0.40 | -0.51 | -0.56 | -0.16 | -0.18 | -0.18 |
| 270 | -1.00 | -1.13 | -1.06 | -0.76 | -0.88 | -0.86 | -0.43 | -0.51 | -0.56 | -0.17 | -0.20 | -0.18 |
| 280 | -1.06 | -1.26 | -1.09 | -0.86 | -0.96 | -0.93 | -0.48 | -0.59 | -0.61 | -0.18 | -0.21 | -0.19 |
| 290 | -1.23 | -1.37 | -1.27 | -0.94 | -1.07 | -1.07 | -0.52 | -0.63 | -0.66 | -0.18 | -0.22 | -0.21 |
| 300 | -1.04 | -1.14 | -1.13 | -0.77 | -0.93 | -0.92 | -0.44 | -0.54 | -0.56 | -0.15 | -0.19 | -0.18 |
| 310 | -0.64 | -0.69 | -0.74 | -0.48 | -0.62 | -0.60 | -0.29 | -0.37 | -0.38 | -0.11 | -0.14 | -0.13 |
| 320 | -0.20 | -0.17 | -0.25 | -0.12 | -0.22 | -0.21 | -0.10 | -0.14 | -0.16 | -0.05 | -0.08 | -0.07 |
| 330 | 0.28 | 0.34 | 0.26 | 0.23 | 0.17 | 0.18 | 0.10 | 0.07 | 0.07 | 0.01 | -0.01 | 0.00 |
| 340 | 0.68 | 0.73 | 0.67 | 0.50 | 0.49 | 0.49 | 0.26 | 0.25 | 0.24 | 0.06 | 0.04 | 0.05 |
| 350 | 0.92 | 0.95 | 0.92 | 0.67 | 0.68 | 0.69 | 0.37 | 0.35 | 0.35 | 0.09 | 0.07 | 0.08 |
| $C_l$ | -0.02 | 0.06 | 0.05 | 0.01 | 0.02 | 0.04 | -0.01 | 0.03 | 0.00 | 0.01 | -0.01 | 0.00 |
| $C_d$ | 1.08 | 1.17 | 1.10 | 0.82 | 0.89 | 0.87 | 0.45 | 0.51 | 0.53 | 0.15 | 0.15 | 0.15 |

Table 3
Pressure Coefficients for 4x1 Right Lay Cable at 0% ppd

| θ,° | β=90° | | β=60° | | β=40° | | β=20° | |
|---|---|---|---|---|---|---|---|---|
| | Re=30k | Re=46k | Re=30k | Re=46k | Re=30k | Re=46k | Re=30k | Re=46k |
| 0 | 0.99 | 0.96 | 0.73 | 0.73 | 0.37 | 0.36 | 0.04 | 0.04 |
| 27 | 0.32 | 0.38 | 0.03 | -0.03 | -0.09 | -0.08 | -0.07 | -0.05 |
| 45 | 0.60 | 0.63 | 0.02 | 0.02 | -0.21 | -0.19 | -0.19 | -0.19 |
| 63 | 0.30 | 0.32 | -0.54 | -0.57 | -0.54 | -0.51 | -0.29 | -0.28 |
| 90 | -0.73 | -0.68 | -1.62 | -1.52 | -0.96 | -0.92 | -0.29 | -0.32 |
| 117 | -0.78 | -0.79 | -1.45 | -1.98 | -1.04 | -0.99 | -0.19 | -0.18 |
| 135 | -0.76 | -0.73 | -0.85 | -1.07 | -0.24 | -0.26 | -0.10 | -0.19 |
| 153 | -0.79 | -0.73 | -0.94 | -1.14 | -0.38 | -0.39 | -0.18 | -0.20 |
| 180 | -0.79 | -0.78 | -0.56 | -0.55 | -0.36 | -0.34 | -0.19 | -0.20 |
| 207 | -0.79 | -0.78 | -0.59 | -0.48 | -0.27 | -0.30 | -0.07 | -0.07 |
| 225 | -0.78 | -0.71 | -0.61 | -0.62 | -0.36 | -0.34 | -0.13 | -0.12 |
| 243 | -0.82 | -0.76 | -0.97 | -0.84 | -0.45 | -0.41 | -0.12 | -0.11 |
| 270 | -0.76 | -0.75 | -1.42 | -1.57 | -0.77 | -0.85 | -0.26 | -0.28 |
| 297 | -0.47 | -0.51 | 0.09 | 0.06 | 0.29 | 0.27 | 0.08 | 0.08 |
| 315 | 0.43 | 0.35 | 0.43 | 0.45 | 0.38 | 0.43 | 0.03 | 0.05 |
| 333 | 0.24 | 0.13 | 0.32 | 0.32 | 0.28 | 0.25 | 0.02 | 0.03 |
| $C_l$ | -0.11 | -0.16 | 0.31 | 0.40 | 0.29 | 0.25 | 0.10 | 0.11 |
| $C_d$ | 1.03 | 0.99 | 0.98 | 1.06 | 0.55 | 0.53 | 0.10 | 0.10 |

Table 4
Pressure Coefficients for 4x1 Right Lay Cable at 25% ppd

| θ,° | β=90° | | β=60° | | β=40° | | β=20° | |
|---|---|---|---|---|---|---|---|---|
| | Re=30k | Re=46k | Re=30k | Re=46k | Re=30k | Re=46k | Re=30k | Re=46k |
| 23 | 0.58 | 0.67 | 0.30 | 0.28 | 0.19 | 0.18 | 0.03 | 0.03 |
| 50 | -0.52 | -0.48 | -0.62 | -0.69 | -0.56 | -0.57 | -0.23 | -0.22 |
| 68 | -0.02 | 0.04 | -0.51 | -0.51 | -0.45 | -0.43 | -0.26 | -0.28 |
| 86 | 0.11 | 0.13 | -0.75 | -0.79 | -0.75 | -0.74 | -0.32 | -0.35 |
| 113 | -0.69 | -0.70 | -0.60 | -0.68 | -0.67 | -0.69 | -0.22 | -0.21 |
| 140 | -0.82 | -0.80 | -1.04 | -1.04 | -0.53 | -0.51 | -0.05 | -0.07 |
| 158 | -0.72 | -0.75 | -0.65 | -0.62 | -0.21 | -0.17 | -0.07 | -0.05 |
| 176 | -0.76 | -0.78 | -0.77 | -0.75 | -0.31 | -0.29 | -0.13 | -0.13 |
| 203 | -0.82 | -0.83 | -0.71 | -0.76 | -0.36 | -0.35 | -0.14 | -0.15 |
| 230 | -0.77 | -0.82 | -1.02 | -1.06 | -0.39 | -0.35 | -0.07 | -0.06 |
| 248 | -0.79 | -0.87 | -0.75 | -0.81 | -0.48 | -0.52 | -0.13 | -0.13 |
| 266 | -0.86 | -0.85 | -0.75 | -0.81 | -0.55 | -0.58 | -0.16 | -0.16 |
| 293 | -0.78 | -0.70 | -0.88 | -0.90 | -0.55 | -0.60 | -0.27 | -0.30 |
| 320 | 0.15 | 0.09 | 0.46 | 0.43 | 0.43 | 0.43 | 0.31 | 0.27 |
| 338 | 0.88 | 0.84 | 0.76 | 0.76 | 0.41 | 0.41 | 0.15 | 0.14 |
| 356 | 0.82 | 0.74 | 0.69 | 0.69 | 0.39 | 0.40 | 0.09 | 0.09 |
| $C_l$ | -0.10 | -0.14 | 0.02 | 0.02 | 0.18 | 0.17 | 0.09 | 0.08 |
| $C_d$ | 1.05 | 1.06 | 0.87 | 0.87 | 0.47 | 0.46 | 0.14 | 0.12 |

Table 5
Pressure Coefficients for 4x1 Right Lay Cable at 50% ppd

| θ,° | β=90° | | β=60° | | β=40° | | β=20° | |
|---|---|---|---|---|---|---|---|---|
| | Re=30k | Re=46k | Re=30k | Re=46k | Re=30k | Re=46k | Re=30k | Re=46k |
| 0 | 1.00 | 0.97 | 0.73 | 0.72 | 0.43 | 0.41 | 0.12 | 0.11 |
| 18 | 1.00 | 0.99 | 0.65 | 0.64 | 0.33 | 0.33 | 0.04 | 0.05 |
| 45 | -0.78 | -0.70 | -0.88 | -0.88 | -0.42 | -0.41 | -0.14 | -0.12 |
| 72 | -0.78 | -1.16 | -1.07 | -1.16 | -0.73 | -0.72 | -0.30 | -0.31 |
| 90 | -1.24 | -0.95 | -1.05 | -1.03 | -0.61 | -0.58 | -0.25 | -0.27 |
| 108 | -0.15 | -0.12 | -0.59 | -0.61 | -0.52 | -0.50 | -0.24 | -0.26 |
| 135 | -0.78 | -0.82 | -0.46 | -0.54 | -0.44 | -0.44 | -0.24 | -0.21 |
| 162 | -0.87 | -0.83 | -0.55 | -0.54 | -0.29 | -0.27 | -0.05 | -0.04 |
| 180 | -0.74 | -0.80 | -0.63 | -0.62 | -0.29 | -0.26 | -0.10 | -0.09 |
| 198 | -0.74 | -0.82 | -0.79 | -0.78 | -0.32 | -0.29 | -0.12 | -0.12 |
| 225 | -0.74 | -0.84 | -0.54 | -0.53 | -0.49 | -0.49 | -0.13 | -0.13 |
| 252 | -0.90 | -0.95 | -1.02 | -0.84 | -0.49 | -0.48 | -0.07 | -0.05 |
| 270 | -1.14 | -0.80 | -0.63 | -0.63 | -0.42 | -0.41 | -0.09 | -0.09 |
| 288 | -1.31 | -0.91 | -0.67 | -0.69 | -0.42 | -0.43 | -0.11 | -0.12 |
| 315 | -0.89 | -0.94 | -1.00 | -0.99 | -0.41 | -0.40 | -0.17 | -0.20 |
| 342 | 0.87 | 0.80 | 0.76 | 0.76 | 0.52 | 0.51 | 0.24 | 0.24 |
| $C_l$ | -0.28 | -0.14 | 0.00 | 0.07 | 0.06 | 0.06 | 0.09 | 0.09 |
| $C_d$ | 0.93 | 0.95 | 0.55 | 0.58 | 0.39 | 0.38 | 0.13 | 0.12 |

Table 6
Pressure Coefficients for 4x1 Right Lay Cable at 75% ppd

| θ,° | β=90° | | β=60° | | β=40° | | β=20° | |
|---|---|---|---|---|---|---|---|---|
| | Re=30k | Re=46k | Re=30k | Re=46k | Re=30k | Re=46k | Re=30k | Re=46k |
| 5 | 0.95 | 0.95 | 0.64 | 0.62 | 0.36 | 0.36 | 0.11 | 0.13 |
| 23 | 0.91 | 0.91 | 0.42 | 0.42 | 0.15 | 0.14 | -0.04 | -0.03 |
| 41 | 0.74 | 0.76 | 0.13 | 0.13 | -0.08 | -0.06 | -0.13 | -0.11 |
| 68 | -0.79 | -0.84 | -1.98 | -1.93 | -1.03 | -0.99 | -0.32 | -0.31 |
| 95 | -0.75 | -0.97 | -1.45 | -1.59 | -0.87 | -0.87 | -0.29 | -0.32 |
| 113 | -0.68 | -0.77 | -1.14 | -1.22 | -0.64 | -0.57 | -0.31 | -0.22 |
| 131 | -0.75 | -0.82 | -1.01 | -0.98 | -0.54 | -0.47 | -0.26 | -0.20 |
| 158 | -0.80 | -0.81 | -0.44 | -0.43 | -0.34 | -0.34 | -0.27 | -0.25 |
| 185 | -0.80 | -0.80 | -0.45 | -0.41 | -0.30 | -0.27 | -0.07 | -0.06 |
| 203 | -0.72 | -0.75 | -0.70 | -0.67 | -0.34 | -0.31 | -0.12 | -0.10 |
| 221 | -0.74 | -0.76 | -1.04 | -0.89 | -0.38 | -0.36 | -0.11 | -0.10 |
| 248 | -0.73 | -0.75 | -0.97 | -1.40 | -0.41 | -0.44 | -0.18 | -0.17 |
| 275 | -0.61 | -0.62 | -0.08 | -0.12 | -0.27 | -0.28 | -0.11 | -0.07 |
| 293 | -0.50 | -0.62 | -0.25 | -0.22 | -0.23 | -0.21 | -0.07 | -0.08 |
| 311 | -0.70 | -0.79 | -0.39 | -0.42 | -0.33 | -0.31 | -0.07 | -0.08 |
| 338 | 0.22 | 0.05 | 0.09 | 0.13 | -0.02 | -0.02 | -0.05 | -0.06 |
| $C_l$ | -0.18 | -0.16 | 0.48 | 0.40 | 0.21 | 0.19 | 0.11 | 0.09 |
| $C_d$ | 0.97 | 0.98 | 0.79 | 0.81 | 0.33 | 0.33 | 0.10 | 0.10 |

Table 7

Pressure Coefficients for 7x1 Left Lay Cable at 0% ppd

| θ,° | β=90° | | β=60° | | β=40° | | β=20° | |
|---|---|---|---|---|---|---|---|---|
| | Re=30k | Re=46k | Re=30k | Re=46k | Re=30k | Re=46k | Re=30k | Re=46k |
| 0 | 1.00 | 0.99 | 0.72 | 0.73 | 0.37 | 0.37 | 0.07 | 0.07 |
| 13 | 0.73 | 0.63 | 0.43 | 0.44 | 0.35 | 0.36 | 0.06 | 0.06 |
| 24 | 0.60 | 0.49 | 0.48 | 0.45 | 0.24 | 0.24 | 0.05 | 0.06 |
| 30 | 0.70 | 0.62 | 0.54 | 0.55 | 0.34 | 0.34 | 0.11 | 0.11 |
| 36 | 0.88 | 0.85 | 0.69 | 0.70 | 0.50 | 0.54 | 0.24 | 0.22 |
| 47 | 0.27 | 0.17 | -0.10 | -0.11 | 0.03 | 0.02 | -0.02 | -0.03 |
| 60 | -0.98 | -1.05 | -1.33 | -1.05 | -0.57 | -0.61 | -0.20 | -0.21 |
| 73 | -0.95 | -0.95 | -0.70 | -0.72 | -0.46 | -0.49 | -0.16 | -0.16 |
| 84 | -1.05 | -0.97 | -1.00 | -1.02 | -0.51 | -0.53 | -0.12 | -0.12 |
| 90 | -1.05 | -1.00 | -0.93 | -0.93 | -0.52 | -0.48 | -0.20 | -0.19 |
| 96 | -1.06 | -1.02 | -0.94 | -0.95 | -0.65 | -0.62 | -0.19 | -0.18 |
| 107 | -1.05 | -0.96 | -0.78 | -0.88 | -0.55 | -0.44 | -0.12 | -0.11 |
| 120 | -1.06 | -1.02 | -0.73 | -0.77 | -0.50 | -0.43 | -0.14 | -0.14 |
| 133 | -0.97 | -0.95 | -0.75 | -0.77 | -0.35 | -0.32 | -0.12 | -0.11 |
| 144 | -0.91 | -0.88 | -0.72 | -0.71 | -0.41 | -0.40 | -0.12 | -0.10 |
| 150 | -0.96 | -0.90 | -0.68 | -0.64 | -0.40 | -0.38 | -0.15 | -0.14 |
| 156 | -0.97 | -0.90 | -0.63 | -0.60 | -0.40 | -0.40 | -0.09 | -0.07 |
| 167 | -0.96 | -0.92 | -0.71 | -0.67 | -0.32 | -0.32 | -0.13 | -0.13 |
| 180 | -0.89 | -0.85 | -0.85 | -0.92 | -0.39 | -0.39 | -0.18 | -0.19 |
| 193 | -0.93 | -0.92 | -1.43 | -1.45 | -0.43 | -0.40 | -0.17 | -0.18 |
| 204 | -0.95 | -0.93 | -1.18 | -0.93 | -0.42 | -0.41 | -0.19 | -0.17 |
| 210 | -0.94 | -0.91 | -1.33 | -1.34 | -0.38 | -0.37 | -0.16 | -0.15 |
| 216 | -0.93 | -0.94 | -1.21 | -1.20 | -0.37 | -0.37 | -0.10 | -0.07 |
| 227 | -0.95 | -0.90 | -0.60 | -0.66 | -0.58 | -0.57 | -0.19 | -0.20 |
| 240 | -1.01 | -1.00 | -1.03 | -1.13 | -0.56 | -0.54 | -0.29 | -0.31 |
| 253 | -0.95 | -0.91 | -0.86 | -0.94 | -0.50 | -0.53 | -0.27 | -0.29 |
| 264 | -1.04 | -1.19 | -1.45 | -1.67 | -0.44 | -0.42 | -0.22 | -0.23 |
| 270 | -1.07 | -1.17 | -1.76 | -1.72 | -0.88 | -0.86 | -0.35 | -0.36 |
| 276 | -1.06 | -1.24 | -1.44 | -2.01 | -0.97 | -0.99 | -0.34 | -0.35 |
| 287 | -0.98 | -0.99 | -1.25 | -1.41 | -0.99 | -1.02 | -0.31 | -0.33 |
| 300 | -1.02 | -1.06 | -1.53 | -1.67 | -1.02 | -1.04 | -0.35 | -0.36 |
| 313 | -0.56 | -0.49 | -0.32 | -0.30 | -0.55 | -0.55 | -0.24 | -0.24 |
| 324 | 0.81 | 0.80 | 0.35 | 0.41 | -0.01 | 0.00 | -0.10 | -0.08 |
| 330 | 0.75 | 0.80 | 0.38 | 0.39 | 0.10 | 0.13 | -0.13 | -0.12 |
| 336 | 0.73 | 0.78 | 0.39 | 0.39 | 0.08 | 0.09 | -0.06 | -0.03 |
| 347 | 0.59 | 0.67 | 0.54 | 0.49 | 0.30 | 0.31 | 0.04 | 0.05 |
| $C_l$ | 0.00 | 0.00 | -0.29 | -0.38 | -0.16 | -0.17 | -0.11 | -0.12 |
| $C_d$ | 1.18 | 1.14 | 0.92 | 1.01 | 0.47 | 0.47 | 0.12 | 0.12 |

Table 8

Pressure Coefficients for 7x1 Left Lay Cable at 25% ppd

| θ,° | β=90° | | β=60° | | β=40° | | β=20° | |
|---|---|---|---|---|---|---|---|---|
| | Re=30k | Re=46k | Re=30k | Re=46k | Re=30k | Re=46k | Re=30k | Re=46k |
| 2 | 0.97 | 0.98 | 0.72 | 0.73 | 0.42 | 0.42 | 0.09 | 0.09 |
| 15 | 0.91 | 0.84 | 0.40 | 0.45 | 0.29 | 0.29 | 0.02 | 0.03 |
| 28 | 0.08 | -0.04 | 0.03 | 0.01 | 0.14 | 0.15 | 0.00 | 0.01 |
| 39 | 0.04 | -0.03 | 0.02 | -0.05 | -0.01 | -0.01 | 0.02 | 0.02 |
| 45 | 0.17 | 0.03 | 0.08 | 0.10 | 0.07 | 0.08 | 0.01 | 0.02 |
| 51 | 0.51 | 0.35 | 0.22 | 0.24 | 0.22 | 0.26 | 0.07 | 0.08 |
| 62 | -0.02 | -0.06 | -0.48 | -0.42 | -0.13 | -0.14 | -0.08 | -0.09 |
| 75 | -1.13 | -0.98 | -1.41 | -1.56 | -0.79 | -0.85 | -0.22 | -0.23 |
| 88 | -0.92 | -0.89 | -0.83 | -0.87 | -0.58 | -0.63 | -0.18 | -0.18 |
| 99 | -0.94 | -0.92 | -1.17 | -1.23 | -0.67 | -0.68 | -0.13 | -0.12 |
| 105 | -0.94 | -0.92 | -0.87 | -1.16 | -0.36 | -0.34 | -0.21 | -0.20 |
| 111 | -0.95 | -0.94 | -0.85 | -1.34 | -0.33 | -0.32 | -0.18 | -0.15 |
| 122 | -0.93 | -0.91 | -0.53 | -0.45 | -0.36 | -0.36 | -0.13 | -0.11 |
| 135 | -0.95 | -0.94 | -0.72 | -0.81 | -0.38 | -0.36 | -0.15 | -0.15 |
| 148 | -0.93 | -0.90 | -0.60 | -0.62 | -0.34 | -0.34 | -0.13 | -0.13 |
| 159 | -0.89 | -0.87 | -0.74 | -0.73 | -0.34 | -0.34 | -0.12 | -0.10 |
| 165 | -0.91 | -0.90 | -0.58 | -0.57 | -0.35 | -0.35 | -0.14 | -0.12 |
| 171 | -0.92 | -0.91 | -0.56 | -0.54 | -0.34 | -0.35 | -0.09 | -0.07 |
| 182 | -0.93 | -0.89 | -0.60 | -0.57 | -0.33 | -0.33 | -0.15 | -0.16 |
| 195 | -0.91 | -0.90 | -0.91 | -0.92 | -0.39 | -0.38 | -0.21 | -0.21 |
| 208 | -0.97 | -0.95 | -1.46 | -1.08 | -0.42 | -0.40 | -0.21 | -0.20 |
| 219 | -0.94 | -0.92 | -0.81 | -0.83 | -0.41 | -0.40 | -0.19 | -0.16 |
| 225 | -0.96 | -0.95 | -0.62 | -1.65 | -0.47 | -0.45 | -0.16 | -0.14 |
| 231 | -0.99 | -0.96 | -0.62 | -1.41 | -0.60 | -0.62 | -0.10 | -0.09 |
| 242 | -1.07 | -1.08 | -0.75 | -0.76 | -0.80 | -0.82 | -0.28 | -0.26 |
| 255 | -0.94 | -0.91 | -1.63 | -1.63 | -0.75 | -0.78 | -0.32 | -0.34 |
| 268 | -1.07 | -1.15 | -0.76 | -0.75 | -0.74 | -0.76 | -0.31 | -0.34 |
| 279 | -0.60 | -0.02 | -1.25 | -1.18 | -0.53 | -0.53 | -0.26 | -0.26 |
| 285 | -1.26 | -1.11 | -1.03 | -1.17 | -0.65 | -0.62 | -0.37 | -0.37 |
| 291 | -1.46 | -1.39 | -1.05 | -1.23 | -0.74 | -0.75 | -0.33 | -0.34 |
| 302 | -0.99 | -1.08 | -0.97 | -1.37 | -0.77 | -0.78 | -0.26 | -0.26 |
| 315 | -1.16 | -1.06 | -0.83 | -0.82 | -0.66 | -0.67 | -0.24 | -0.23 |
| 328 | 0.22 | 0.29 | 0.22 | 0.26 | -0.14 | -0.15 | -0.12 | -0.10 |
| 339 | 0.95 | 0.94 | 0.62 | 0.62 | 0.23 | 0.23 | -0.04 | -0.03 |
| 345 | 0.98 | 0.97 | 0.64 | 0.62 | 0.32 | 0.32 | -0.03 | -0.01 |
| 351 | 0.97 | 0.96 | 0.65 | 0.64 | 0.30 | 0.30 | 0.05 | 0.08 |
| $C_l$ | -0.19 | -0.17 | -0.29 | -0.21 | -0.19 | -0.19 | -0.11 | -0.11 |
| $C_d$ | 1.26 | 1.30 | 0.81 | 0.92 | 0.51 | 0.52 | 0.10 | 0.11 |

Table 9

Pressure Coefficients for 7x1 Left Lay Cable at 50% ppd

| θ,° | β=90° | | β=60° | | β=40° | | β=20° | |
|---|---|---|---|---|---|---|---|---|
| | Re=30k | Re=46k | Re=30k | Re=46k | Re=30k | Re=46k | Re=30k | Re=46k |
| 0 | 1.03 | 1.00 | 0.76 | 0.76 | 0.44 | 0.44 | 0.05 | 0.07 |
| 6 | 1.02 | 0.99 | 0.79 | 0.80 | 0.44 | 0.44 | 0.14 | 0.17 |
| 17 | 0.99 | 0.93 | 0.59 | 0.60 | 0.36 | 0.36 | 0.08 | 0.08 |
| 30 | 0.38 | 0.23 | -0.27 | -0.21 | -0.01 | -0.01 | -0.05 | -0.05 |
| 43 | -0.68 | -0.74 | -0.51 | -0.54 | -0.16 | -0.18 | -0.05 | -0.05 |
| 54 | -0.77 | -0.95 | -0.57 | -0.61 | -0.33 | -0.33 | -0.03 | -0.03 |
| 60 | -0.29 | -0.49 | -0.49 | -0.46 | -0.30 | -0.29 | -0.08 | -0.07 |
| 66 | -0.55 | -0.84 | -0.52 | -0.46 | -0.29 | -0.28 | -0.07 | -0.06 |
| 77 | -0.12 | -0.12 | -0.62 | -0.72 | -0.36 | -0.39 | -0.13 | -0.12 |
| 90 | -0.96 | -0.98 | -1.30 | -1.45 | -0.72 | -0.71 | -0.21 | -0.21 |
| 103 | -0.89 | -0.87 | -1.35 | -1.29 | -0.47 | -0.46 | -0.16 | -0.16 |
| 114 | -0.89 | -0.86 | -0.64 | -0.59 | -0.43 | -0.42 | -0.14 | -0.14 |
| 120 | -0.95 | -0.91 | -0.92 | -0.89 | -0.40 | -0.42 | -0.18 | -0.17 |
| 126 | -0.96 | -0.92 | -0.97 | -0.87 | -0.41 | -0.44 | -0.13 | -0.11 |
| 137 | -0.92 | -0.89 | -0.59 | -0.55 | -0.32 | -0.33 | -0.13 | -0.12 |
| 150 | -0.94 | -0.92 | -0.58 | -0.59 | -0.42 | -0.40 | -0.15 | -0.15 |
| 163 | -0.91 | -0.86 | -0.69 | -0.71 | -0.38 | -0.38 | -0.15 | -0.15 |
| 174 | -0.93 | -0.91 | -0.68 | -0.52 | -0.34 | -0.34 | -0.12 | -0.12 |
| 180 | -0.88 | -0.86 | -0.64 | -0.63 | -0.34 | -0.33 | -0.14 | -0.14 |
| 186 | -0.89 | -0.86 | -0.62 | -0.59 | -0.33 | -0.33 | -0.11 | -0.10 |
| 197 | -0.93 | -0.87 | -0.52 | -0.49 | -0.33 | -0.33 | -0.17 | -0.16 |
| 210 | -0.97 | -1.05 | -1.18 | -1.17 | -0.34 | -0.34 | -0.21 | -0.20 |
| 223 | -0.96 | -0.93 | -0.90 | -1.09 | -0.35 | -0.33 | -0.20 | -0.19 |
| 234 | -0.93 | -0.88 | -1.05 | -1.06 | -0.39 | -0.37 | -0.17 | -0.16 |
| 240 | -1.01 | -1.01 | -0.97 | -1.75 | -0.72 | -0.72 | -0.16 | -0.18 |
| 246 | -1.02 | -1.04 | -1.00 | -1.70 | -1.13 | -1.24 | -0.20 | -0.21 |
| 257 | -0.92 | -0.91 | -1.09 | -1.09 | -0.96 | -0.98 | -0.28 | -0.29 |
| 270 | -0.94 | -0.86 | -1.96 | -1.97 | -0.95 | -0.98 | -0.35 | -0.38 |
| 283 | -1.06 | -1.09 | -0.97 | -0.98 | -0.99 | -1.01 | -0.34 | -0.37 |
| 294 | 0.46 | 0.58 | -0.49 | -0.22 | -0.52 | -0.52 | -0.24 | -0.23 |
| 300 | -0.42 | -0.30 | -0.46 | -0.45 | -0.38 | -0.35 | -0.31 | -0.31 |
| 306 | -0.57 | -0.52 | -0.47 | -0.48 | -0.47 | -0.47 | -0.27 | -0.26 |
| 317 | -0.57 | -0.47 | -0.61 | -0.84 | -0.38 | -0.39 | -0.17 | -0.15 |
| 330 | -0.20 | -0.08 | -0.01 | -0.01 | -0.19 | -0.22 | -0.10 | -0.09 |
| 343 | 0.85 | 0.88 | 0.63 | 0.64 | 0.19 | 0.20 | -0.03 | -0.01 |
| 354 | 1.02 | 0.99 | 0.71 | 0.72 | 0.35 | 0.36 | 0.01 | 0.03 |
| $C_l$ | -0.09 | -0.02 | -0.15 | -0.18 | -0.16 | -0.15 | -0.09 | -0.10 |
| $C_d$ | 1.26 | 1.22 | 0.75 | 0.90 | 0.45 | 0.46 | 0.10 | 0.11 |

Table 10

Pressure Coefficients for 7x1 Left Lay Cable at 75% ppd

| θ,° | β=90° | | β=60° | | β=40° | | β=20° | |
|---|---|---|---|---|---|---|---|---|
| | Re=30k | Re=46k | Re=30k | Re=46k | Re=30k | Re=46k | Re=30k | Re=46k |
| 9 | 0.92 | 0.85 | 0.70 | 0.70 | 0.37 | 0.37 | 0.04 | 0.07 |
| 15 | 0.96 | 0.92 | 0.73 | 0.74 | 0.44 | 0.42 | 0.10 | 0.11 |
| 21 | 0.98 | 0.94 | 0.84 | 0.83 | 0.50 | 0.49 | 0.20 | 0.22 |
| 32 | 0.69 | 0.57 | 0.26 | 0.26 | 0.21 | 0.21 | 0.04 | 0.03 |
| 45 | -0.46 | -0.65 | -0.98 | -1.00 | -0.32 | -0.32 | -0.13 | -0.14 |
| 58 | -1.14 | -1.21 | -0.75 | -0.77 | -0.38 | -0.39 | -0.10 | -0.11 |
| 69 | -1.29 | -1.22 | -1.06 | -1.12 | -0.37 | -0.39 | -0.09 | -0.08 |
| 75 | -1.04 | -1.15 | -1.04 | -1.07 | -0.42 | -0.41 | -0.14 | -0.13 |
| 81 | -1.86 | -1.90 | -1.15 | -1.21 | -0.43 | -0.43 | -0.14 | -0.12 |
| 92 | 0.01 | -0.20 | -0.69 | -0.70 | -0.46 | -0.48 | -0.13 | -0.13 |
| 105 | -1.02 | -1.21 | -0.61 | -0.60 | -0.53 | -0.55 | -0.16 | -0.15 |
| 118 | -0.92 | -0.93 | -0.64 | -0.55 | -0.50 | -0.50 | -0.15 | -0.14 |
| 129 | -0.88 | -0.86 | -0.63 | -0.61 | -0.46 | -0.47 | -0.15 | -0.13 |
| 135 | -0.93 | -0.92 | -0.90 | -0.84 | -0.44 | -0.44 | -0.17 | -0.16 |
| 141 | -0.94 | -0.93 | -0.91 | -0.86 | -0.44 | -0.46 | -0.12 | -0.10 |
| 152 | -0.91 | -0.92 | -0.90 | -0.86 | -0.29 | -0.30 | -0.12 | -0.12 |
| 165 | -0.91 | -0.87 | -0.65 | -0.66 | -0.38 | -0.38 | -0.16 | -0.16 |
| 178 | -0.92 | -0.84 | -1.05 | -1.04 | -0.38 | -0.38 | -0.16 | -0.16 |
| 189 | -0.94 | -0.93 | -0.93 | -0.66 | -0.37 | -0.37 | -0.16 | -0.16 |
| 195 | -0.88 | -0.84 | -0.90 | -0.88 | -0.36 | -0.35 | -0.16 | -0.16 |
| 201 | -0.88 | -0.84 | -0.84 | -0.86 | -0.35 | -0.34 | -0.14 | -0.10 |
| 212 | -0.91 | -0.88 | -0.53 | -0.50 | -0.40 | -0.39 | -0.15 | -0.15 |
| 225 | -0.97 | -1.02 | -1.06 | -1.06 | -0.39 | -0.38 | -0.23 | -0.24 |
| 238 | -0.93 | -0.88 | -0.55 | -0.55 | -0.35 | -0.33 | -0.22 | -0.22 |
| 249 | -0.95 | -0.88 | -1.10 | -1.22 | -0.33 | -0.35 | -0.21 | -0.20 |
| 255 | -0.99 | -1.05 | -1.05 | -1.85 | -0.90 | -0.89 | -0.28 | -0.28 |
| 261 | -0.98 | -1.05 | -1.15 | -2.20 | -1.13 | -1.17 | -0.31 | -0.30 |
| 272 | -0.91 | -0.89 | -1.10 | -1.17 | -1.03 | -1.05 | -0.32 | -0.34 |
| 285 | -0.93 | -0.89 | -1.91 | -2.05 | -1.12 | -1.13 | -0.39 | -0.42 |
| 298 | -0.90 | -0.88 | -0.68 | -0.70 | -0.93 | -0.95 | -0.33 | -0.33 |
| 309 | 0.71 | 0.68 | 0.11 | 0.13 | -0.32 | -0.31 | -0.18 | -0.16 |
| 315 | 0.27 | 0.38 | 0.04 | 0.06 | -0.13 | -0.12 | -0.24 | -0.22 |
| 321 | 0.23 | 0.35 | 0.02 | 0.01 | -0.19 | -0.19 | -0.18 | -0.15 |
| 332 | 0.03 | 0.13 | 0.01 | -0.12 | 0.03 | 0.03 | -0.04 | -0.04 |
| 345 | 0.62 | 0.69 | 0.54 | 0.54 | 0.19 | 0.19 | 0.01 | 0.03 |
| 358 | 1.01 | 0.98 | 0.69 | 0.71 | 0.37 | 0.37 | 0.05 | 0.05 |
| $C_l$ | 0.03 | 0.15 | -0.10 | -0.16 | -0.16 | -0.16 | -0.10 | -0.11 |
| $C_d$ | 1.10 | 1.04 | 0.78 | 0.90 | 0.47 | 0.47 | 0.12 | 0.12 |

Table 11

Pressure Coefficients for 4x7 Right Lay Cable at Re=10,000

| θ,° | β=90° | β=60° | β=40° | β=20° | β=90° | β=60° | β=40° | β=20° |
|---|---|---|---|---|---|---|---|---|
| | 0%ppd | | | | 50%ppd | | | |
| 0 | 0.96 | 0.72 | 0.36 | 0.06 | 0.96 | 0.72 | 0.45 | 0.15 |
| 45 | 0.60 | -0.03 | -0.08 | -0.08 | -0.27 | -0.29 | -0.38 | 0.00 |
| 90 | -0.67 | -1.18 | -0.74 | -0.25 | -0.82 | -1.24 | -0.69 | -0.19 |
| 135 | -0.73 | -0.94 | -0.55 | -0.13 | -0.73 | -0.53 | -0.33 | -0.16 |
| 180 | -0.66 | -0.76 | -0.33 | -0.14 | -0.67 | -0.52 | -0.28 | -0.12 |
| 225 | -0.71 | -0.62 | -0.36 | -0.13 | -0.68 | -0.62 | -0.42 | -0.16 |
| 270 | -0.68 | -0.93 | -0.66 | -0.14 | -0.71 | -0.69 | -0.40 | -0.14 |
| 315 | 0.42 | 0.29 | 0.11 | 0.04 | -0.33 | -0.22 | -0.17 | -0.11 |
| $C_l$ | -0.05 | 0.28 | 0.14 | 0.08 | 0.04 | 0.21 | 0.15 | -0.01 |
| $C_d$ | 1.32 | 1.09 | 0.53 | 0.14 | 0.87 | 0.66 | 0.34 | 0.16 |

| θ,° | β=90° | β=60° | β=40° | β=20° | β=90° | β=60° | β=40° | β=20° |
|---|---|---|---|---|---|---|---|---|
| | 25%ppd | | | | 75%ppd | | | |
| 23 | 0.75 | 0.56 | 0.22 | 0.07 | 0.89 | 0.44 | 0.16 | 0.03 |
| 68 | -0.27 | -0.42 | -0.48 | -0.20 | -1.02 | -1.21 | -0.78 | -0.18 |
| 113 | -0.66 | -1.04 | -0.59 | -0.20 | -0.70 | -1.14 | -0.56 | -0.14 |
| 158 | -0.64 | -0.65 | -0.29 | -0.11 | -0.65 | -0.60 | -0.30 | -0.14 |
| 203 | -0.68 | -0.68 | -0.32 | -0.13 | -0.66 | -0.56 | -0.30 | -0.12 |
| 248 | -0.79 | -0.65 | -0.49 | -0.16 | -0.61 | -1.11 | -0.66 | -0.18 |
| 293 | -0.95 | -0.67 | -0.40 | -0.16 | -0.44 | -0.51 | -0.29 | -0.06 |
| 338 | 0.88 | 0.69 | 0.44 | 0.17 | 0.68 | 0.44 | 0.12 | -0.02 |
| $C_l$ | -0.28 | 0.06 | 0.09 | 0.04 | 0.21 | 0.27 | 0.13 | 0.02 |
| $C_d$ | 1.10 | 1.02 | 0.49 | 0.17 | 1.02 | 0.82 | 0.34 | 0.11 |

Table 12

Pressure Coefficients for 4x7 Right Lay Cable at 0% ppd

| θ,° | β=90° | | β=60° | | β=40° | | β=20° | |
|---|---|---|---|---|---|---|---|---|
| | Re=30k | Re=43k | Re=30k | Re=43k | Re=30k | Re=43k | Re=30k | Re=44k |
| -3 | 1.00 | 1.00 | 0.75 | 0.71 | 0.36 | 0.42 | 0.10 | 0.09 |
| 18 | 0.19 | 0.23 | 0.37 | 0.43 | 0.29 | 0.22 | 0.14 | 0.15 |
| 33 | 0.19 | 0.20 | 0.23 | 0.24 | 0.24 | 0.15 | 0.16 | 0.18 |
| 36 | 0.39 | 0.48 | 0.66 | 0.68 | 0.49 | 0.46 | 0.29 | 0.30 |
| 54 | 0.63 | 0.69 | 0.48 | 0.53 | 0.27 | 0.22 | 0.11 | 0.10 |
| 66 | -0.77 | -0.78 | -0.64 | -0.62 | -0.30 | -0.32 | -0.01 | -0.01 |
| 84 | -0.51 | -0.47 | -0.61 | -0.62 | -0.64 | -0.70 | -0.21 | -0.23 |
| 101 | -0.52 | -0.49 | -0.62 | -0.62 | -0.44 | -0.47 | -0.12 | -0.12 |
| 117 | -0.53 | -0.50 | -0.66 | -0.65 | -0.47 | -0.50 | -0.13 | -0.13 |
| 124 | -0.51 | -0.48 | -0.63 | -0.64 | -0.43 | -0.44 | -0.09 | -0.09 |
| 140 | -0.51 | -0.50 | -0.64 | -0.64 | -0.44 | -0.44 | -0.09 | -0.09 |
| 158 | -0.53 | -0.52 | -0.68 | -0.68 | -0.46 | -0.44 | -0.10 | -0.10 |
| 176 | -0.54 | -0.53 | -0.66 | -0.68 | -0.36 | -0.31 | -0.10 | -0.09 |
| 197 | -0.57 | -0.55 | -0.55 | -0.55 | -0.29 | -0.28 | -0.05 | -0.06 |
| 215 | -0.56 | -0.55 | -0.52 | -0.50 | -0.23 | -0.34 | -0.03 | -0.03 |
| 219 | -0.62 | -0.63 | -0.55 | -0.51 | -0.24 | -0.24 | -0.05 | -0.05 |
| 234 | -0.60 | -0.59 | -0.52 | -0.51 | -0.23 | -0.24 | -0.05 | -0.04 |
| 241 | -0.63 | -0.62 | -0.58 | -0.57 | -0.25 | -0.30 | -0.03 | -0.04 |
| 245 | -0.60 | -0.60 | -0.67 | -0.72 | -0.28 | -0.34 | -0.05 | -0.06 |
| 260 | -0.58 | -0.61 | -0.62 | -0.68 | -0.26 | -0.30 | -0.07 | -0.08 |
| 278 | -0.58 | -0.60 | -0.65 | -0.68 | -1.16 | -1.17 | -0.13 | -0.14 |
| 294 | 0.29 | 0.28 | 0.64 | 0.64 | 0.62 | 0.64 | 0.24 | 0.22 |
| 298 | 0.73 | 0.70 | 0.70 | 0.61 | 0.44 | 0.57 | 0.07 | 0.06 |
| 324 | 0.70 | 0.69 | 0.66 | 0.49 | 0.42 | 0.30 | 0.11 | 0.11 |
| 332 | 0.39 | 0.36 | 0.25 | 0.21 | 0.00 | 0.05 | 0.03 | 0.03 |
| 339 | 0.31 | 0.33 | 0.16 | 0.12 | -0.01 | 0.07 | 0.04 | 0.03 |
| $C_l$ | 0.05 | 0.03 | 0.05 | 0.02 | -0.02 | 0.00 | 0.00 | 0.00 |
| $C_d$ | 0.78 | 0.78 | 0.85 | 0.85 | 0.47 | 0.49 | 0.15 | 0.14 |

Table 13

Pressure Coefficients for 4x7 Right Lay Cable at 12.5% ppd

| θ,° | β=90° | | β=60° | | β=40° | | β=20° | |
|---|---|---|---|---|---|---|---|---|
| | Re=30k | Re=43k | Re=30k | Re=43k | Re=30k | Re=43k | Re=30k | Re=44k |
| 9 | 0.95 | 0.95 | 0.77 | 0.77 | 0.44 | 0.45 | 0.13 | 0.15 |
| 29 | -0.22 | -0.21 | -0.02 | 0.11 | 0.15 | 0.15 | 0.11 | 0.06 |
| 44 | -0.10 | -0.09 | -0.06 | 0.01 | 0.10 | 0.09 | 0.13 | 0.11 |
| 47 | 0.43 | 0.38 | 0.44 | 0.48 | 0.40 | 0.39 | 0.23 | 0.20 |
| 65 | -0.12 | -0.06 | 0.28 | 0.35 | 0.15 | 0.16 | 0.05 | 0.00 |
| 77 | -0.92 | -0.92 | -0.63 | -0.61 | -0.37 | -0.34 | -0.03 | -0.05 |
| 95 | -0.55 | -0.53 | -0.70 | -0.72 | -0.78 | -0.73 | -0.21 | -0.18 |
| 112 | -0.55 | -0.52 | -0.68 | -0.65 | -0.54 | -0.50 | -0.11 | -0.07 |
| 128 | -0.55 | -0.54 | -0.72 | -0.69 | -0.56 | -0.51 | -0.11 | -0.08 |
| 135 | -0.54 | -0.53 | -0.73 | -0.70 | -0.45 | -0.40 | -0.09 | -0.09 |
| 151 | -0.54 | -0.53 | -0.73 | -0.71 | -0.46 | -0.40 | -0.09 | -0.09 |
| 169 | -0.56 | -0.55 | -0.75 | -0.74 | -0.46 | -0.41 | -0.09 | -0.09 |
| 187 | -0.58 | -0.57 | -0.67 | -0.68 | -0.34 | -0.31 | -0.09 | -0.08 |
| 208 | -0.60 | -0.59 | -0.60 | -0.57 | -0.32 | -0.28 | -0.05 | -0.05 |
| 226 | -0.61 | -0.59 | -0.69 | -0.70 | -0.29 | -0.30 | -0.02 | -0.03 |
| 230 | -0.66 | -0.65 | -0.53 | -0.49 | -0.33 | -0.25 | -0.05 | -0.05 |
| 245 | -0.63 | -0.62 | -0.52 | -0.48 | -0.33 | -0.24 | -0.05 | -0.04 |
| 252 | -0.66 | -0.73 | -0.62 | -0.62 | -0.34 | -0.31 | -0.03 | -0.03 |
| 256 | -0.64 | -0.65 | -0.64 | -0.66 | -0.45 | -0.37 | -0.05 | -0.05 |
| 271 | -0.62 | -0.65 | -0.64 | -0.65 | -0.43 | -0.32 | -0.08 | -0.13 |
| 289 | -0.65 | -0.65 | -0.72 | -0.68 | -0.60 | -1.22 | -0.14 | -0.17 |
| 305 | 0.48 | 0.48 | 0.70 | 0.68 | 0.67 | 0.64 | 0.25 | 0.24 |
| 309 | 0.85 | 0.84 | 0.85 | 0.82 | 0.66 | 0.66 | 0.11 | 0.16 |
| 335 | 0.89 | 0.89 | 0.68 | 0.68 | 0.36 | 0.29 | 0.14 | 0.11 |
| 343 | 0.60 | 0.59 | 0.39 | 0.38 | 0.14 | 0.14 | 0.06 | 0.14 |
| 350 | 0.57 | 0.56 | 0.34 | 0.30 | 0.09 | 0.12 | 0.06 | 0.12 |
| $C_l$ | 0.05 | 0.04 | 0.01 | -0.02 | -0.01 | -0.07 | -0.01 | 0.00 |
| $C_d$ | 0.74 | 0.74 | 0.88 | 0.88 | 0.5[illegible] | 0.49 | 0.14 | 0.13 |

Table 14

Pressure Coefficients for 4x7 Right Lay Cable at 25% ppd

| θ,° | β=90° | | β=60° | | β=40° | | β=20° | |
|---|---|---|---|---|---|---|---|---|
| | Re=30k | Re=43k | Re=30k | Re=43k | Re=30k | Re=43k | Re=30k | Re=44k |
| 2 | 0.89 | 0.88 | 0.62 | 0.58 | 0.30 | 0.29 | 0.10 | 0.12 |
| 20 | 0.52 | 0.54 | 0.64 | 0.67 | 0.41 | 0.42 | 0.15 | 0.15 |
| 40 | -0.51 | -0.41 | -0.30 | -0.26 | -0.02 | 0.01 | 0.07 | 0.06 |
| 55 | -0.51 | -0.45 | -0.34 | -0.32 | -0.06 | -0.05 | 0.10 | 0.11 |
| 59 | 0.16 | 0.04 | 0.33 | 0.36 | 0.26 | 0.27 | 0.19 | 0.20 |
| 77 | -0.43 | -0.38 | 0.01 | 0.07 | 0.04 | 0.04 | 0.01 | 0.00 |
| 89 | -0.71 | -0.68 | -0.55 | -0.53 | -0.34 | -0.34 | -0.05 | -0.05 |
| 107 | -0.56 | -0.58 | -0.68 | -0.71 | -0.67 | -0.67 | -0.18 | -0.18 |
| 124 | -0.52 | -0.53 | -0.56 | -0.56 | -0.48 | -0.44 | -0.09 | -0.07 |
| 140 | -0.55 | -0.54 | -0.57 | -0.57 | -0.48 | -0.40 | -0.09 | -0.08 |
| 147 | -0.51 | -0.52 | -0.55 | -0.58 | -0.39 | -0.35 | -0.09 | -0.09 |
| 163 | -0.51 | -0.51 | -0.56 | -0.58 | -0.39 | -0.37 | -0.09 | -0.09 |
| 181 | -0.53 | -0.52 | -0.60 | -0.60 | -0.40 | -0.38 | -0.08 | -0.09 |
| 199 | -0.54 | -0.54 | -0.58 | -0.59 | -0.31 | -0.30 | -0.08 | -0.08 |
| 219 | -0.55 | -0.56 | -0.59 | -0.58 | -0.30 | -0.27 | -0.05 | -0.05 |
| 238 | -0.56 | -0.56 | -0.63 | -0.63 | -0.28 | -0.23 | -0.03 | -0.03 |
| 242 | -0.64 | -0.61 | -0.50 | -0.49 | -0.31 | -0.29 | -0.05 | -0.05 |
| 257 | -0.59 | -0.59 | -0.49 | -0.46 | -0.30 | -0.30 | -0.04 | -0.04 |
| 263 | -0.59 | -0.67 | -0.63 | -0.59 | -0.34 | -0.29 | -0.03 | -0.03 |
| 268 | -0.59 | -0.58 | -0.62 | -0.64 | -0.45 | -0.45 | -0.06 | -0.05 |
| 283 | -0.62 | -0.59 | -0.74 | -0.71 | -0.37 | -0.58 | -0.10 | -0.13 |
| 300 | -0.75 | -0.72 | -0.89 | -0.79 | -0.57 | -0.68 | -0.15 | -0.17 |
| 317 | 0.75 | 0.75 | 0.80 | 0.79 | 0.66 | 0.66 | 0.26 | 0.24 |
| 321 | 0.89 | 0.88 | 0.89 | 0.89 | 0.81 | 0.81 | 0.13 | 0.16 |
| 347 | 0.83 | 0.81 | 0.47 | 0.50 | 0.31 | 0.31 | 0.12 | 0.11 |
| 355 | 0.75 | 0.73 | 0.49 | 0.48 | 0.32 | 0.30 | 0.10 | 0.14 |
| $C_l$ | 0.05 | 0.04 | -0.11 | -0.11 | -0.05 | -0.10 | -0.03 | -0.03 |
| $C_d$ | 0.70 | 0.73 | 0.76 | 0.78 | 0.56 | 0.53 | 0.13 | 0.13 |

Table 15

Pressure Coefficients for 4x7 Right Lay Cable at 37.5% ppd

| θ,° | β=90° | | β=60° | | β=40° | | β=20° | |
|---|---|---|---|---|---|---|---|---|
| | Re=30k | Re=43k | Re=30k | Re=43k | Re=30k | Re=43k | Re=30k | Re=44k |
| 6 | 0.82 | 0.81 | 0.66 | 0.63 | 0.42 | 0.42 | 0.16 | 0.17 |
| 13 | 1.01 | 1.00 | 0.78 | 0.78 | 0.45 | 0.45 | 0.15 | 0.16 |
| 31 | -0.21 | -0.19 | 0.26 | 0.30 | 0.29 | 0.29 | 0.14 | 0.12 |
| 51 | -0.66 | -0.70 | -0.57 | -0.59 | -0.16 | -0.16 | 0.02 | 0.01 |
| 66 | -0.69 | -0.72 | -0.69 | -0.69 | -0.21 | -0.11 | 0.07 | 0.06 |
| 70 | -0.33 | -0.27 | 0.04 | 0.07 | 0.14 | 0.15 | 0.12 | 0.09 |
| 88 | -0.68 | -0.66 | -0.27 | -0.25 | -0.07 | -0.07 | -0.04 | -0.04 |
| 100 | -0.72 | -0.74 | -0.49 | -0.48 | -0.34 | -0.33 | -0.05 | -0.05 |
| 118 | -0.55 | -0.56 | -0.52 | -0.58 | -0.45 | -0.45 | -0.13 | -0.12 |
| 135 | -0.52 | -0.51 | -0.48 | -0.48 | -0.36 | -0.35 | -0.06 | -0.05 |
| 151 | -0.55 | -0.53 | -0.48 | -0.49 | -0.35 | -0.34 | -0.06 | -0.05 |
| 158 | -0.51 | -0.52 | -0.46 | -0.46 | -0.30 | -0.29 | -0.07 | -0.06 |
| 174 | -0.52 | -0.53 | -0.46 | -0.47 | -0.31 | -0.30 | -0.07 | -0.06 |
| 192 | -0.52 | -0.53 | -0.47 | -0.48 | -0.31 | -0.31 | -0.07 | -0.06 |
| 210 | -0.54 | -0.54 | -0.49 | -0.49 | -0.26 | -0.26 | -0.07 | -0.06 |
| 230 | -0.56 | -0.54 | -0.49 | -0.50 | -0.24 | -0.25 | -0.05 | -0.05 |
| 249 | -0.55 | -0.56 | -0.52 | -0.51 | -0.25 | -0.25 | -0.04 | -0.05 |
| 253 | -0.60 | -0.56 | -0.43 | -0.42 | -0.30 | -0.30 | -0.05 | -0.04 |
| 268 | -0.59 | -0.50 | -0.43 | -0.42 | -0.28 | -0.29 | -0.05 | -0.03 |
| 274 | -0.68 | -0.63 | -0.53 | -0.53 | -0.33 | -0.33 | -0.03 | -0.03 |
| 279 | -0.66 | -0.66 | -0.54 | -0.56 | -0.41 | -0.41 | -0.06 | -0.06 |
| 294 | -0.60 | -0.79 | -0.54 | -0.57 | -0.30 | -0.33 | -0.16 | -0.18 |
| 311 | -0.96 | -0.98 | -0.78 | -0.88 | -0.61 | -0.80 | -0.14 | -0.12 |
| 328 | 0.94 | 0.94 | 0.87 | 0.86 | 0.64 | 0.63 | 0.27 | 0.24 |
| 332 | 0.89 | 0.89 | 0.87 | 0.89 | 0.77 | 0.74 | 0.18 | 0.18 |
| 358 | 0.77 | 0.76 | 0.35 | 0.33 | 0.23 | 0.19 | 0.10 | 0.07 |
| $C_l$ | 0.03 | 0.02 | -0.06 | -0.07 | -0.10 | -0.13 | -0.05 | -0.04 |
| $C_d$ | 0.64 | 0.62 | 0.64 | 0.64 | 0.46 | 0.42 | 0.12 | 0.11 |

Table 16

Pressure Coefficients for 4x7 Right Lay Cable at 50% ppd

| θ,° | β=90° | | β=60° | | β=40° | | β=20° | |
|---|---|---|---|---|---|---|---|---|
| | Re=30k | Re=43k | Re=30k | Re=43k | Re=30k | Re=43k | Re=30k | Re=44k |
| 9 | 0.68 | 0.67 | 0.13 | 0.13 | 0.12 | 0.10 | 0.05 | 0.03 |
| 17 | 0.90 | 0.89 | 0.69 | 0.69 | 0.45 | 0.45 | 0.18 | 0.18 |
| 24 | 0.95 | 0.96 | 0.72 | 0.71 | 0.46 | 0.46 | 0.16 | 0.16 |
| 43 | -0.84 | -0.87 | -0.31 | -0.30 | 0.09 | 0.08 | 0.08 | 0.05 |
| 63 | -0.84 | -0.98 | -0.89 | -0.96 | -0.36 | -0.36 | -0.01 | -0.02 |
| 78 | -0.66 | -0.66 | -0.77 | -0.80 | -0.35 | -0.34 | 0.02 | 0.02 |
| 81 | -0.47 | -0.47 | -0.17 | -0.13 | 0.02 | 0.04 | 0.04 | 0.04 |
| 99 | -0.63 | -0.61 | -0.60 | -0.59 | -0.21 | -0.22 | -0.04 | -0.03 |
| 111 | -0.59 | -0.58 | -0.46 | -0.44 | -0.29 | -0.30 | -0.04 | -0.04 |
| 129 | -0.55 | -0.53 | -0.40 | -0.42 | -0.30 | -0.31 | -0.09 | -0.08 |
| 146 | -0.53 | -0.51 | -0.42 | -0.44 | -0.27 | -0.27 | -0.05 | -0.04 |
| 162 | -0.55 | -0.55 | -0.44 | -0.45 | -0.28 | -0.28 | -0.04 | -0.04 |
| 169 | -0.51 | -0.51 | -0.41 | -0.41 | -0.27 | -0.28 | -0.05 | -0.05 |
| 185 | -0.52 | -0.52 | -0.41 | -0.42 | -0.27 | -0.28 | -0.05 | -0.06 |
| 203 | -0.53 | -0.53 | -0.42 | -0.42 | -0.26 | -0.28 | -0.05 | -0.05 |
| 221 | -0.59 | -0.58 | -0.42 | -0.42 | -0.25 | -0.27 | -0.07 | -0.06 |
| 242 | -0.70 | -0.69 | -0.42 | -0.43 | -0.23 | -0.26 | -0.06 | -0.06 |
| 260 | -0.91 | -0.80 | -0.46 | -0.46 | -0.24 | -0.26 | -0.05 | -0.06 |
| 264 | -0.52 | -0.54 | -0.40 | -0.40 | -0.27 | -0.28 | -0.05 | -0.04 |
| 279 | -0.50 | -0.51 | -0.39 | -0.39 | -0.25 | -0.27 | -0.04 | -0.03 |
| 286 | -0.78 | -0.73 | -0.45 | -0.45 | -0.30 | -0.32 | -0.03 | -0.04 |
| 290 | -0.64 | -0.66 | -0.45 | -0.47 | -0.33 | -0.37 | -0.07 | -0.07 |
| 305 | -0.62 | -0.63 | -0.43 | -0.46 | -0.31 | -0.34 | -0.19 | -0.21 |
| 323 | -0.23 | -0.26 | -0.38 | -0.45 | -0.36 | -0.39 | -0.07 | -0.04 |
| 339 | 1.00 | 0.99 | 0.85 | 0.85 | 0.60 | 0.61 | 0.26 | 0.24 |
| 343 | 0.88 | 0.87 | 0.68 | 0.70 | 0.55 | 0.58 | 0.20 | 0.21 |
| $C_l$ | -0.04 | -0.02 | 0.03 | 0.03 | -0.08 | -0.10 | -0.06 | -0.06 |
| $C_d$ | 0.66 | 0.65 | 0.51 | 0.51 | 0.37 | 0.37 | 0.10 | 0.10 |

Table 17

Pressure Coefficients for 4x7 Right Lay Cable at 62.5% ppd

| θ,° | β=90° | | β=60° | | β=40° | | β=20° | |
|---|---|---|---|---|---|---|---|---|
| | Re=30k | Re=43k | Re=30k | Re=43k | Re=30k | Re=43k | Re=30k | Re=44k |
| 20 | 0.56 | 0.55 | 0.08 | 0.08 | -0.01 | -0.03 | 0.01 | -0.01 |
| 28 | 0.94 | 0.94 | 0.67 | 0.66 | 0.42 | 0.43 | 0.18 | 0.18 |
| 35 | 0.72 | 0.73 | 0.52 | 0.51 | 0.35 | 0.36 | 0.14 | 0.13 |
| 54 | -0.85 | -0.79 | -0.82 | -0.83 | -0.18 | -0.19 | 0.01 | 0.00 |
| 74 | -0.63 | -0.62 | -0.97 | -0.97 | -0.41 | -0.41 | -0.03 | -0.03 |
| 89 | -0.65 | -0.63 | -1.25 | -1.24 | -0.48 | -0.49 | 0.00 | 0.01 |
| 92 | -0.59 | -0.59 | -0.51 | -0.50 | -0.10 | -0.06 | 0.01 | 0.01 |
| 110 | -0.68 | -0.71 | -0.85 | -0.84 | -0.29 | -0.28 | -0.03 | -0.03 |
| 122 | -0.66 | -0.67 | -0.52 | -0.52 | -0.26 | -0.26 | -0.03 | -0.02 |
| 140 | -0.59 | -0.58 | -0.48 | -0.45 | -0.21 | -0.21 | -0.07 | -0.06 |
| 157 | -0.55 | -0.54 | -0.44 | -0.42 | -0.24 | -0.24 | -0.04 | -0.04 |
| 173 | -0.58 | -0.57 | -0.43 | -0.42 | -0.25 | -0.25 | -0.03 | -0.02 |
| 180 | -0.56 | -0.53 | -0.43 | -0.42 | -0.26 | -0.30 | -0.05 | -0.05 |
| 196 | -0.55 | -0.54 | -0.46 | -0.43 | -0.26 | -0.31 | -0.05 | -0.05 |
| 214 | -0.56 | -0.55 | -0.44 | -0.41 | -0.25 | -0.27 | -0.05 | -0.05 |
| 232 | -0.62 | -0.60 | -0.45 | -0.42 | -0.23 | -0.25 | -0.07 | -0.07 |
| 253 | -0.75 | -0.73 | -0.53 | -0.54 | -0.22 | -0.26 | -0.06 | -0.07 |
| 271 | -0.71 | -0.72 | -0.52 | -0.48 | -0.24 | -0.28 | -0.07 | -0.06 |
| 275 | -0.19 | -0.25 | -0.34 | -0.35 | -0.25 | -0.29 | -0.06 | -0.04 |
| 290 | -0.19 | -0.30 | -0.35 | -0.35 | -0.23 | -0.28 | -0.05 | -0.04 |
| 297 | -0.24 | -0.52 | -0.41 | -0.42 | -0.28 | -0.32 | -0.05 | -0.04 |
| 301 | -0.52 | -0.55 | -0.36 | -0.38 | -0.30 | -0.35 | -0.09 | -0.09 |
| 316 | -0.50 | -0.58 | -0.37 | -0.37 | -0.31 | -0.33 | -0.20 | -0.21 |
| 334 | 0.51 | 0.45 | 0.19 | 0.17 | -0.06 | -0.09 | 0.00 | 0.02 |
| 350 | 0.91 | 0.91 | 0.75 | 0.75 | 0.53 | 0.54 | 0.24 | 0.22 |
| 354 | 0.80 | 0.79 | 0.62 | 0.62 | 0.44 | 0.42 | 0.20 | 0.23 |
| $C_l$ | -0.04 | -0.08 | 0.11 | 0.11 | -0.07 | -0.09 | -0.08 | -0.08 |
| $C_d$ | 0.69 | 0.69 | 0.56 | 0.54 | 0.32 | 0.32 | 0.09 | 0.09 |

Table 18

Pressure Coefficients for 4x7 Right Lay Cable at 75% ppd

| θ,° | β=90° | | β=60° | | β=40° | | β=20° | |
|---|---|---|---|---|---|---|---|---|
| | Re=30k | Re=43k | Re=30k | Re=43k | Re=30k | Re=43k | Re=30k | Re=44k |
| 2 | 0.65 | 0.66 | 0.52 | 0.51 | 0.38 | 0.39 | 0.18 | 0.16 |
| 6 | 0.62 | 0.62 | 0.39 | 0.39 | 0.25 | 0.27 | 0.21 | 0.23 |
| 32 | 0.43 | 0.43 | -0.05 | -0.05 | -0.14 | -0.17 | -0.03 | -0.04 |
| 40 | 0.94 | 0.94 | 0.60 | 0.59 | 0.34 | 0.34 | 0.16 | 0.16 |
| 47 | 0.42 | 0.43 | 0.20 | 0.17 | 0.17 | 0.15 | 0.08 | 0.07 |
| 65 | -0.74 | -0.83 | -1.20 | -1.24 | -0.44 | -0.45 | -0.05 | -0.06 |
| 85 | -0.64 | -0.65 | -1.13 | -1.12 | -0.44 | -0.44 | -0.04 | -0.03 |
| 100 | -0.61 | -0.61 | -1.16 | -1.10 | -0.51 | -0.53 | -0.01 | 0.00 |
| 104 | -0.63 | -0.63 | -0.86 | -0.86 | -0.24 | -0.17 | -0.01 | 0.00 |
| 122 | -0.61 | -0.61 | -1.14 | -1.14 | -0.34 | -0.31 | -0.03 | -0.03 |
| 134 | -0.58 | -0.57 | -0.78 | -0.76 | -0.21 | -0.21 | -0.03 | -0.02 |
| 152 | -0.56 | -0.56 | -0.52 | -0.50 | -0.19 | -0.18 | -0.07 | -0.06 |
| 169 | -0.53 | -0.54 | -0.44 | -0.44 | -0.22 | -0.24 | -0.04 | -0.04 |
| 185 | -0.56 | -0.56 | -0.44 | -0.45 | -0.21 | -0.24 | -0.02 | -0.02 |
| 192 | -0.59 | -0.59 | -0.43 | -0.43 | -0.26 | -0.29 | -0.05 | -0.05 |
| 208 | -0.55 | -0.56 | -0.44 | -0.43 | -0.25 | -0.30 | -0.04 | -0.05 |
| 226 | -0.54 | -0.55 | -0.44 | -0.44 | -0.26 | -0.28 | -0.05 | -0.05 |
| 244 | -0.61 | -0.60 | -0.53 | -0.53 | -0.26 | -0.29 | -0.09 | -0.08 |
| 264 | -0.72 | -0.72 | -0.80 | -0.86 | -0.29 | -0.32 | -0.08 | -0.08 |
| 283 | -0.35 | -0.35 | -0.48 | -0.48 | -0.32 | -0.36 | -0.07 | -0.05 |
| 287 | 0.05 | 0.05 | -0.26 | -0.26 | -0.22 | -0.23 | -0.07 | -0.05 |
| 302 | 0.09 | 0.08 | -0.26 | -0.25 | -0.22 | -0.23 | -0.06 | -0.04 |
| 308 | -0.18 | -0.18 | -0.33 | -0.32 | -0.23 | -0.24 | -0.07 | -0.05 |
| 313 | -0.23 | -0.21 | -0.36 | -0.33 | -0.25 | -0.27 | -0.11 | -0.09 |
| 328 | -0.26 | -0.26 | -0.36 | -0.35 | -0.25 | -0.26 | -0.19 | -0.18 |
| 345 | 0.91 | 0.91 | 0.63 | 0.62 | 0.24 | 0.24 | 0.08 | 0.09 |
| $C_l$ | -0.04 | -0.03 | 0.18 | 0.18 | -0.05 | -0.07 | -0.09 | -0.08 |
| $C_d$ | 0.72 | 0.72 | 0.52 | 0.50 | 0.26 | 0.27 | 0.07 | 0.06 |

Table 19

Pressure Coefficients for 4x7 Right Lay Cable at 87.5% ppd

| θ,° | β=90° | | β=60° | | β=40° | | β=20° | |
|---|---|---|---|---|---|---|---|---|
| | Re=30k | Re=43k | Re=30k | Re=43k | Re=30k | Re=43k | Re=30k | Re=44k |
| 13 | 0.27 | 0.27 | 0.25 | 0.21 | 0.20 | 0.20 | 0.11 | 0.09 |
| 17 | 0.78 | 0.88 | 0.29 | 0.35 | 0.22 | 0.29 | 0.17 | 0.18 |
| 43 | 0.24 | 0.23 | -0.17 | -0.19 | -0.20 | -0.20 | -0.03 | -0.05 |
| 51 | 0.90 | 0.90 | 0.52 | 0.51 | 0.27 | 0.28 | 0.15 | 0.14 |
| 58 | 0.11 | 0.13 | -0.12 | -0.16 | -0.04 | -0.06 | 0.01 | 0.00 |
| 76 | -0.70 | -0.88 | -1.04 | -1.13 | -0.59 | -0.59 | -0.07 | -0.08 |
| 96 | -0.55 | -0.55 | -0.91 | -0.86 | -0.51 | -0.47 | -0.03 | -0.01 |
| 111 | -0.55 | -0.54 | -0.99 | -0.93 | -0.44 | -0.44 | -0.01 | -0.01 |
| 115 | -0.52 | -0.52 | -0.79 | -0.80 | -0.33 | -0.34 | -0.02 | -0.01 |
| 133 | -0.53 | -0.52 | -0.83 | -0.84 | -0.35 | -0.35 | -0.03 | -0.03 |
| 145 | -0.53 | -0.54 | -0.82 | -0.80 | -0.22 | -0.22 | -0.03 | -0.03 |
| 163 | -0.51 | -0.51 | -0.62 | -0.64 | -0.22 | -0.22 | -0.07 | -0.07 |
| 180 | -0.51 | -0.51 | -0.47 | -0.53 | -0.25 | -0.24 | -0.04 | -0.04 |
| 196 | -0.53 | -0.51 | -0.44 | -0.59 | -0.21 | -0.19 | -0.02 | -0.02 |
| 203 | -0.60 | -0.60 | -0.45 | -0.59 | -0.26 | -0.24 | -0.04 | -0.04 |
| 219 | -0.55 | -0.53 | -0.44 | -0.56 | -0.26 | -0.24 | -0.04 | -0.04 |
| 237 | -0.52 | -0.53 | -0.48 | -0.55 | -0.27 | -0.25 | -0.04 | -0.05 |
| 255 | -0.55 | -0.56 | -0.74 | -0.67 | -0.30 | -0.26 | -0.07 | -0.08 |
| 275 | -0.59 | -0.66 | -1.20 | -1.29 | -0.45 | -0.39 | -0.07 | -0.09 |
| 294 | 0.40 | 0.27 | 0.24 | 0.44 | -0.26 | -0.26 | -0.05 | -0.04 |
| 298 | 0.35 | 0.31 | -0.03 | 0.00 | -0.14 | -0.11 | -0.04 | -0.02 |
| 313 | 0.45 | 0.41 | -0.03 | 0.02 | -0.13 | -0.12 | -0.04 | -0.02 |
| 319 | 0.02 | 0.03 | -0.08 | -0.09 | -0.18 | -0.19 | -0.05 | -0.02 |
| 324 | 0.07 | 0.04 | -0.11 | -0.14 | -0.20 | -0.23 | -0.08 | -0.06 |
| 339 | 0.15 | 0.14 | -0.06 | -0.03 | -0.15 | -0.14 | -0.14 | -0.13 |
| 356 | 1.00 | 1.00 | 0.78 | 0.77 | 0.40 | 0.40 | 0.12 | 0.13 |
| $C_l$ | -0.02 | -0.03 | 0.09 | 0.07 | -0.04 | -0.03 | -0.06 | -0.06 |
| $C_d$ | 0.76 | 0.73 | 0.59 | 0.63 | 0.24 | 0.23 | 0.04 | 0.04 |

Table 20

Pressure Coefficients for 7x7 Left Lay Cable at Re=10,000

| θ,° | β=90° | β=60° | β=40° | β=20° | β=90° | β=60° | β=40° | β=20° |
|---|---|---|---|---|---|---|---|---|
| | 0%ppd | | | | 50%ppd | | | |
| 0 | 0.97 | 0.73 | 0.38 | 0.09 | 0.97 | 0.72 | 0.43 | 0.02 |
| 30 | 0.52 | 0.58 | 0.35 | 0.11 | 0.60 | 0.30 | 0.14 | 0.00 |
| 60 | -0.96 | -0.67 | -0.27 | -0.13 | -1.03 | -0.41 | -0.23 | -0.03 |
| 90 | -1.33 | -0.69 | -0.42 | -0.14 | -1.06 | -0.88 | -0.50 | -0.18 |
| 120 | -1.05 | -0.70 | -0.39 | -0.14 | -1.00 | -0.65 | -0.36 | -0.16 |
| 150 | -0.99 | -0.63 | -0.33 | -0.15 | -1.02 | -0.76 | -0.34 | -0.14 |
| 180 | -0.97 | -0.72 | -0.32 | -0.14 | -0.92 | -0.63 | -0.34 | -0.14 |
| 210 | -1.01 | -0.57 | -0.33 | -0.14 | -0.95 | -0.75 | -0.34 | -0.16 |
| 240 | -1.01 | -0.66 | -0.44 | -0.19 | -1.01 | -0.87 | -0.45 | -0.13 |
| 270 | -1.18 | -0.79 | -0.68 | -0.19 | -0.99 | -1.39 | -0.65 | -0.24 |
| 300 | -1.04 | -0.77 | -0.64 | -0.17 | -0.30 | -0.52 | -0.44 | -0.23 |
| 330 | 0.69 | 0.33 | 0.03 | -0.12 | 0.10 | 0.27 | 0.07 | 0.03 |
| $C_l$ | 0.05 | -0.06 | -0.21 | -0.06 | 0.13 | -0.21 | -0.12 | -0.05 |
| $C_d$ | 1.24 | 0.85 | 0.41 | 0.13 | 1.19 | 0.90 | 0.42 | 0.12 |

| θ,° | β=90° | β=60° | β=40° | β=20° | β=90° | β=60° | β=40° | β=20° |
|---|---|---|---|---|---|---|---|---|
| | 25%ppd | | | | 75%ppd | | | |
| 15 | 0.93 | 0.62 | 0.33 | 0.04 | 0.89 | 0.74 | 0.41 | 0.09 |
| 45 | -0.16 | 0.13 | 0.12 | 0.05 | -0.21 | -0.24 | -0.06 | -0.06 |
| 75 | -1.14 | -0.76 | -0.47 | -0.19 | -1.37 | -0.80 | -0.37 | -0.08 |
| 105 | -1.03 | -0.74 | -0.41 | -0.17 | -1.02 | -0.79 | -0.39 | -0.16 |
| 135 | -1.00 | -0.73 | -0.38 | -0.14 | -1.01 | -0.59 | -0.34 | -0.15 |
| 165 | -0.95 | -0.62 | -0.35 | -0.14 | -1.05 | -0.71 | -0.31 | -0.14 |
| 195 | -0.99 | -0.71 | -0.34 | -0.15 | -0.96 | -0.61 | -0.33 | -0.14 |
| 225 | -1.03 | -0.68 | -0.34 | -0.14 | -0.97 | -0.78 | -0.35 | -0.17 |
| 255 | -0.97 | -0.89 | -0.51 | -0.21 | -1.01 | -0.86 | -0.60 | -0.14 |
| 285 | -1.09 | -0.87 | -0.56 | -0.23 | -0.96 | -0.86 | -0.74 | -0.24 |
| 315 | -0.74 | -0.38 | -0.37 | -0.07 | 0.30 | -0.05 | -0.24 | -0.20 |
| 345 | 0.94 | 0.61 | 0.27 | -0.04 | 0.75 | 0.64 | 0.31 | 0.08 |
| $C_l$ | -0.09 | -0.16 | -0.13 | -0.05 | 0.20 | -0.03 | -0.19 | -0.07 |
| $C_d$ | 1.16 | 0.86 | 0.41 | 0.12 | 1.29 | 0.88 | 0.41 | 0.12 |

Table 21

Pressure Coefficients for 7x7 Left Lay Cable at 0% ppd

| θ,° | β=90° | | β=60° | | β=40° | | β=20° | |
|---|---|---|---|---|---|---|---|---|
| | Re=30k | Re=45k | Re=30k | Re=45k | Re=30k | Re=45k | Re=30k | Re=45k |
| 10 | 0.87 | 0.85 | 0.58 | 0.57 | 0.18 | 0.16 | -0.06 | -0.07 |
| 27 | 0.39 | 0.42 | 0.28 | 0.26 | 0.14 | 0.03 | -0.05 | -0.05 |
| 33 | 0.66 | 0.65 | 0.70 | 0.68 | 0.09 | 0.07 | -0.01 | 0.00 |
| 50 | -1.20 | -1.23 | -0.73 | -0.78 | -0.43 | -0.44 | -0.11 | -0.15 |
| 70 | -1.12 | -1.20 | -0.81 | -0.81 | -0.89 | -0.85 | -0.29 | -0.32 |
| 87 | -0.90 | -0.91 | -0.82 | -0.80 | -0.46 | -0.48 | -0.16 | -0.16 |
| 93 | -0.91 | -0.91 | -0.79 | -0.78 | -0.38 | -0.43 | -0.13 | -0.13 |
| 110 | -0.86 | -0.87 | -0.72 | -0.68 | -0.34 | -0.40 | -0.14 | -0.14 |
| 130 | -0.85 | -0.86 | -0.70 | -0.65 | -0.36 | -0.41 | -0.15 | -0.17 |
| 147 | -0.83 | -0.83 | -0.68 | -0.66 | -0.34 | -0.37 | -0.15 | -0.16 |
| 153 | -0.81 | -0.84 | -0.63 | -0.62 | -0.30 | -0.32 | -0.11 | -0.10 |
| 170 | -0.82 | -0.81 | -0.68 | -0.67 | -0.36 | -0.37 | -0.15 | -0.16 |
| 190 | -0.85 | -0.82 | -0.76 | -0.75 | -0.39 | -0.39 | -0.20 | -0.18 |
| 207 | -0.83 | -0.83 | -0.75 | -0.72 | -0.36 | -0.37 | -0.16 | -0.16 |
| 213 | -0.84 | -0.83 | -0.72 | -0.69 | -0.33 | -0.34 | -0.13 | -0.13 |
| 230 | -0.86 | -0.85 | -0.70 | -0.68 | -0.42 | -0.43 | -0.16 | -0.17 |
| 250 | -0.93 | -0.94 | -0.93 | -0.89 | -0.50 | -0.49 | -0.20 | -0.20 |
| 267 | -0.98 | -0.99 | -1.23 | -1.20 | -0.65 | -0.64 | -0.22 | -0.23 |
| 273 | -0.98 | -1.00 | -1.15 | -1.09 | -0.60 | -0.60 | -0.21 | -0.21 |
| 290 | -0.96 | -1.03 | -1.31 | -1.53 | -0.72 | -0.74 | -0.23 | -0.26 |
| 310 | -1.24 | -1.29 | -1.16 | -1.26 | -0.62 | -0.62 | -0.15 | -0.16 |
| 327 | 0.78 | 0.75 | 0.17 | 0.19 | -0.03 | -0.02 | -0.05 | -0.05 |
| 333 | 0.57 | 0.55 | 0.29 | 0.29 | 0.08 | 0.09 | 0.00 | 0.00 |
| 350 | 0.64 | 0.58 | 0.45 | 0.46 | 0.27 | 0.27 | 0.06 | 0.06 |
| $C_l$ | -0.01 | -0.01 | -0.23 | -0.26 | -0.06 | -0.03 | -0.01 | 0.00 |
| $C_d$ | 0.79 | 0.75 | 0.60 | 0.55 | 0.25 | 0.25 | 0.09 | 0.09 |

Table 22

Pressure Coefficients for 7x7 Left Lay Cable at 12.5% ppd

| θ,° | β=90° | | β=60° | | β=40° | | β=20° | |
|---|---|---|---|---|---|---|---|---|
| | Re=30k | Re=45k | Re=30k | Re=45k | Re=30k | Re=45k | Re=30k | Re=45k |
| 17 | 0.57 | 0.60 | 0.35 | 0.39 | 0.03 | 0.03 | -0.09 | -0.11 |
| 34 | 0.25 | 0.19 | 0.18 | 0.18 | -0.14 | -0.12 | -0.10 | -0.08 |
| 41 | 0.37 | 0.37 | 0.16 | 0.17 | -0.11 | -0.11 | -0.02 | -0.02 |
| 58 | -1.23 | -1.22 | -1.03 | -1.07 | -0.43 | -0.50 | -0.11 | -0.15 |
| 77 | -1.00 | -1.06 | -0.84 | -0.83 | -0.74 | -0.60 | -0.27 | -0.29 |
| 94 | -0.87 | -0.87 | -0.83 | -0.80 | -0.46 | -0.44 | -0.17 | -0.16 |
| 101 | -0.87 | -0.88 | -0.80 | -0.79 | -0.37 | -0.41 | -0.13 | -0.14 |
| 118 | -0.86 | -0.85 | -0.82 | -0.78 | -0.36 | -0.38 | -0.14 | -0.15 |
| 137 | -0.84 | -0.84 | -0.78 | -0.75 | -0.37 | -0.40 | -0.15 | -0.17 |
| 154 | -0.83 | -0.83 | -0.67 | -0.67 | -0.35 | -0.36 | -0.14 | -0.14 |
| 161 | -0.85 | -0.82 | -0.65 | -0.62 | -0.30 | -0.32 | -0.11 | -0.09 |
| 178 | -0.84 | -0.83 | -0.70 | -0.70 | -0.39 | -0.36 | -0.15 | -0.16 |
| 197 | -0.85 | -0.83 | -0.78 | -0.75 | -0.40 | -0.39 | -0.18 | -0.19 |
| 214 | -0.86 | -0.84 | -0.74 | -0.74 | -0.38 | -0.37 | -0.16 | -0.15 |
| 221 | -0.86 | -0.84 | -0.73 | -0.72 | -0.35 | -0.35 | -0.12 | -0.12 |
| 238 | -0.90 | -0.87 | -0.73 | -0.71 | -0.49 | -0.50 | -0.16 | -0.16 |
| 257 | -1.17 | -1.19 | -0.85 | -0.84 | -0.62 | -0.62 | -0.20 | -0.21 |
| 274 | -1.10 | -1.10 | -1.15 | -1.15 | -0.61 | -0.63 | -0.22 | -0.21 |
| 281 | -1.08 | -1.06 | -1.09 | -1.09 | -0.58 | -0.58 | -0.20 | -0.18 |
| 298 | -1.11 | -1.11 | -1.27 | -1.34 | -0.72 | -0.74 | -0.25 | -0.26 |
| 317 | -1.02 | -1.05 | -0.83 | -0.89 | -0.46 | -0.47 | -0.12 | -0.12 |
| 334 | 0.84 | 0.81 | 0.36 | 0.33 | 0.08 | 0.07 | -0.02 | -0.02 |
| 341 | 0.72 | 0.69 | 0.40 | 0.39 | 0.15 | 0.16 | 0.02 | 0.02 |
| 358 | 0.84 | 0.82 | 0.64 | 0.64 | 0.33 | 0.33 | 0.08 | 0.08 |
| $C_l$ | -0.14 | -0.13 | -0.15 | -0.18 | -0.07 | -0.09 | -0.01 | 0.00 |
| $C_d$ | 0.77 | 0.75 | 0.57 | 0.54 | 0.26 | 0.24 | 0.09 | 0.08 |

Table 23

Pressure Coefficients for 7x7 Left Lay Cable at 25% ppd

| θ,° | β=90° | | β=60° | | β=40° | | β=20° | |
|---|---|---|---|---|---|---|---|---|
| | Re=30k | Re=45k | Re=30k | Re=45k | Re=30k | Re=45k | Re=30k | Re=45k |
| 5 | 0.98 | 0.95 | 0.72 | 0.72 | 0.38 | 0.39 | 0.10 | 0.09 |
| 25 | 0.16 | 0.14 | 0.08 | 0.06 | -0.12 | -0.11 | -0.14 | -0.17 |
| 42 | -0.06 | -0.05 | 0.04 | 0.00 | -0.24 | -0.22 | -0.13 | -0.12 |
| 48 | 0.03 | -0.01 | -0.05 | -0.07 | -0.29 | -0.24 | -0.08 | -0.05 |
| 65 | -1.13 | -1.12 | -0.99 | -1.14 | -0.53 | -0.59 | -0.13 | -0.14 |
| 85 | -0.88 | -0.87 | -0.82 | -0.80 | -0.45 | -0.52 | -0.23 | -0.25 |
| 102 | -0.85 | -0.83 | -0.80 | -0.80 | -0.39 | -0.46 | -0.14 | -0.16 |
| 108 | -0.84 | -0.82 | -0.80 | -0.78 | -0.38 | -0.41 | -0.13 | -0.14 |
| 125 | -0.84 | -0.82 | -0.83 | -0.80 | -0.38 | -0.36 | -0.15 | -0.15 |
| 145 | -0.83 | -0.82 | -0.74 | -0.73 | -0.37 | -0.35 | -0.19 | -0.17 |
| 162 | -0.82 | -0.81 | -0.67 | -0.64 | -0.34 | -0.33 | -0.14 | -0.14 |
| 168 | -0.80 | -0.80 | -0.64 | -0.61 | -0.29 | -0.30 | -0.10 | -0.09 |
| 185 | -0.80 | -0.80 | -0.74 | -0.74 | -0.36 | -0.34 | -0.16 | -0.16 |
| 205 | -0.81 | -0.81 | -0.86 | -0.82 | -0.39 | -0.38 | -0.16 | -0.19 |
| 222 | -0.84 | -0.81 | -0.85 | -0.78 | -0.38 | -0.38 | -0.16 | -0.15 |
| 228 | -0.83 | -0.82 | -0.81 | -0.75 | -0.43 | -0.42 | -0.14 | -0.12 |
| 245 | -0.87 | -0.85 | -0.80 | -0.76 | -0.51 | -0.49 | -0.19 | -0.16 |
| 265 | -1.06 | -1.07 | -0.86 | -0.83 | -0.64 | -0.64 | -0.24 | -0.23 |
| 282 | -0.93 | -0.96 | -0.91 | -0.97 | -0.50 | -0.51 | -0.21 | -0.21 |
| 288 | -0.83 | -0.82 | -0.79 | -0.85 | -0.46 | -0.47 | -0.19 | -0.18 |
| 305 | -1.12 | -1.04 | -1.19 | -1.17 | -0.68 | -0.72 | -0.23 | -0.25 |
| 325 | -0.62 | -0.65 | -0.47 | -0.46 | -0.23 | -0.25 | -0.05 | -0.07 |
| 342 | 0.90 | 0.88 | 0.49 | 0.50 | 0.21 | 0.20 | 0.00 | 0.01 |
| 348 | 0.82 | 0.79 | 0.50 | 0.50 | 0.26 | 0.25 | 0.06 | 0.06 |
| $C_l$ | -0.10 | -0.10 | -0.14 | -0.11 | -0.08 | -0.06 | -0.01 | -0.01 |
| $C_d$ | 0.75 | 0.72 | 0.61 | 0.57 | 0.24 | 0.23 | 0.10 | 0.09 |

Table 24

Pressure Coefficients for 7x7 Left Lay Cable at 37.5% ppd

| θ,° | β=90° | | β=60° | | β=40° | | β=20° | |
|---|---|---|---|---|---|---|---|---|
| | Re=30k | Re=45k | Re=30k | Re=45k | Re=30k | Re=45k | Re=30k | Re=45k |
| 13 | 0.98 | 0.95 | 0.72 | 0.73 | 0.38 | 0.39 | 0.11 | 0.10 |
| 32 | -0.28 | -0.32 | -0.33 | -0.30 | -0.23 | -0.21 | -0.21 | -0.22 |
| 49 | -0.40 | -0.38 | -0.31 | -0.25 | -0.25 | -0.20 | -0.15 | -0.16 |
| 56 | -0.35 | -0.36 | -0.35 | -0.26 | -0.31 | -0.23 | -0.10 | -0.06 |
| 73 | -1.09 | -1.10 | -1.03 | -1.04 | -0.61 | -0.64 | -0.14 | -0.14 |
| 92 | -0.88 | -0.86 | -0.86 | -0.88 | -0.70 | -0.74 | -0.21 | -0.22 |
| 109 | -0.85 | -0.85 | -0.85 | -0.82 | -0.41 | -0.42 | -0.14 | -0.16 |
| 116 | -0.84 | -0.85 | -0.76 | -0.74 | -0.35 | -0.35 | -0.13 | -0.13 |
| 133 | -0.84 | -0.85 | -0.76 | -0.74 | -0.33 | -0.32 | -0.16 | -0.15 |
| 152 | -0.84 | -0.83 | -0.70 | -0.69 | -0.35 | -0.35 | -0.17 | -0.17 |
| 169 | -0.83 | -0.82 | -0.66 | -0.64 | -0.34 | -0.33 | -0.15 | -0.14 |
| 176 | -0.82 | -0.82 | -0.62 | -0.61 | -0.29 | -0.28 | -0.11 | -0.10 |
| 193 | -0.82 | -0.83 | -0.75 | -0.76 | -0.33 | -0.32 | -0.15 | -0.17 |
| 212 | -0.85 | -0.84 | -0.81 | -0.83 | -0.37 | -0.36 | -0.19 | -0.19 |
| 229 | -0.84 | -0.84 | -0.79 | -0.78 | -0.44 | -0.44 | -0.16 | -0.15 |
| 236 | -0.83 | -0.83 | -0.76 | -0.76 | -0.58 | -0.59 | -0.15 | -0.13 |
| 253 | -0.85 | -0.85 | -0.85 | -0.81 | -0.60 | -0.59 | -0.19 | -0.18 |
| 272 | -0.90 | -0.91 | -0.93 | -0.89 | -0.71 | -0.74 | -0.23 | -0.23 |
| 289 | -0.84 | -0.80 | -0.71 | -0.76 | -0.40 | -0.43 | -0.21 | -0.20 |
| 296 | -0.74 | -0.64 | -0.66 | -0.66 | -0.37 | -0.39 | -0.18 | -0.17 |
| 313 | -0.96 | -0.99 | -0.94 | -0.98 | -0.63 | -0.66 | -0.23 | -0.22 |
| 332 | -0.19 | -0.20 | -0.10 | -0.10 | -0.05 | -0.06 | -0.02 | -0.02 |
| 349 | 0.96 | 0.93 | 0.61 | 0.62 | 0.30 | 0.30 | 0.05 | 0.05 |
| 356 | 0.89 | 0.87 | 0.60 | 0.59 | 0.32 | 0.34 | 0.06 | 0.07 |
| $C_l$ | -0.03 | -0.02 | -0.05 | -0.07 | -0.06 | -0.07 | -0.02 | -0.01 |
| $C_d$ | 0.77 | 0.74 | 0.61 | 0.62 | 0.29 | 0.30 | 0.10 | 0.10 |

Table 25

Pressure Coefficients for 7x7 Left Lay Cable at 50% ppd

| θ,° | β=90° | | β=60° | | β=40° | | β=20° | |
|---|---|---|---|---|---|---|---|---|
| | Re=30k | Re=45k | Re=30k | Re=45k | Re=30k | Re=45k | Re=30k | Re=45k |
| 3 | 0.97 | 0.92 | 0.69 | 0.70 | 0.38 | 0.40 | 0.06 | 0.08 |
| 20 | 0.85 | 0.82 | 0.64 | 0.65 | 0.34 | 0.35 | 0.10 | 0.09 |
| 40 | -0.70 | -0.71 | -0.57 | -0.56 | -0.32 | -0.34 | -0.25 | -0.28 |
| 57 | -0.79 | -0.83 | -0.52 | -0.49 | -0.34 | -0.33 | -0.17 | -0.17 |
| 63 | -0.64 | -0.66 | -0.49 | -0.53 | -0.39 | -0.38 | -0.11 | -0.09 |
| 80 | -1.12 | -1.08 | -1.09 | -1.19 | -0.66 | -0.67 | -0.12 | -0.14 |
| 100 | -0.88 | -0.88 | -0.85 | -0.87 | -0.69 | -0.70 | -0.19 | -0.20 |
| 117 | -0.86 | -0.84 | -0.78 | -0.81 | -0.43 | -0.43 | -0.17 | -0.15 |
| 123 | -0.84 | -0.85 | -0.67 | -0.70 | -0.38 | -0.38 | -0.14 | -0.13 |
| 140 | -0.84 | -0.84 | -0.64 | -0.70 | -0.38 | -0.38 | -0.15 | -0.15 |
| 160 | -0.85 | -0.83 | -0.68 | -0.68 | -0.40 | -0.40 | -0.17 | -0.18 |
| 177 | -0.82 | -0.81 | -0.65 | -0.65 | -0.36 | -0.35 | -0.14 | -0.14 |
| 183 | -0.82 | -0.82 | -0.62 | -0.62 | -0.31 | -0.31 | -0.10 | -0.11 |
| 200 | -0.84 | -0.82 | -0.79 | -0.77 | -0.34 | -0.33 | -0.15 | -0.16 |
| 220 | -0.84 | -0.84 | -0.93 | -0.92 | -0.38 | -0.37 | -0.19 | -0.19 |
| 237 | -0.87 | -0.85 | -0.90 | -0.89 | -0.50 | -0.47 | -0.16 | -0.16 |
| 243 | -0.84 | -0.85 | -0.88 | -0.88 | -0.64 | -0.64 | -0.15 | -0.16 |
| 260 | -0.88 | -0.87 | -0.93 | -0.92 | -0.74 | -0.72 | -0.20 | -0.20 |
| 280 | -0.88 | -0.89 | -1.13 | -1.12 | -0.74 | -0.75 | -0.23 | -0.24 |
| 297 | -0.48 | -0.50 | -0.55 | -0.60 | -0.31 | -0.34 | -0.19 | -0.19 |
| 303 | -0.46 | -0.43 | -0.48 | -0.48 | -0.27 | -0.29 | -0.15 | -0.14 |
| 320 | -0.86 | -0.90 | -0.81 | -0.82 | -0.51 | -0.52 | -0.16 | -0.17 |
| 340 | 0.27 | 0.22 | 0.21 | 0.23 | 0.11 | 0.13 | 0.02 | 0.01 |
| 357 | 0.99 | 0.94 | 0.69 | 0.70 | 0.34 | 0.36 | 0.08 | 0.08 |
| $C_l$ | 0.05 | 0.05 | -0.12 | -0.09 | -0.06 | -0.05 | -0.02 | -0.01 |
| $C_d$ | 0.81 | 0.77 | 0.64 | 0.63 | 0.35 | 0.34 | 0.11 | 0.10 |

Table 26

Pressure Coefficients for 7x7 Left Lay Cable at 62.5% ppd

| θ,° | β=90° | | β=60° | | β=40° | | β=20° | |
|---|---|---|---|---|---|---|---|---|
| | Re=30k | Re=45k | Re=30k | Re=45k | Re=30k | Re=45k | Re=30k | Re=45k |
| 4 | 0.94 | 0.92 | 0.71 | 0.72 | 0.36 | 0.39 | 0.07 | 0.08 |
| 11 | 0.97 | 0.94 | 0.78 | 0.78 | 0.43 | 0.49 | 0.07 | 0.07 |
| 28 | 0.58 | 0.56 | 0.45 | 0.46 | 0.26 | 0.27 | 0.11 | 0.09 |
| 47 | -1.03 | -1.05 | -0.77 | -0.77 | -0.46 | -0.40 | -0.30 | -0.34 |
| 64 | -1.13 | -1.23 | -0.70 | -0.69 | -0.44 | -0.41 | -0.19 | -0.17 |
| 71 | -0.93 | -0.89 | -0.79 | -0.79 | -0.51 | -0.43 | -0.13 | -0.12 |
| 88 | -1.15 | -1.14 | -1.12 | -1.12 | -0.58 | -0.55 | -0.15 | -0.15 |
| 107 | -0.91 | -0.89 | -0.76 | -0.76 | -0.58 | -0.51 | -0.18 | -0.19 |
| 124 | -0.85 | -0.83 | -0.70 | -0.70 | -0.39 | -0.36 | -0.16 | -0.15 |
| 131 | -0.84 | -0.84 | -0.68 | -0.69 | -0.37 | -0.33 | -0.15 | -0.14 |
| 148 | -0.84 | -0.83 | -0.71 | -0.70 | -0.38 | -0.33 | -0.14 | -0.15 |
| 167 | -0.82 | -0.80 | -0.70 | -0.68 | -0.38 | -0.35 | -0.17 | -0.18 |
| 184 | -0.81 | -0.80 | -0.65 | -0.65 | -0.34 | -0.32 | -0.15 | -0.15 |
| 191 | -0.83 | -0.81 | -0.63 | -0.62 | -0.30 | -0.28 | -0.11 | -0.11 |
| 208 | -0.85 | -0.83 | -0.78 | -0.77 | -0.31 | -0.29 | -0.16 | -0.16 |
| 227 | -0.83 | -0.82 | -0.87 | -0.90 | -0.37 | -0.35 | -0.19 | -0.19 |
| 244 | -0.83 | -0.83 | -0.87 | -0.89 | -0.56 | -0.56 | -0.17 | -0.17 |
| 251 | -0.86 | -0.84 | -0.87 | -0.90 | -0.66 | -0.68 | -0.16 | -0.16 |
| 268 | -0.89 | -0.88 | -0.86 | -0.95 | -0.83 | -0.84 | -0.24 | -0.23 |
| 287 | -0.94 | -0.95 | -0.97 | -1.03 | -0.73 | -0.74 | -0.23 | -0.22 |
| 304 | -0.03 | -0.09 | -0.26 | -0.32 | -0.23 | -0.26 | -0.16 | -0.17 |
| 311 | 0.07 | -0.01 | -0.13 | -0.19 | -0.17 | -0.19 | -0.11 | -0.11 |
| 328 | -0.64 | -0.69 | -0.48 | -0.52 | -0.34 | -0.35 | -0.12 | -0.11 |
| 347 | 0.64 | 0.60 | 0.48 | 0.49 | 0.25 | 0.26 | 0.04 | 0.03 |
| $C_l$ | 0.15 | 0.14 | 0.00 | -0.05 | -0.07 | -0.12 | -0.01 | 0.00 |
| $C_d$ | 0.85 | 0.81 | 0.66 | 0.65 | 0.34 | 0.34 | 0.11 | 0.11 |

Table 27

Pressure Coefficients for 7x7 Left Lay Cable at 75% ppd

| θ,° | β=90° | | β=60° | | β=40° | | β=20° | |
|---|---|---|---|---|---|---|---|---|
| | Re=30k | Re=45k | Re=30k | Re=45k | Re=30k | Re=45k | Re=30k | Re=45k |
| 12 | 0.83 | 0.81 | 0.69 | 0.70 | 0.35 | 0.37 | 0.05 | 0.07 |
| 18 | 0.95 | 0.93 | 0.79 | 0.81 | 0.48 | 0.54 | 0.05 | 0.07 |
| 35 | 0.22 | 0.17 | 0.25 | 0.23 | 0.18 | 0.16 | 0.08 | 0.08 |
| 55 | -1.02 | -1.03 | -0.79 | -0.77 | -0.51 | -0.53 | -0.32 | -0.35 |
| 72 | -1.12 | -1.24 | -0.78 | -0.78 | -0.52 | -0.54 | -0.19 | -0.18 |
| 78 | -1.06 | -1.05 | -0.80 | -0.82 | -0.49 | -0.50 | -0.16 | -0.15 |
| 95 | -1.19 | -1.19 | -0.78 | -0.86 | -0.37 | -0.38 | -0.15 | -0.16 |
| 115 | -0.91 | -0.86 | -0.67 | -0.69 | -0.37 | -0.40 | -0.17 | -0.18 |
| 132 | -0.86 | -0.83 | -0.71 | -0.71 | -0.39 | -0.36 | -0.16 | -0.17 |
| 138 | -0.85 | -0.83 | -0.66 | -0.68 | -0.38 | -0.35 | -0.14 | -0.13 |
| 155 | -0.84 | -0.83 | -0.70 | -0.68 | -0.40 | -0.36 | -0.15 | -0.15 |
| 175 | -0.85 | -0.81 | -0.67 | -0.65 | -0.39 | -0.37 | -0.17 | -0.18 |
| 192 | -0.83 | -0.81 | -0.65 | -0.64 | -0.35 | -0.32 | -0.16 | -0.14 |
| 198 | -0.82 | -0.80 | -0.61 | -0.61 | -0.31 | -0.29 | -0.11 | -0.11 |
| 215 | -0.83 | -0.85 | -0.69 | -0.66 | -0.32 | -0.30 | -0.16 | -0.16 |
| 235 | -0.85 | -0.83 | -0.94 | -0.91 | -0.35 | -0.33 | -0.18 | -0.18 |
| 252 | -0.87 | -0.86 | -1.14 | -1.06 | -0.56 | -0.56 | -0.19 | -0.18 |
| 258 | -0.87 | -0.86 | -1.18 | -1.14 | -0.62 | -0.61 | -0.17 | -0.16 |
| 275 | -0.89 | -0.93 | -1.43 | -1.49 | -0.83 | -0.85 | -0.26 | -0.26 |
| 295 | -0.88 | -0.92 | -1.20 | -1.18 | -0.64 | -0.64 | -0.20 | -0.19 |
| 312 | 0.31 | 0.29 | -0.13 | -0.13 | -0.16 | -0.18 | -0.13 | -0.13 |
| 318 | 0.54 | 0.49 | 0.08 | 0.04 | -0.08 | -0.09 | -0.08 | -0.07 |
| 335 | -0.20 | -0.18 | -0.23 | -0.22 | -0.15 | -0.14 | -0.06 | -0.05 |
| 355 | 0.90 | 0.88 | 0.63 | 0.65 | 0.34 | 0.34 | 0.04 | 0.04 |
| $C_l$ | 0.17 | 0.17 | -0.26 | -0.24 | -0.10 | -0.10 | -0.01 | 0.00 |
| $C_d$ | 0.92 | 0.89 | 0.70 | 0.69 | 0.37 | 0.35 | 0.11 | 0.12 |

Table 28

Pressure Coefficients for 7x7 Left Lay Cable at 87.5% ppd

| θ,° | β=90° | | β=60° | | β=40° | | β=20° | |
|---|---|---|---|---|---|---|---|---|
| | Re=30k | Re=45k | Re=30k | Re=45k | Re=30k | Re=45k | Re=30k | Re=45k |
| 2 | 0.98 | 0.95 | 0.70 | 0.71 | 0.36 | 0.35 | 0.02 | 0.02 |
| 19 | 0.66 | 0.64 | 0.57 | 0.58 | 0.30 | 0.27 | 0.02 | 0.04 |
| 26 | 0.91 | 0.88 | 0.56 | 0.57 | 0.38 | 0.32 | 0.06 | 0.07 |
| 43 | -0.19 | -0.23 | -0.01 | -0.02 | 0.03 | -0.02 | 0.05 | 0.05 |
| 62 | -1.12 | -1.16 | -0.82 | -0.81 | -0.55 | -1.21 | -0.31 | -0.33 |
| 79 | -1.10 | -1.19 | -0.86 | -0.84 | -0.58 | -0.52 | -0.20 | -0.19 |
| 86 | -1.07 | -1.11 | -0.87 | -0.85 | -0.52 | -0.46 | -0.17 | -0.16 |
| 103 | -1.07 | -1.09 | -0.76 | -0.75 | -0.34 | -0.39 | -0.17 | -0.17 |
| 122 | -0.86 | -0.84 | -0.74 | -0.71 | -0.39 | -0.39 | -0.17 | -0.17 |
| 139 | -0.86 | -0.83 | -0.76 | -0.74 | -0.39 | -0.40 | -0.16 | -0.16 |
| 146 | -0.82 | -0.83 | -0.72 | -0.70 | -0.37 | -0.39 | -0.14 | -0.13 |
| 163 | -0.82 | -0.81 | -0.75 | -0.72 | -0.37 | -0.39 | -0.13 | -0.14 |
| 182 | -0.83 | -0.81 | -0.71 | -0.70 | -0.41 | -0.39 | -0.17 | -0.18 |
| 199 | -0.82 | -0.81 | -0.67 | -0.67 | -0.36 | -0.35 | -0.15 | -0.14 |
| 206 | -0.82 | -0.79 | -0.65 | -0.64 | -0.33 | -0.32 | -0.12 | -0.11 |
| 223 | -0.86 | -0.84 | -0.72 | -0.68 | -0.33 | -0.32 | -0.16 | -0.15 |
| 242 | -0.86 | -0.85 | -0.91 | -0.87 | -0.41 | -0.37 | -0.19 | -0.18 |
| 259 | -0.89 | -0.86 | -1.12 | -1.16 | -0.61 | -0.61 | -0.19 | -0.20 |
| 266 | -0.93 | -0.92 | -1.11 | -1.20 | -0.65 | -0.63 | -0.18 | -0.18 |
| 283 | -0.97 | -0.95 | -1.39 | -1.64 | -0.90 | -0.91 | -0.27 | -0.27 |
| 302 | -0.73 | -0.70 | -0.94 | -0.96 | -0.52 | -0.51 | -0.16 | -0.16 |
| 319 | 0.41 | 0.34 | 0.03 | 0.00 | -0.10 | -0.11 | -0.09 | -0.09 |
| 326 | 0.70 | 0.69 | 0.21 | 0.22 | 0.01 | 0.01 | -0.03 | -0.04 |
| 343 | 0.27 | 0.30 | 0.09 | 0.09 | 0.04 | 0.04 | 0.00 | 0.00 |
| $C_l$ | 0.13 | 0.17 | -0.21 | -0.27 | -0.12 | 0.00 | 0.00 | -0.01 |
| $C_d$ | 0.96 | 0.93 | 0.73 | 0.71 | 0.38 | 0.34 | 0.12 | 0.12 |

Table 29

Integrated Drag Coefficients

| Cable | Cylinder | | | 7x1 Cable | | 4x1 Cable | |
|---|---|---|---|---|---|---|---|
| Angle, β | Re=10k | Re=30k | Re=46k | Re=30k | Re=46k | Re=30k | Re=46k |
| 90° | 1.08 | 1.17 | 1.10 | 1.20 | 1.18 | 1.00 | 1.00 |
| 60° | 0.82 | 0.89 | 0.87 | 0.82 | 0.93 | 0.80 | 0.83 |
| 40° | 0.45 | 0.51 | 0.53 | 0.48 | 0.48 | 0.44 | 0.43 |
| 20° | 0.15 | 0.15 | 0.15 | 0.11 | 0.12 | 0.12 | 0.11 |

| Cable | 7x7 Cable | | | 4x7 Serrated Cable | | |
|---|---|---|---|---|---|---|
| Angle, β | Re=10,000 | Re=30,000 | Re=45,000 | Re=10,000 | Re=30,000 | Re=43,000 |
| 90° | 1.22 | 0.83 | 0.80 | 1.08 | 0.71 | 0.71 |
| 60° | 0.87 | 0.64 | 0.62 | 0.90 | 0.66 | 0.67 |
| 40° | 0.41 | 0.31 | 0.30 | 0.43 | 0.41 | 0.39 |
| 20° | 0.12 | 0.10 | 0.10 | 0.15 | 0.11 | 0.10 |

Table 30

Integrated Lift Coefficients

| Cable | Cylinder | | | 7x1 Cable | | 4x1 Cable | |
|---|---|---|---|---|---|---|---|
| Angle, β | Re=10k | Re=30k | Re=46k | Re=30k | Re=46k | Re=30k | Re=46k |
| 90° | -0.02 | 0.06 | 0.05 | -0.06 | -0.01 | -0.17 | -0.15 |
| 60° | 0.01 | 0.02 | 0.04 | -0.21 | -0.23 | 0.20 | 0.22 |
| 40° | -0.01 | 0.03 | 0.00 | -0.17 | -0.17 | 0.19 | 0.17 |
| 20° | 0.01 | -0.01 | 0.00 | -0.10 | -0.11 | 0.10 | 0.09 |

| Cable | 7x7 Cable | | | 4x7 Serrated Cable | | |
|---|---|---|---|---|---|---|
| Angle, β | Re=10,000 | Re=30,000 | Re=45,000 | Re=10,000 | Re=30,000 | Re=43,000 |
| 90° | 0.07 | 0.03 | 0.03 | -0.02 | 0.01 | 0.00 |
| 60° | -0.12 | -0.15 | -0.16 | 0.21 | 0.04 | 0.03 |
| 40° | -0.16 | -0.08 | -0.07 | 0.13 | -0.05 | -0.07 |
| 20° | -0.06 | -0.01 | -0.01 | 0.03 | -0.05 | -0.04 |

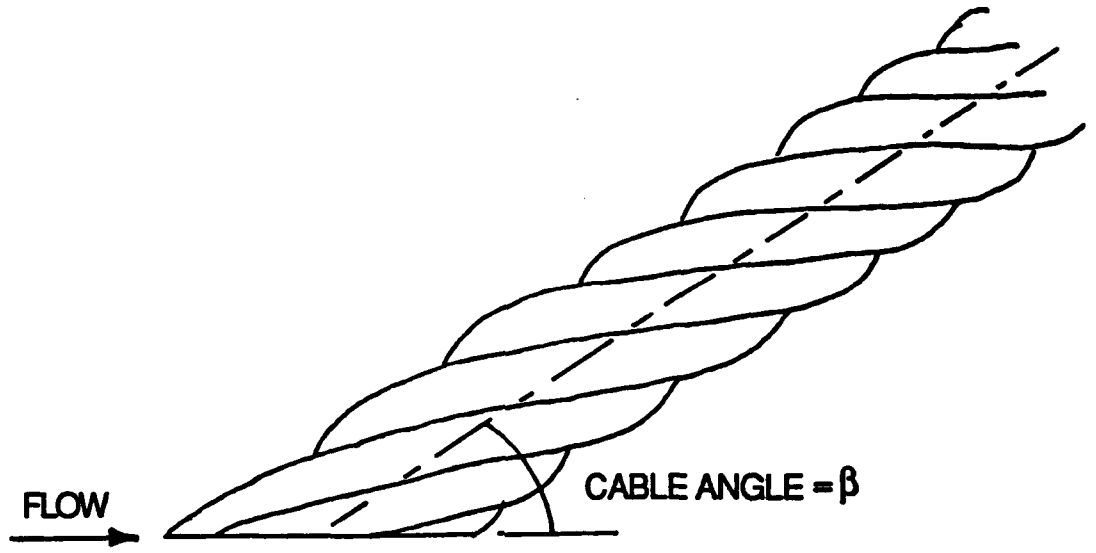


(a) PLAN VIEW

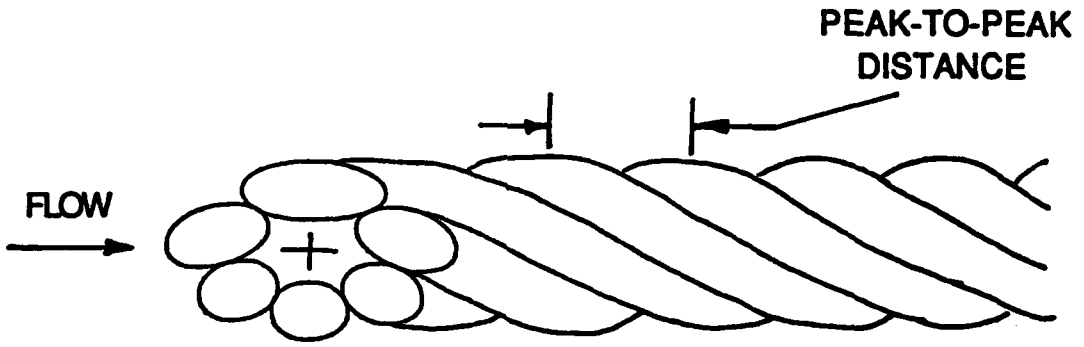


(b) SIDE VIEW

**Figure 1. Cross Section of Stranded Cable**

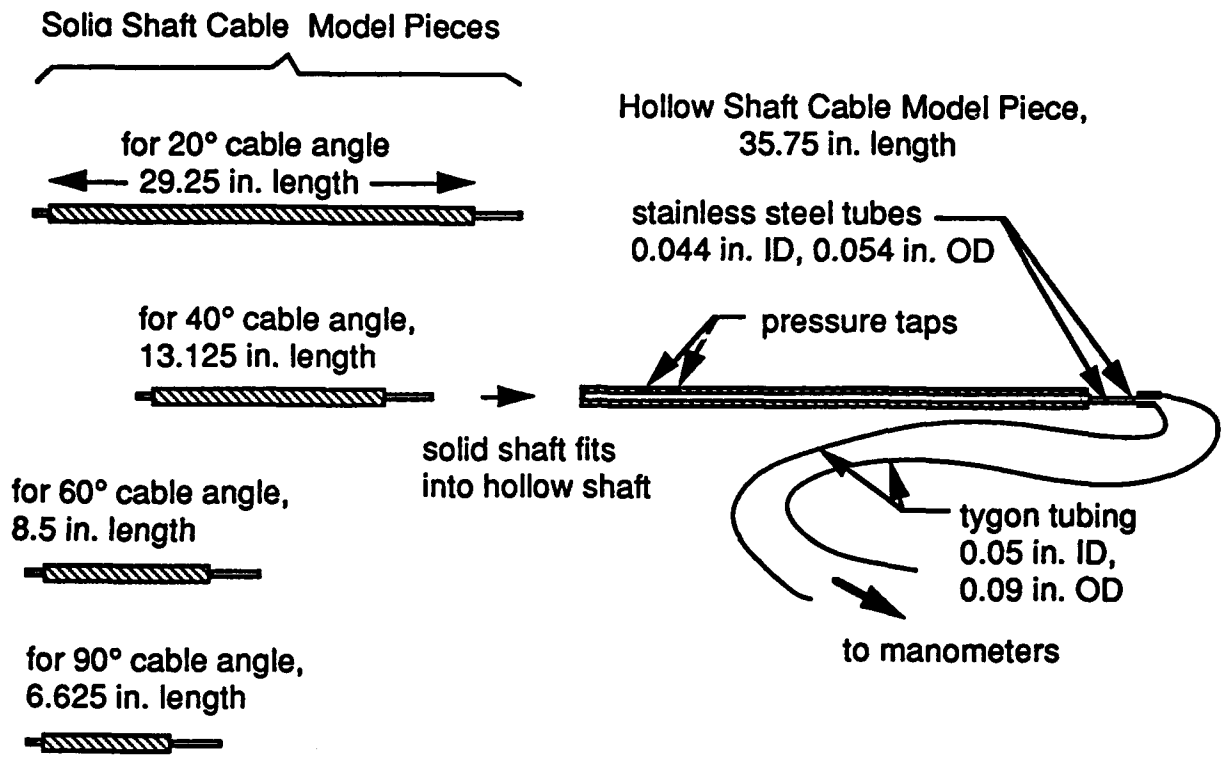


Figure 2 . Schematic of Pressure Models

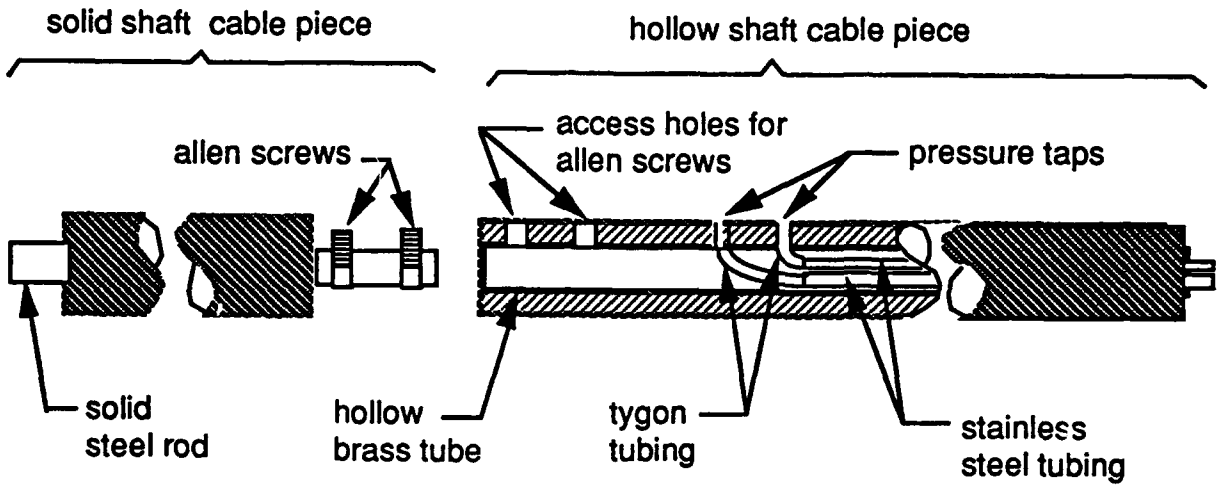


Figure 3. Two Piece Cable Model Assembly for Pressure Measurements

angular spacings between the taps are all equal to $\Delta\theta=45°$

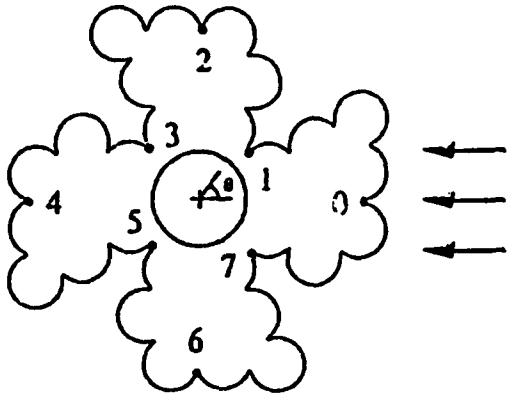


Schematic of 4x7 Cable
for Low Reynolds Number Tests

angular spacings between the taps are all equal to $\Delta\theta=30°$

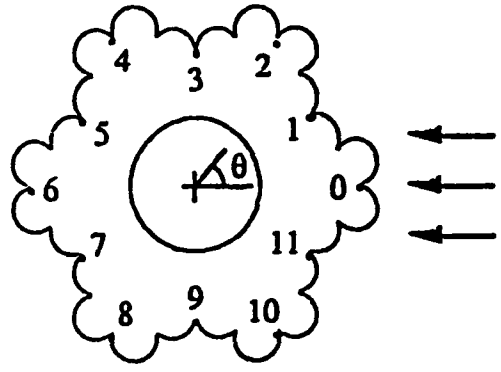


Schematic of 7x7 Cable
for Low Reynolds Number Tests

Figure 4. Schematic of Pressure Tap Locations on Cast Epoxy Models

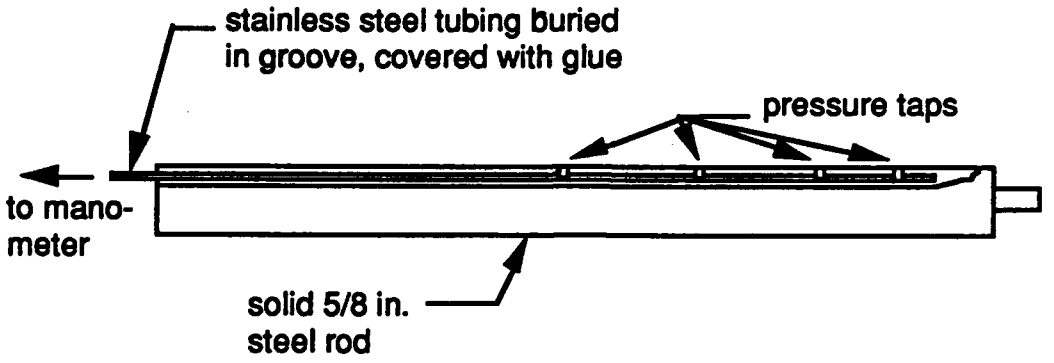


Figure 5 . Small Diameter Cylinder Model for Pressure Measurements

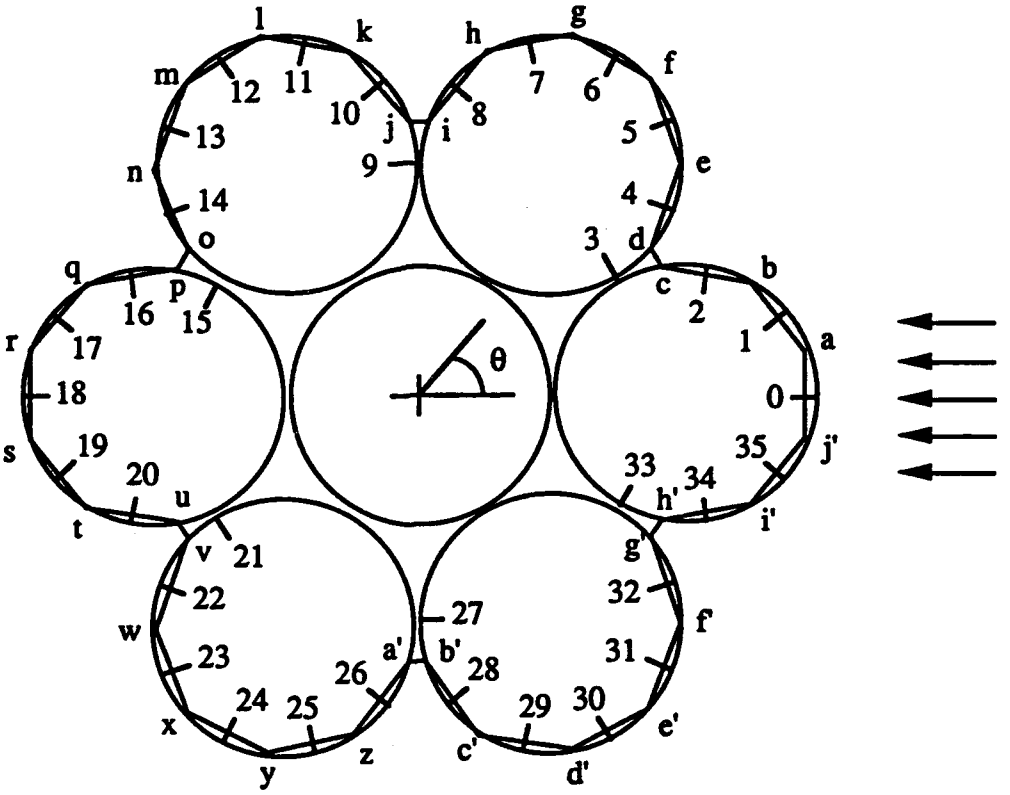


| Tap | θ° | Tap | θ° | Tap | θ° | Pt. | r/D | θ° | Pt. | r/D | θ° | Pt. | r/D | θ° |
|---|---|---|---|---|---|---|---|---|---|---|---|---|---|---|
| 0 | 0 | 12 | 120 | 24 | 240 | a | 0.49 | 7 | m | 0.49 | 127 | w | 0.49 | 247 |
| 1 | 13 | 13 | 133 | 25 | 253 | b | 0.44 | 19 | n | 0.44 | 139 | z | 0.44 | 259 |
| 2 | 24 | 14 | 144 | 26 | 264 | c | 0.29 | 28 | o | 0.29 | 148 | a' | 0.29 | 268 |
| 3 | 30 | 15 | 150 | 27 | 270 | d | 0.29 | 32 | p | 0.29 | 152 | b' | 0.29 | 272 |
| 4 | 36 | 16 | 156 | 28 | 276 | e | 0.44 | 41 | q | 0.44 | 161 | c' | 0.44 | 281 |
| 5 | 47 | 17 | 167 | 29 | 287 | f | 0.49 | 53 | r | 0.49 | 173 | d' | 0.49 | 293 |
| 6 | 60 | 18 | 180 | 30 | 300 | g | 0.49 | 67 | s | 0.49 | 187 | e' | 0.49 | 307 |
| 7 | 73 | 19 | 193 | 31 | 313 | h | 0.44 | 79 | t | 0.44 | 199 | f' | 0.44 | 319 |
| 8 | 84 | 20 | 204 | 32 | 324 | i | 0.29 | 88 | u | 0.29 | 208 | g' | 0.29 | 328 |
| 9 | 90 | 21 | 210 | 33 | 330 | j | 0.29 | 92 | v | 0.29 | 212 | h' | 0.29 | 332 |
| 10 | 96 | 22 | 216 | 34 | 336 | k | 0.44 | 101 | w | 0.44 | 221 | i' | 0.44 | 341 |
| 11 | 107 | 23 | 227 | 35 | 347 | l | 0.49 | 113 | x | 0.49 | 233 | j' | 0.49 | 353 |

Figure 6. Schematic of 7x1 Cable Model

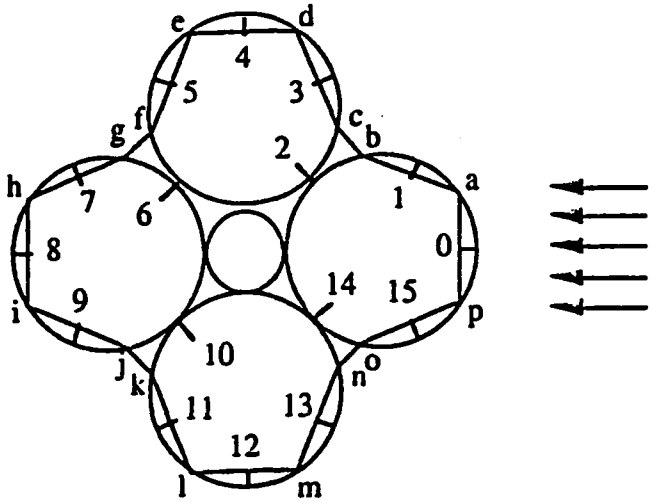


| Tap | θ° | Tap | θ° | Tap | θ° | Pt. | r/D | θ° | Pt. | r/D | θ° | Pt. | r/D | θ° |
|---|---|---|---|---|---|---|---|---|---|---|---|---|---|---|
| 0 | 0 | 6 | 135 | 11 | 243 | a | 0.48 | 14 | g | 0.32 | 141 | l | 0.48 | 256 |
| 1 | 27 | 7 | 153 | 12 | 270 | b | 0.32 | 39 | h | 0.48 | 166 | m | 0.48 | 284 |
| 2 | 45 | 8 | 180 | 13 | 297 | c | 0.32 | 51 | i | 0.48 | 194 | n | 0.32 | 309 |
| 3 | 63 | 9 | 207 | 14 | 315 | *d* | 0.48 | 76 | j | 0.32 | 219 | o | 0.32 | 321 |
| 4 | 90 | 10 | 225 | 15 | 333 | e | 0.48 | 104 | k | 0.32 | 231 | p | 0.48 | 346 |
| 5 | 117 | | | | | f | 0.32 | 129 | | | | | | |

Figure 7. Schematic of 4x1 Cable

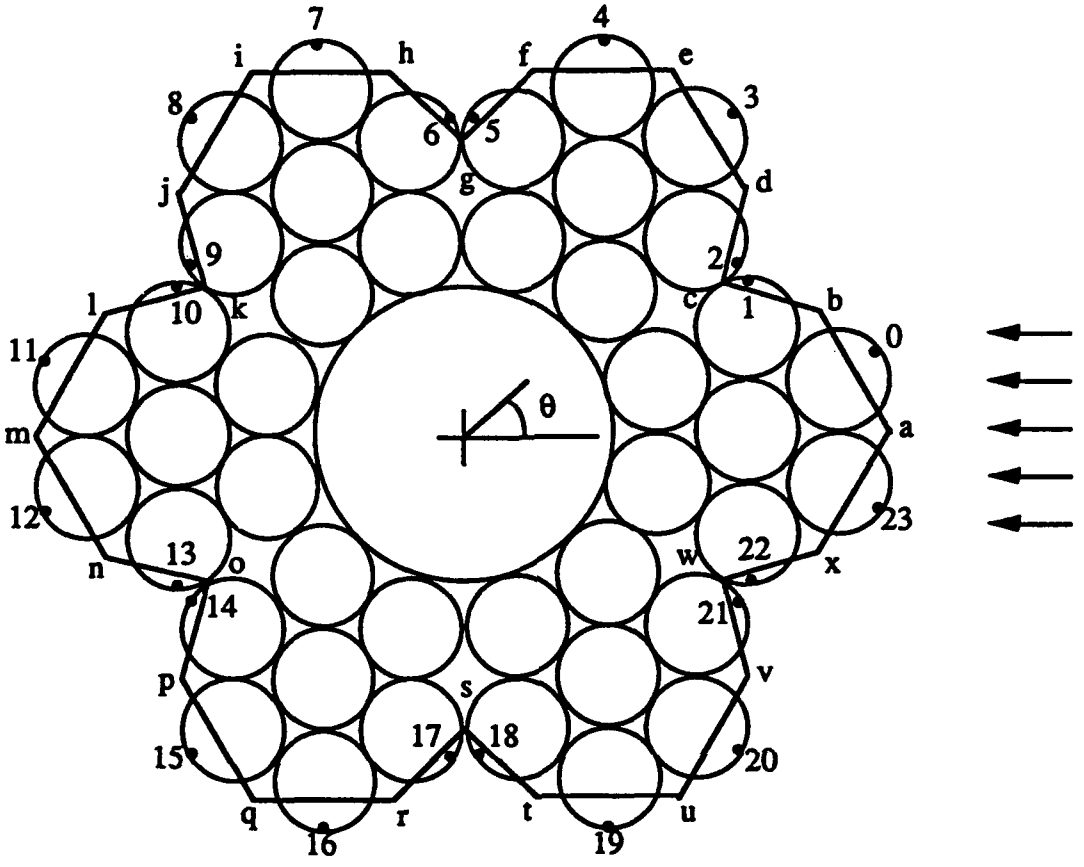


| Tap | θ° | Tap | θ° | Tap | θ° | Pt. | r/D | θ° | Pt. | r/D | θ° | Pt. | r/D | θ° |
|---|---|---|---|---|---|---|---|---|---|---|---|---|---|---|
| 0 | 10 | 8 | 130 | 16 | 250 | a | 0.50 | 0 | i | 0.50 | 120 | q | 0.50 | 240 |
| 1 | 27 | 9 | 147 | 17 | 267 | b | 0.44 | 19 | j | 0.44 | 139 | r | 0.44 | 259 |
| 2 | 33 | 10 | 153 | 18 | 273 | c | 0.35 | 30 | k | 0.35 | 150 | s | 0.35 | 270 |
| 3 | 50 | 11 | 170 | 19 | 290 | d | 0.44 | 41 | l | 0.44 | 161 | t | 0.44 | 281 |
| 4 | 70 | 12 | 190 | 20 | 310 | e | 0.50 | 60 | m | 0.50 | 180 | u | 0.50 | 300 |
| 5 | 87 | 13 | 207 | 21 | 327 | f | 0.44 | 79 | n | 0.44 | 199 | v | 0.44 | 319 |
| 6 | 93 | 14 | 213 | 22 | 333 | g | 0.35 | 90 | o | 0.35 | 210 | w | 0.35 | 330 |
| 7 | 110 | 15 | 230 | 23 | 350 | h | 0.44 | 101 | p | 0.44 | 221 | x | 0.44 | 341 |

Figure 8. Schematic of the 7x7 Cable for High Reynolds Number Tests

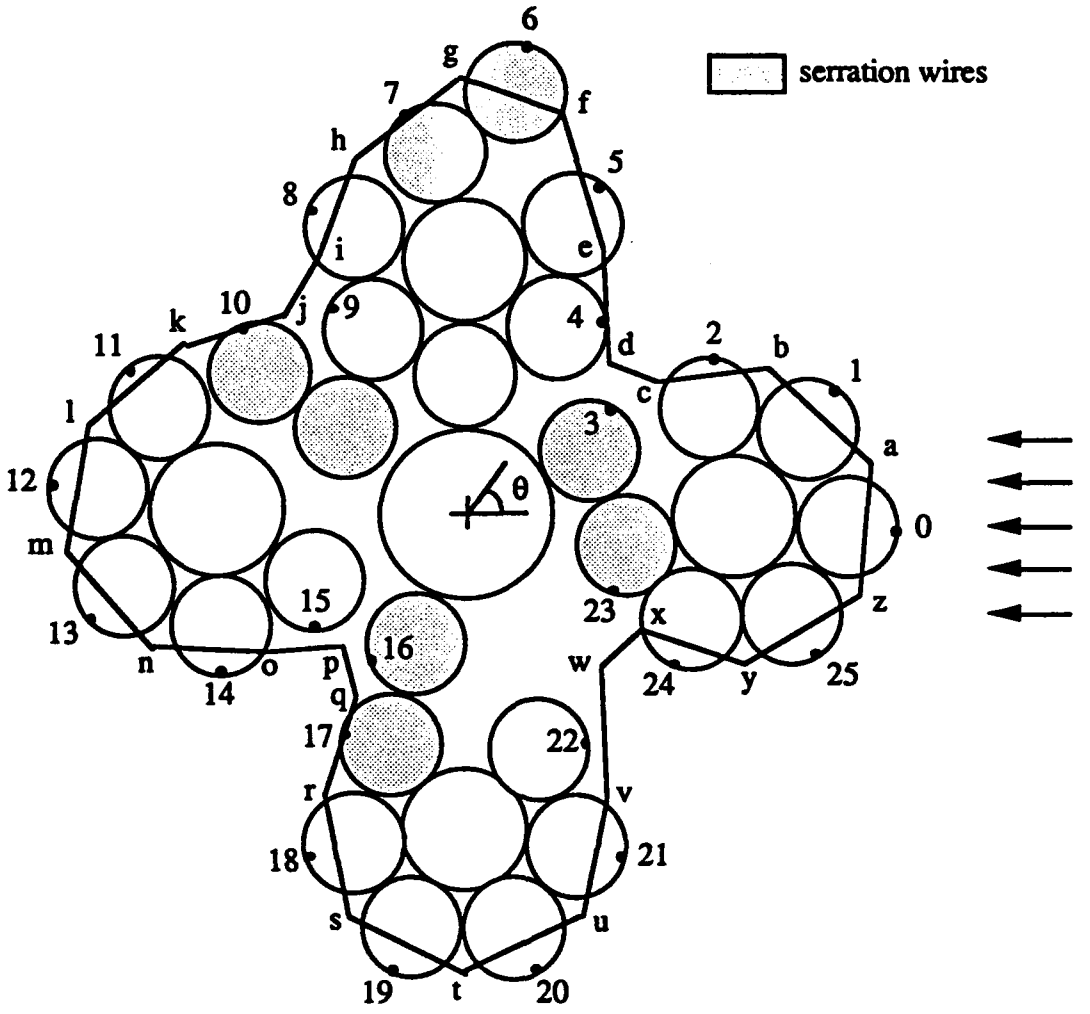


| Tap | θ° | Tap | θ° | Tap | θ° | Pt. | r/D | θ° | Pt. | r/D | θ° | Pt. | r/D | θ° |
|---|---|---|---|---|---|---|---|---|---|---|---|---|---|---|
| 0 | -3 | 9 | 124 | 18 | 245 | a | 0.42 | 7 | j | 0.29 | 133 | s | 0.45 | 253 |
| 1 | 18 | 10 | 140 | 19 | 260 | b | 0.36 | 24 | k | 0.36 | 150 | t | 0.49 | 269 |
| 2 | 33 | 11 | 158 | 20 | 278 | c | 0.25 | 34 | l | 0.42 | 167 | u | 0.45 | 285 |
| 3 | 36 | 12 | 176 | 21 | 294 | d | 0.22 | 45 | m | 0.42 | 186 | v | 0.35 | 296 |
| 4 | 54 | 13 | 197 | 22 | 298 | e | 0.31 | 61 | n | 0.36 | 204 | w | 0.23 | 311 |
| 5 | 66 | 14 | 215 | 23 | 324 | f | 0.43 | 76 | o | 0.26 | 216 | x | 0.23 | 327 |
| 6 | 84 | 15 | 219 | 24 | 332 | g | 0.46 | 92 | p | 0.19 | 226 | y | 0.34 | 333 |
| 7 | 101 | 16 | 234 | 25 | 339 | h | 0.39 | 109 | q | 0.23 | 237 | z | 0.42 | 348 |
| 8 | 117 | 17 | 241 | | | i | 0.32 | 121 | r | 0.34 | 243 | | | |

Figure 9. Schematic of the 4x7 Serrated Cable for High Reynolds Number Tests

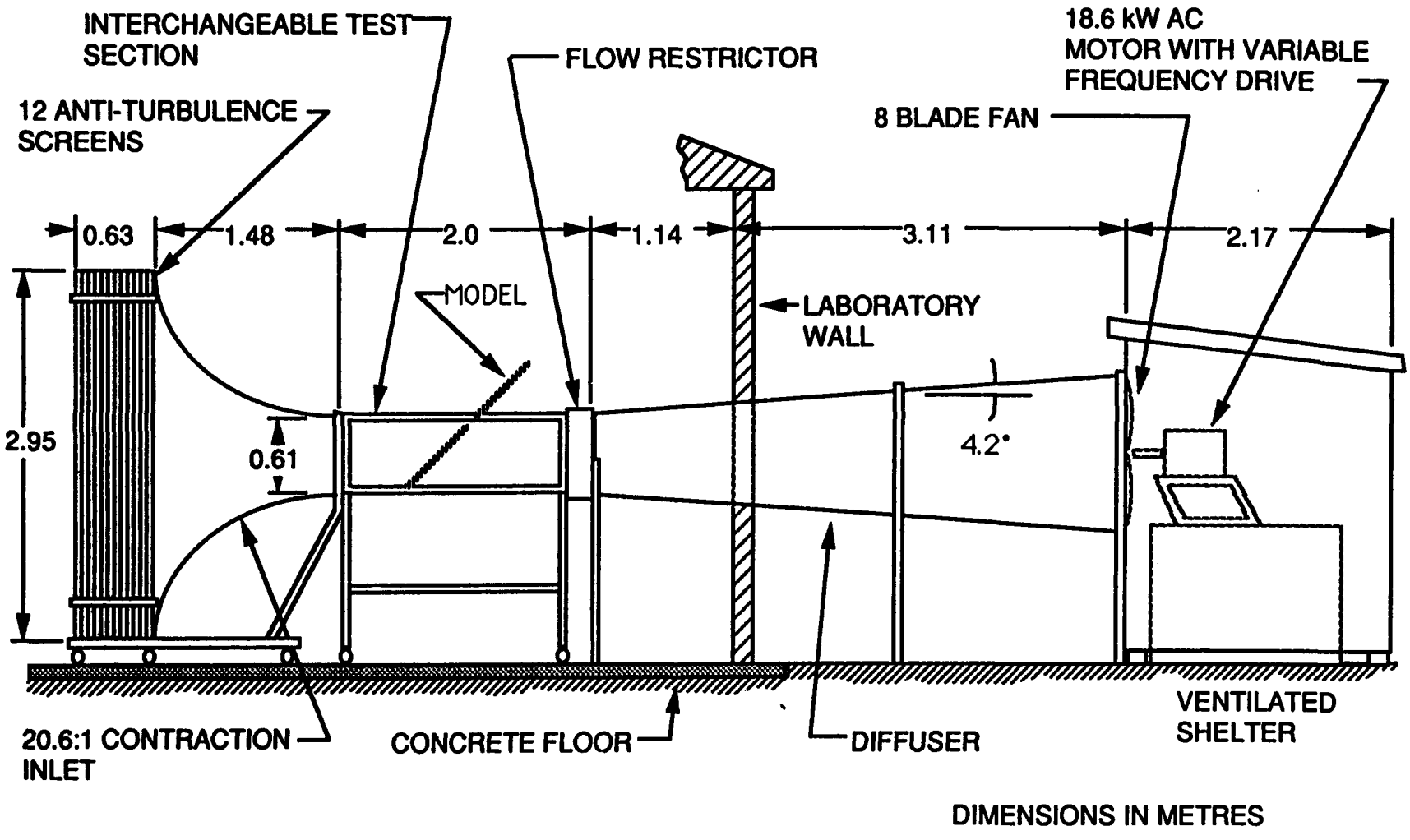


Figure 10: University of Notre Dame Wind Tunnel Facility

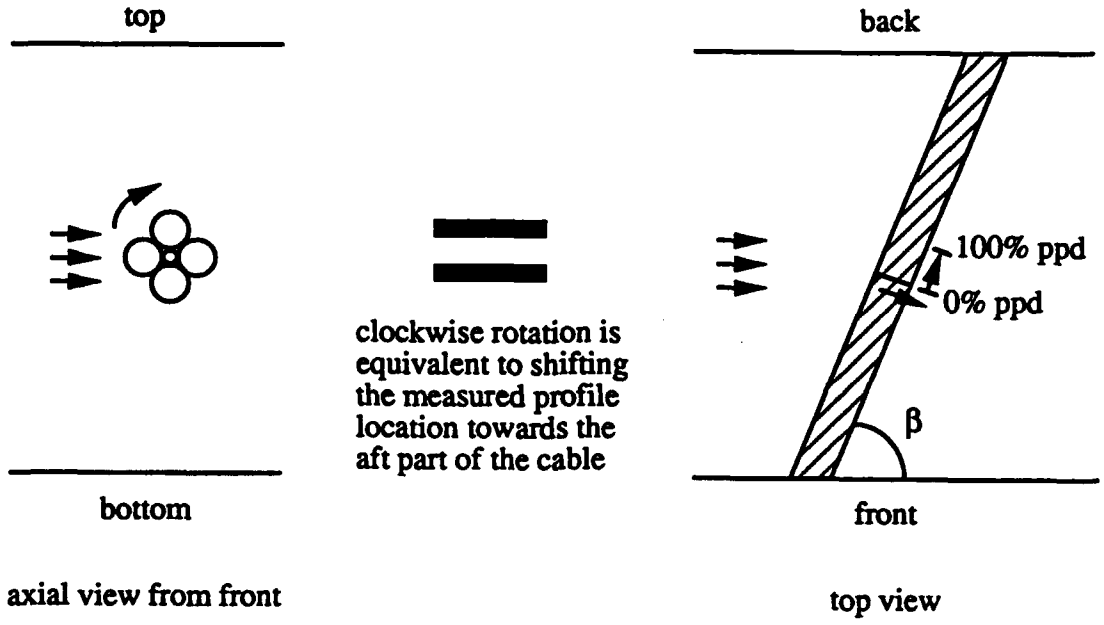


Right Lay Cable, e.g., 4x1 Cable

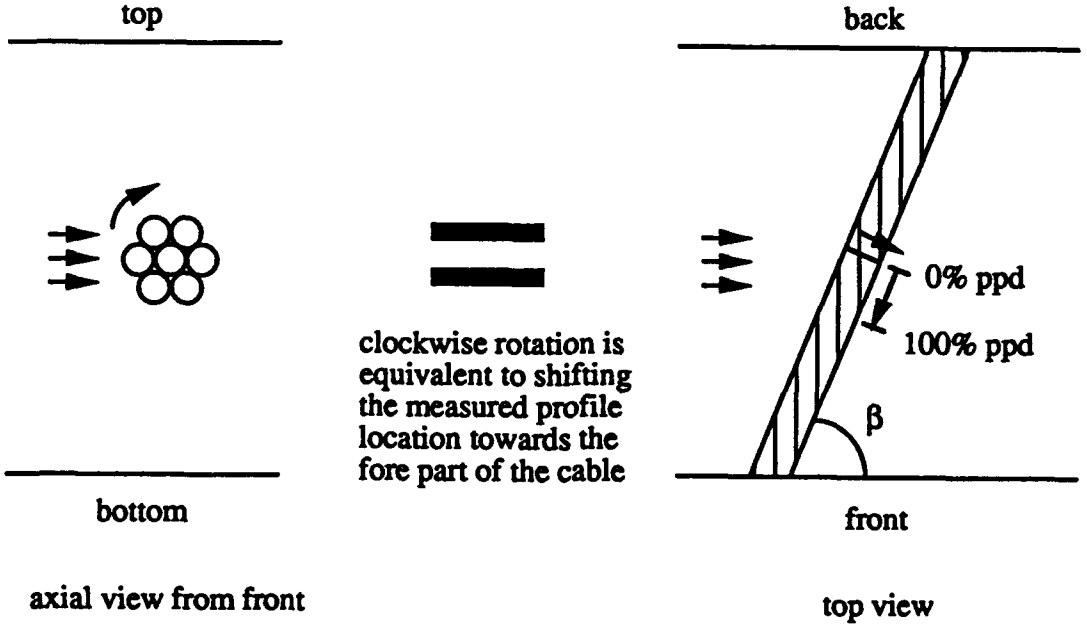


Left Lay Cable, e.g., 7x1 Cable

Figure 11. Equivalence of Rotation to the Spanwise Shift of the Measured Profile

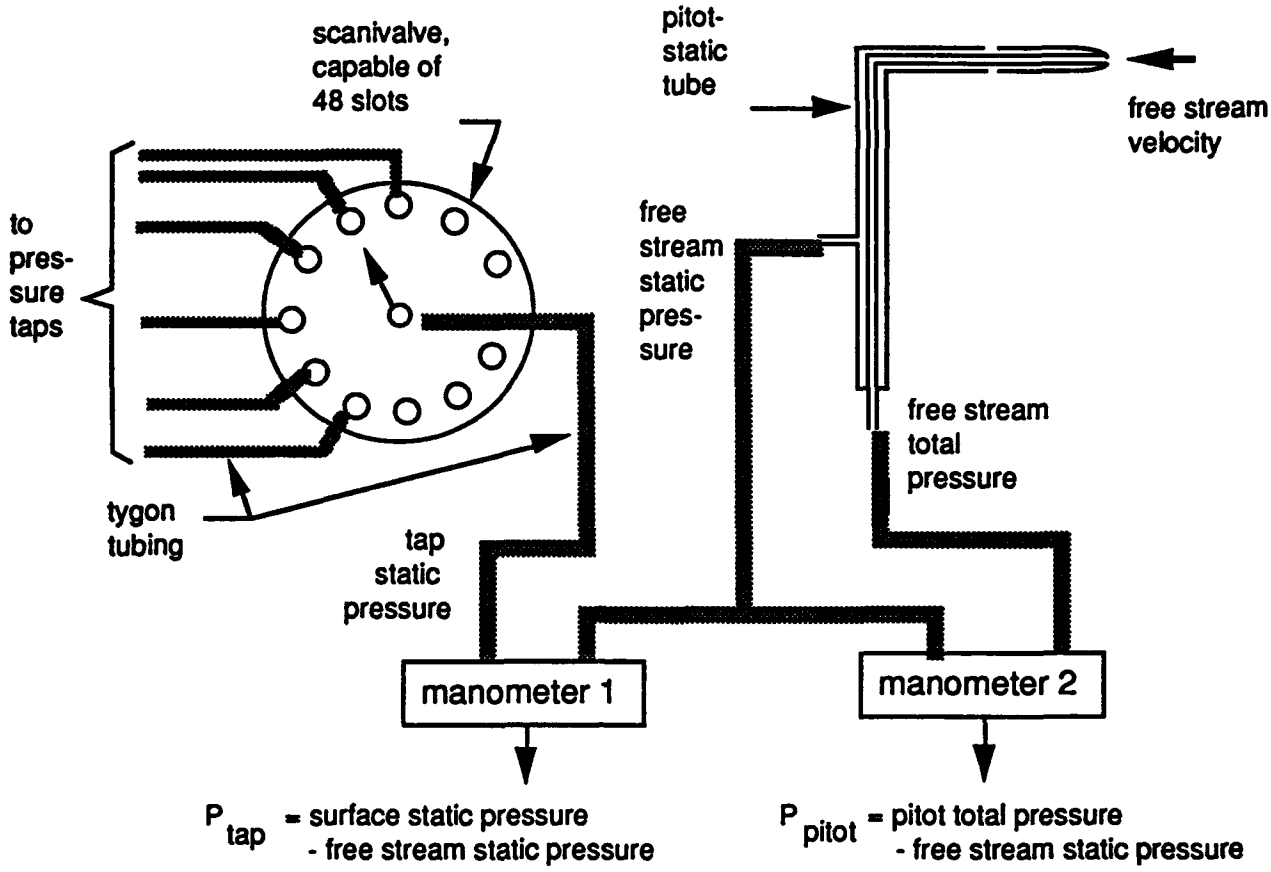


Figure 12. Schematic of the Pressure Measurement System

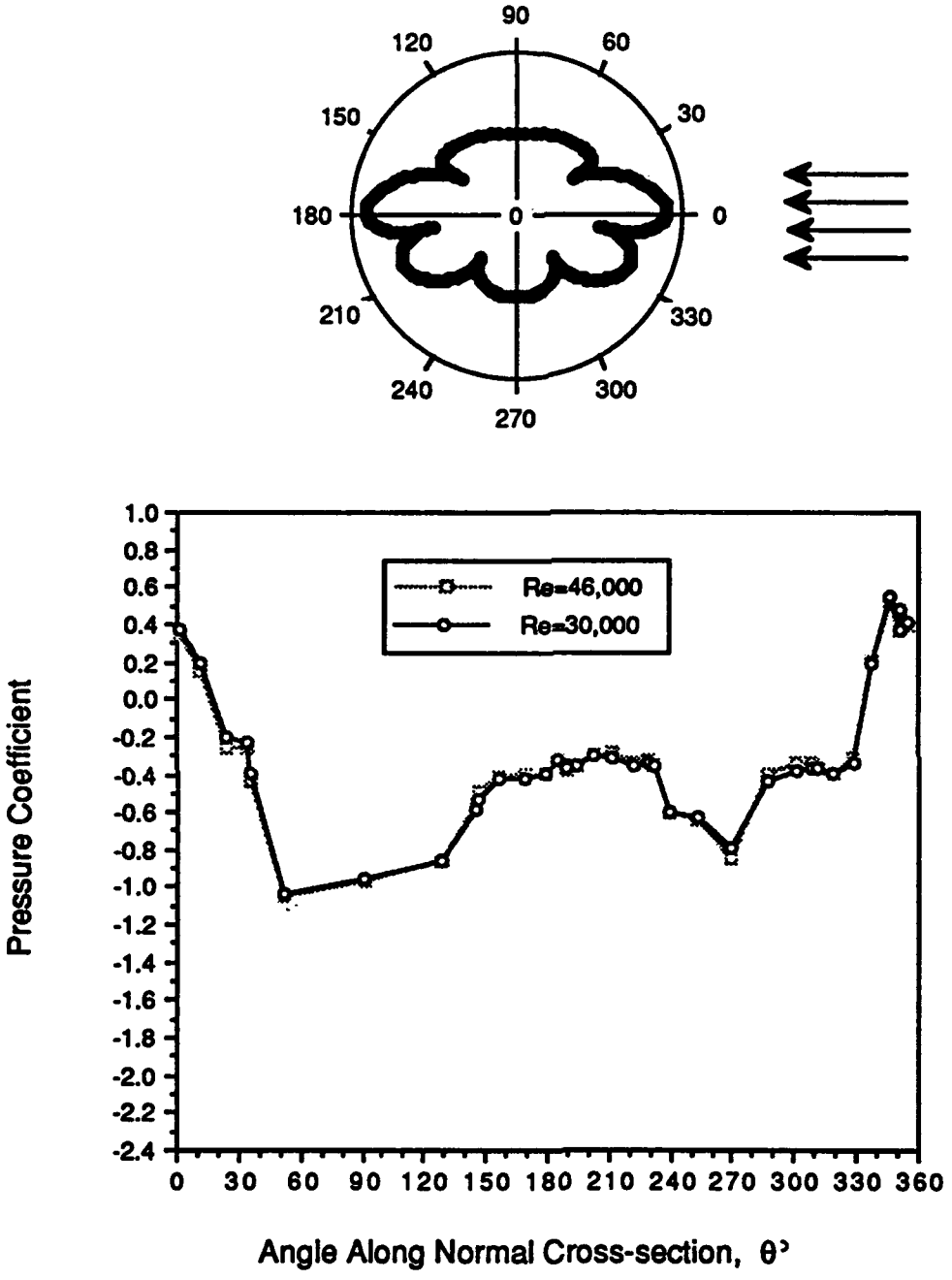


Figure 13: Pressure Profile Along a Streamwise Cross-section, 7x1 Cable
40° Cable Angle, 50% Peak to Peak Distance

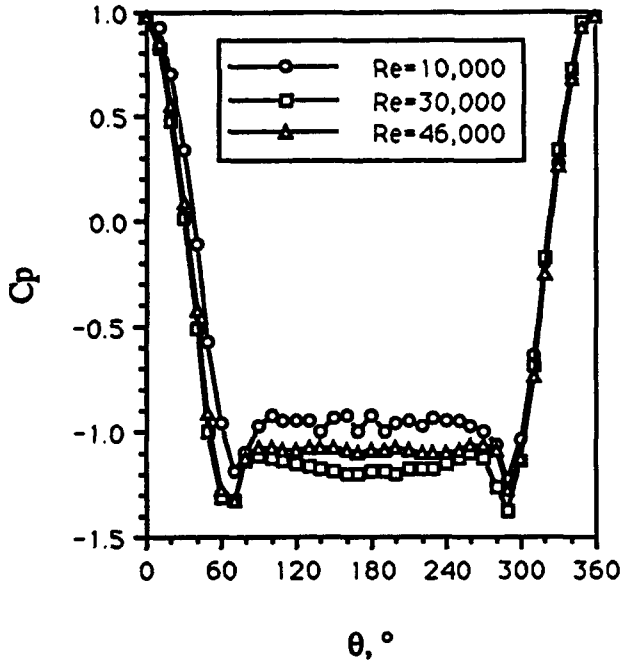


a) 90° Cable Angle

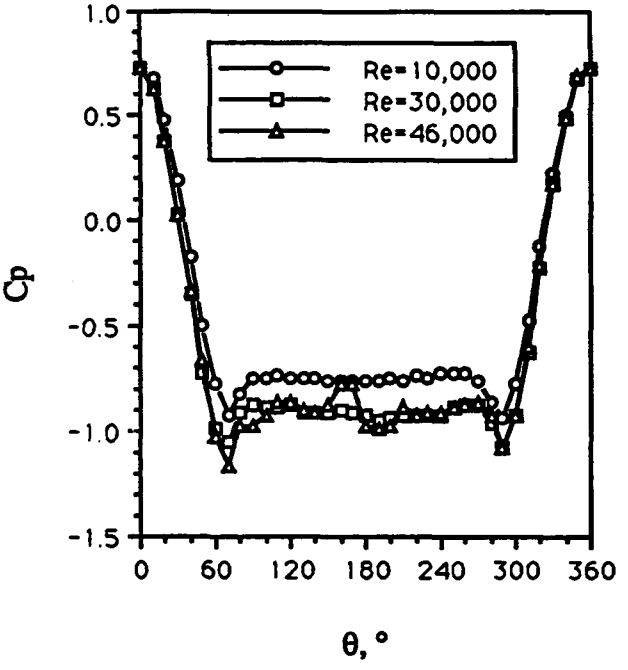


b) 60° Cable Angle

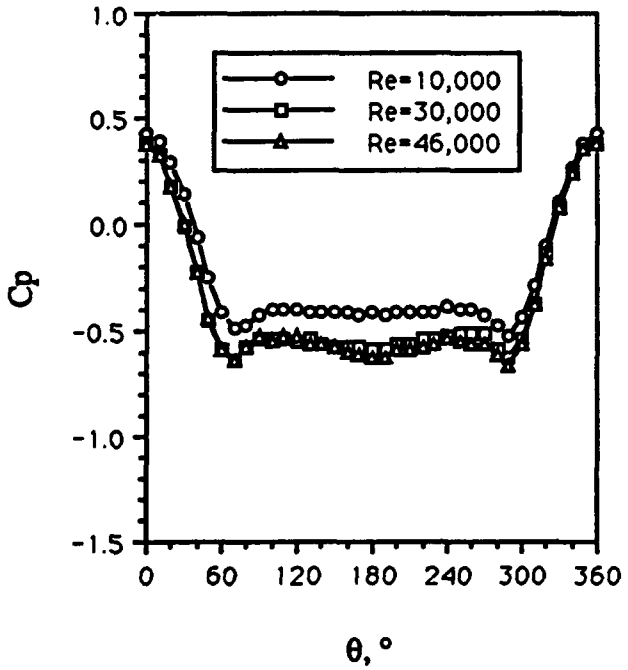


c) 40° Cable Angle

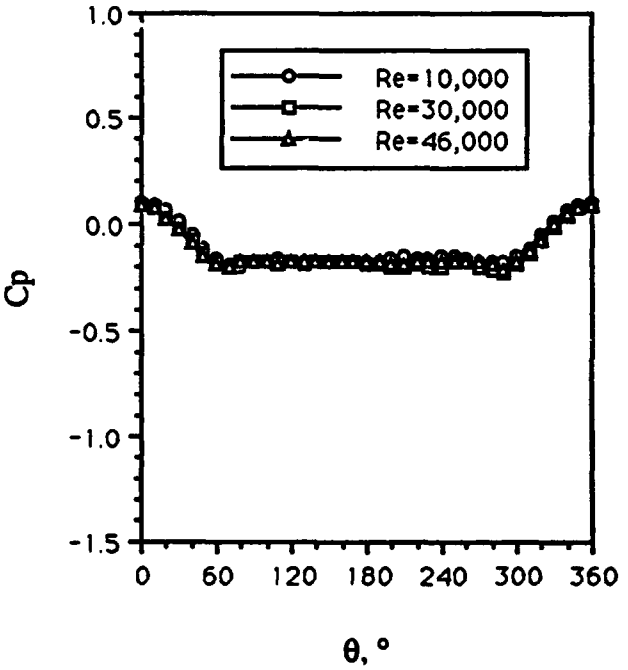


d) 20° Cable Angle

Figure 14. Pressure Distribution around the Circular Cylinder

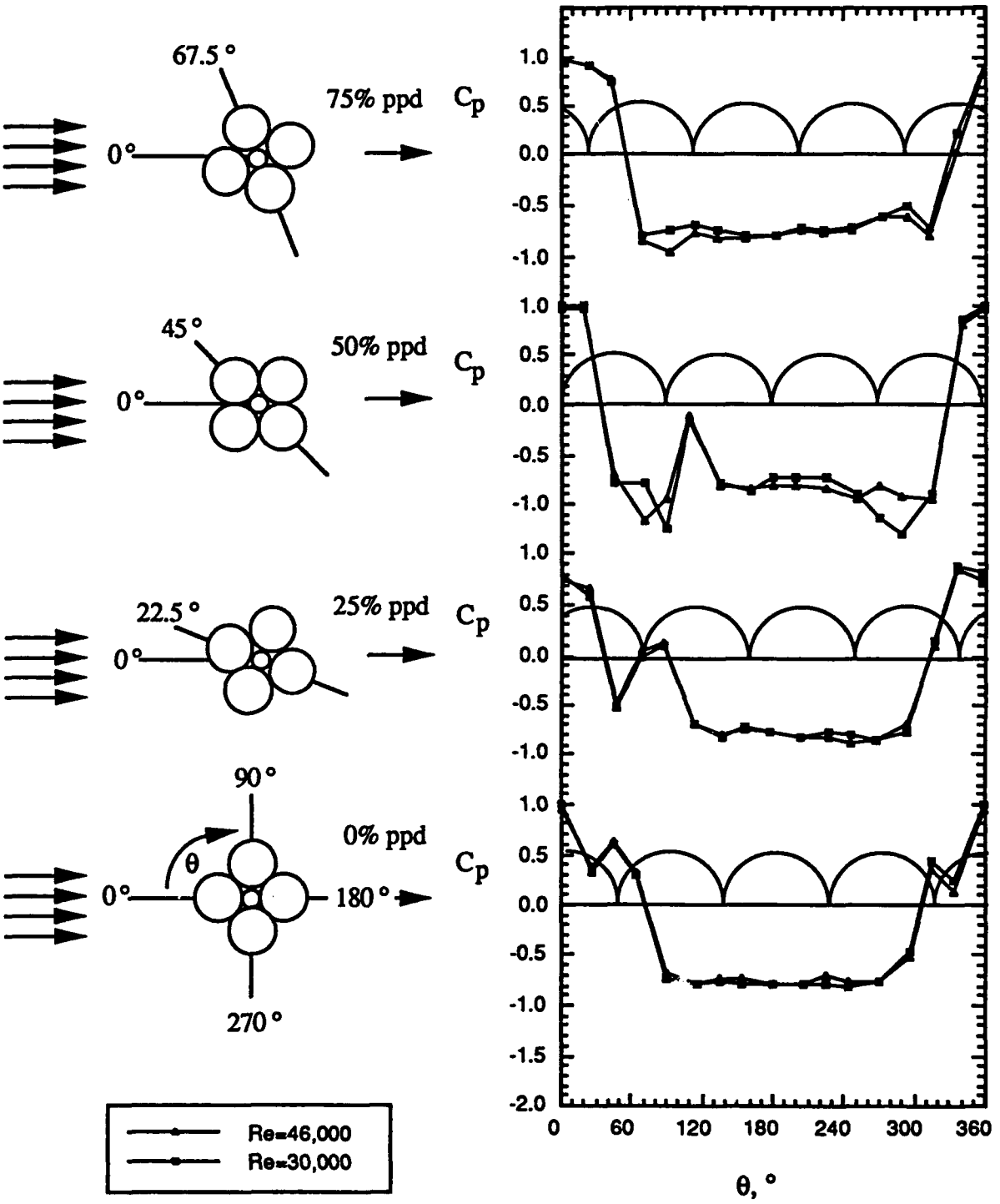


Figure 15. 4x1 cable, right lay, 90° cable angle

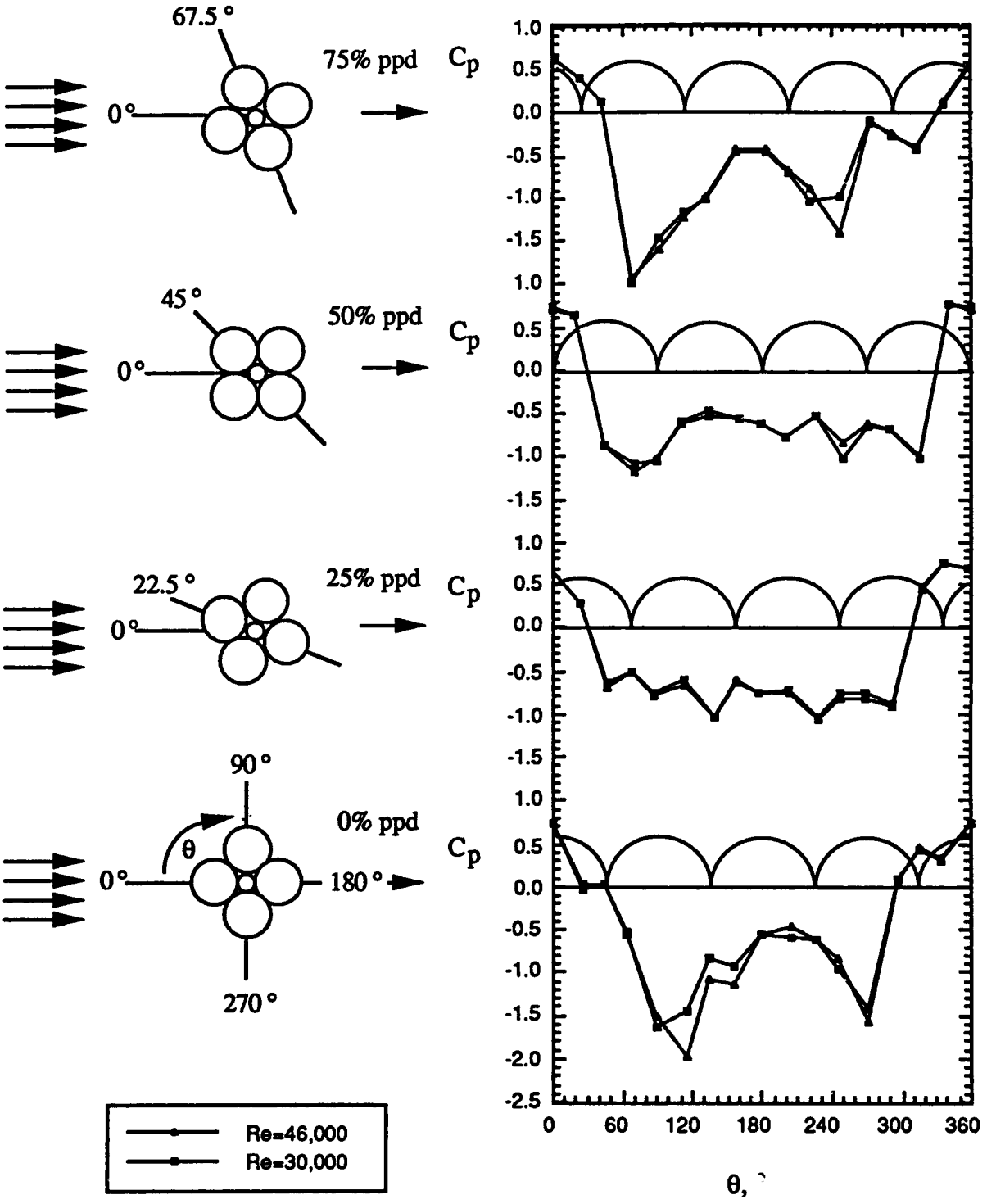


Figure 16. 4x1 cable, right lay, 60° cable angle

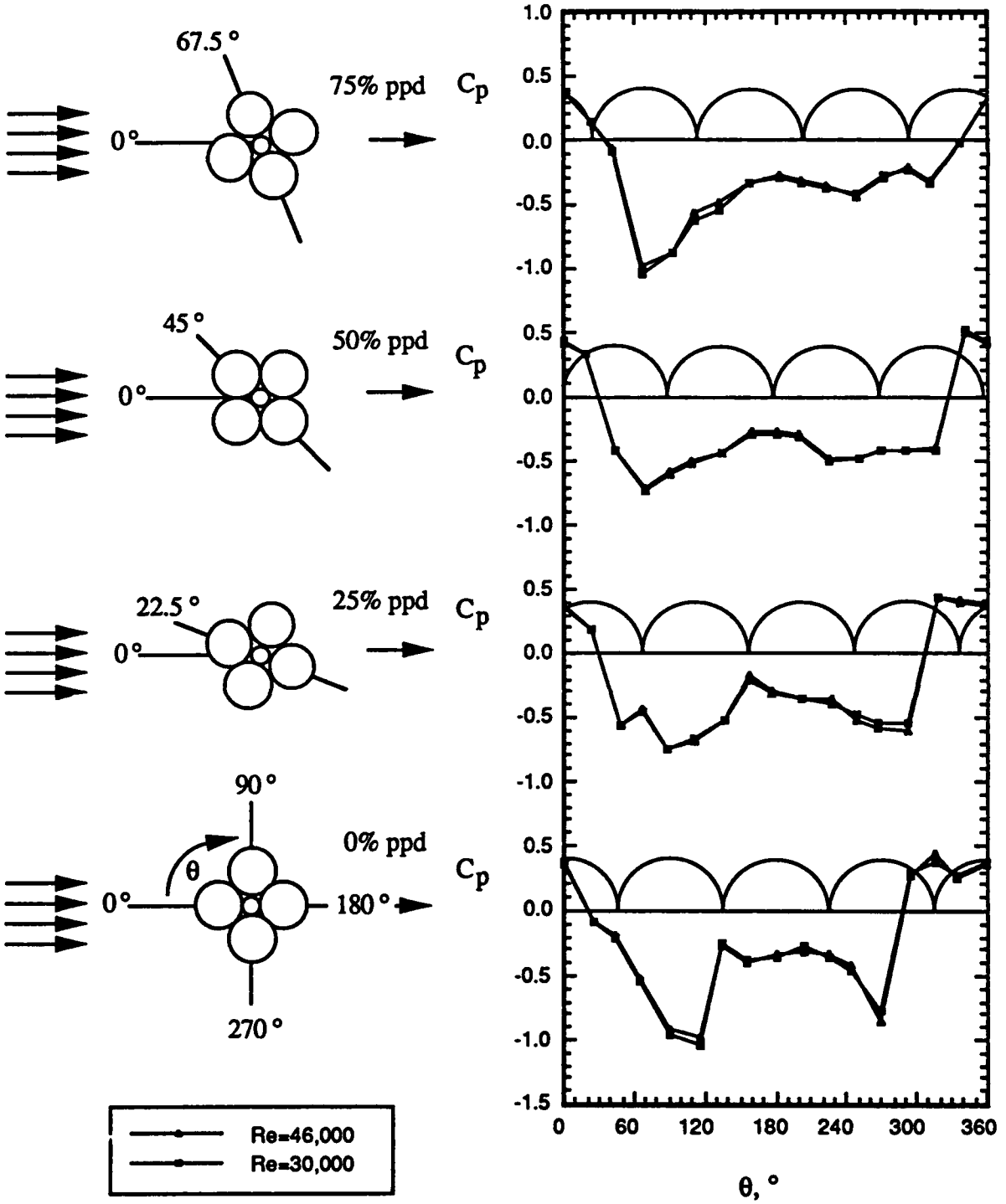


Figure 17. 4x1 cable, right lay, 40° cable angle

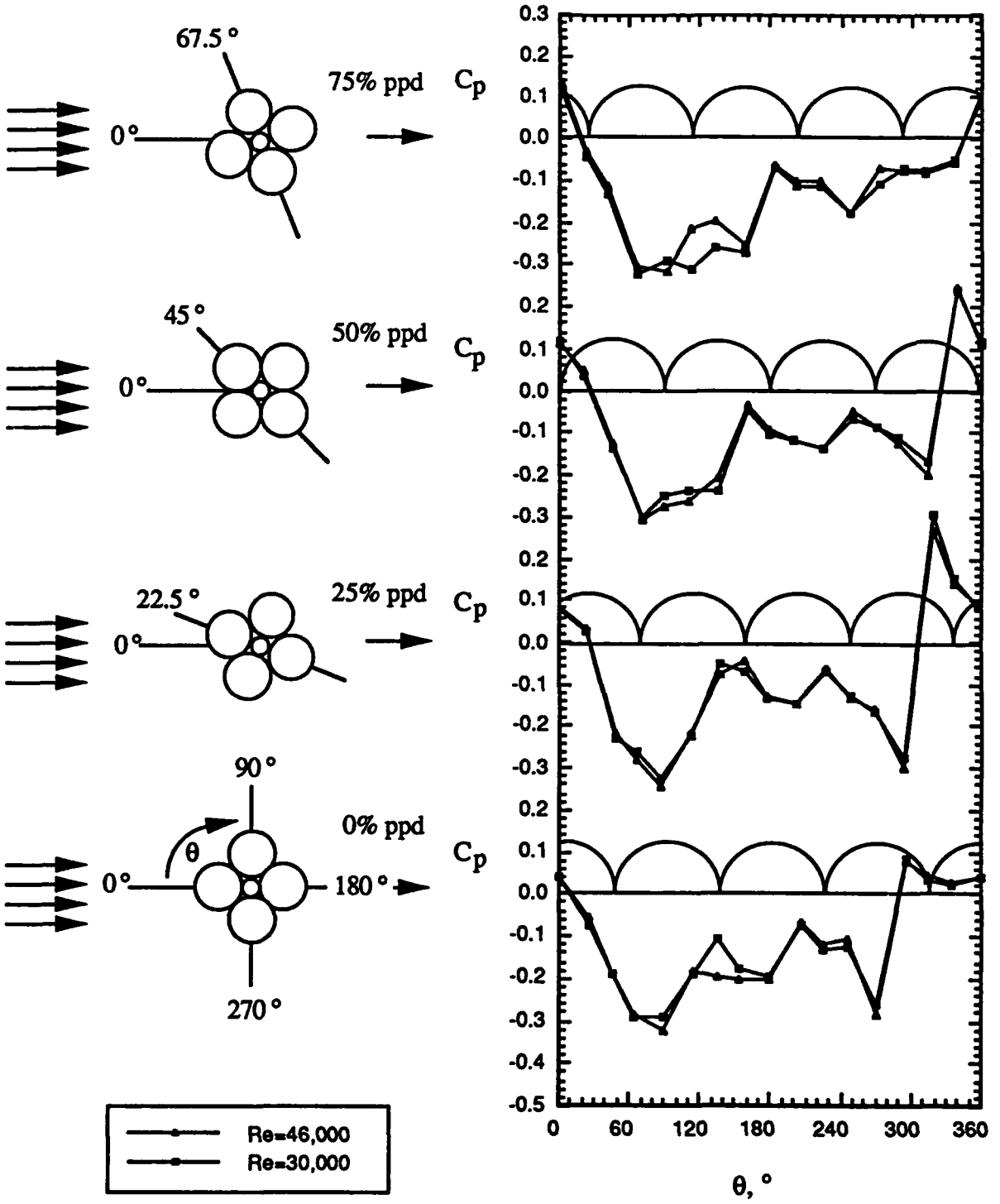


Figure 18. 4x1 cable, right lay, 20° cable angle

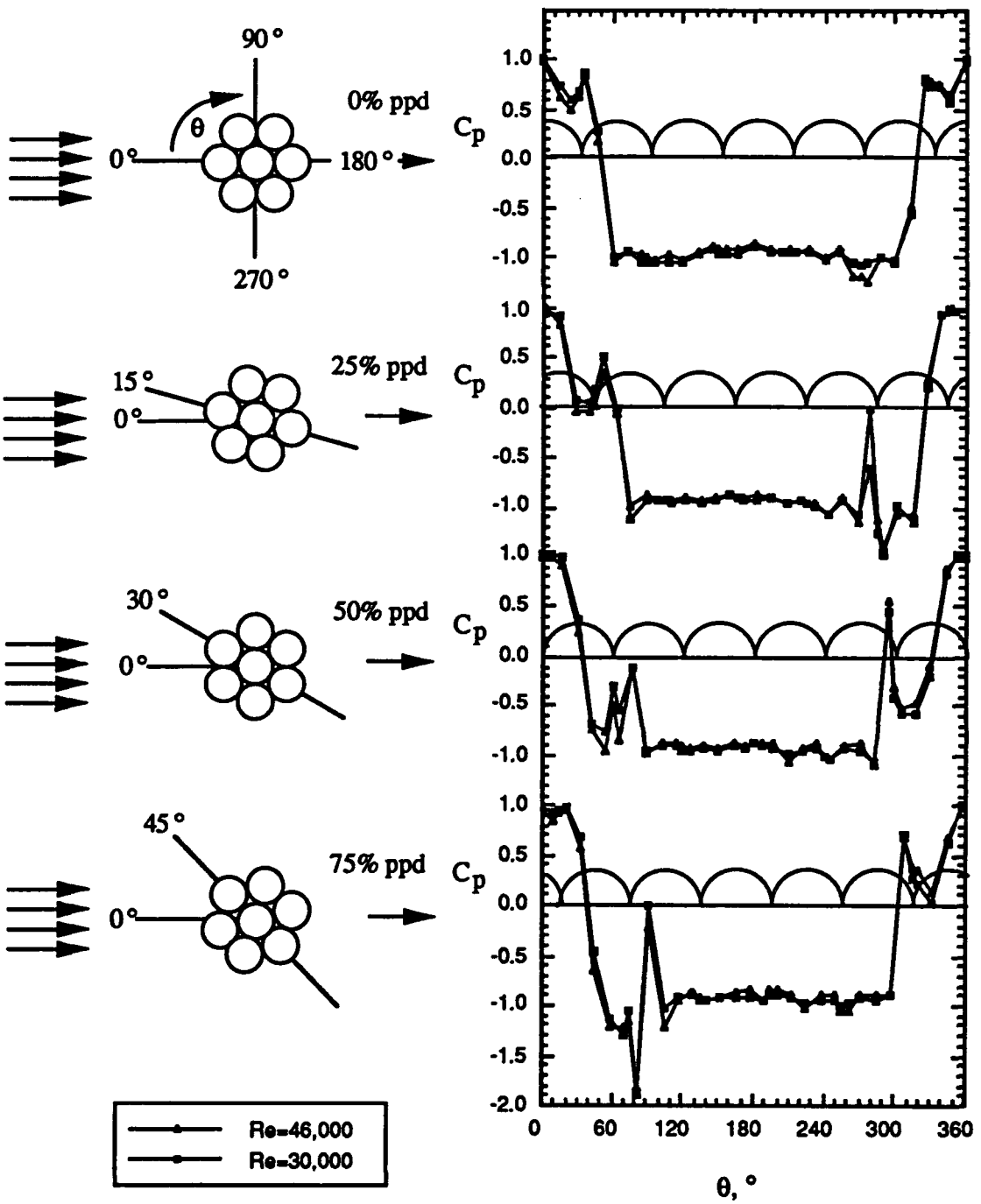


Figure 19. 7x1 cable, left lay, 90° cable angle

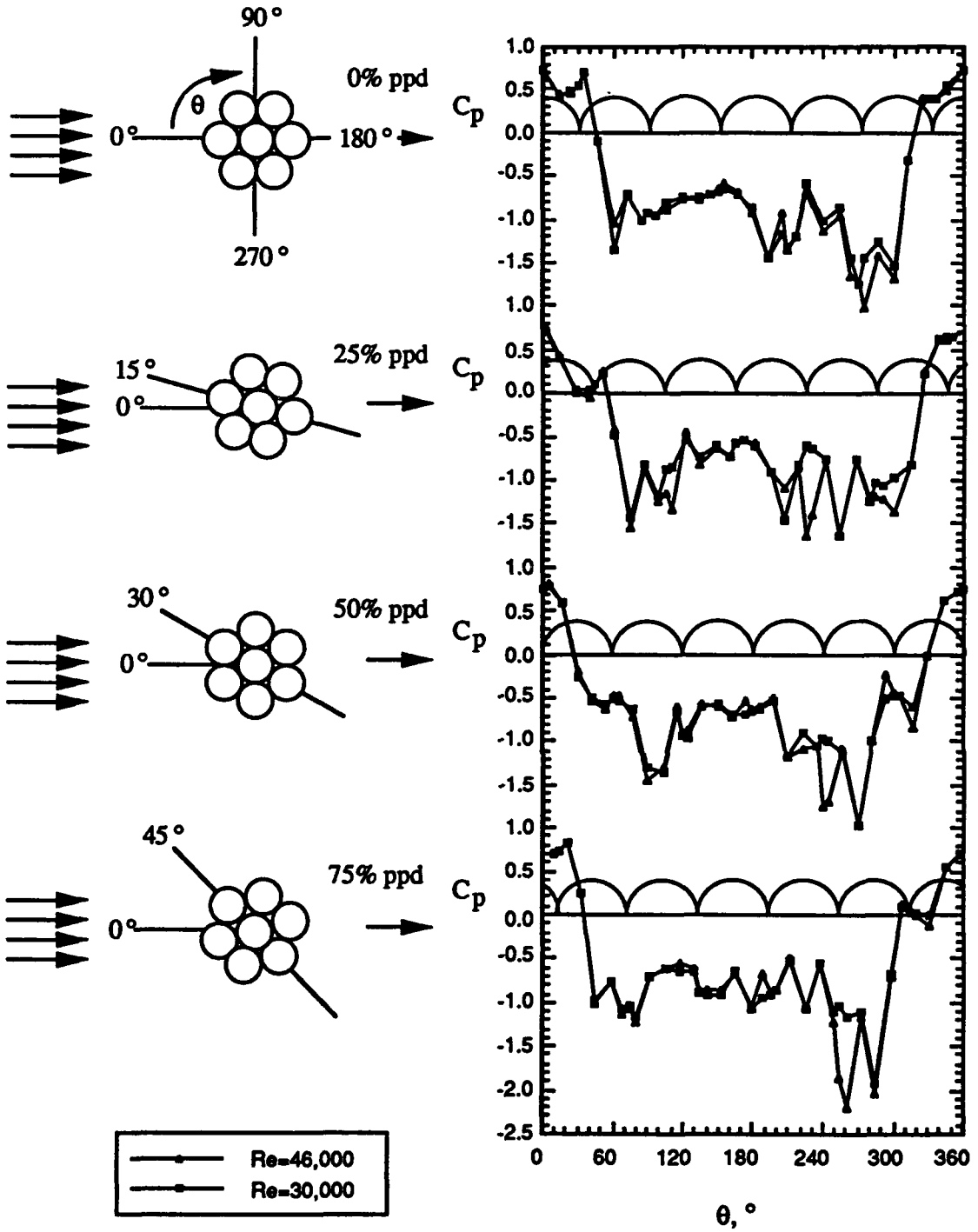


Figure 20. 7x1 cable, left lay, 60° cable angle

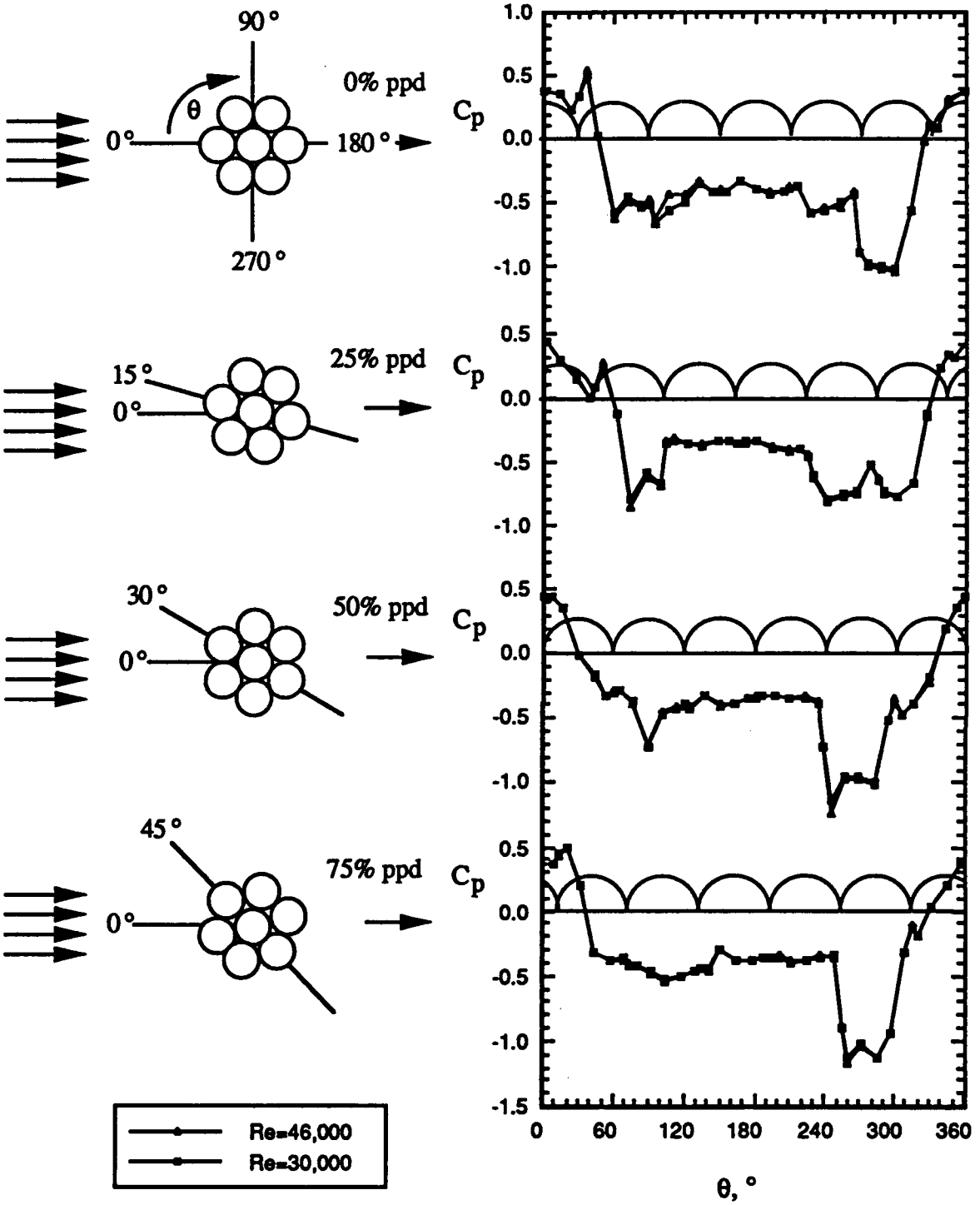


Figure 21. 7x1 cable, left lay, 40° cable angle

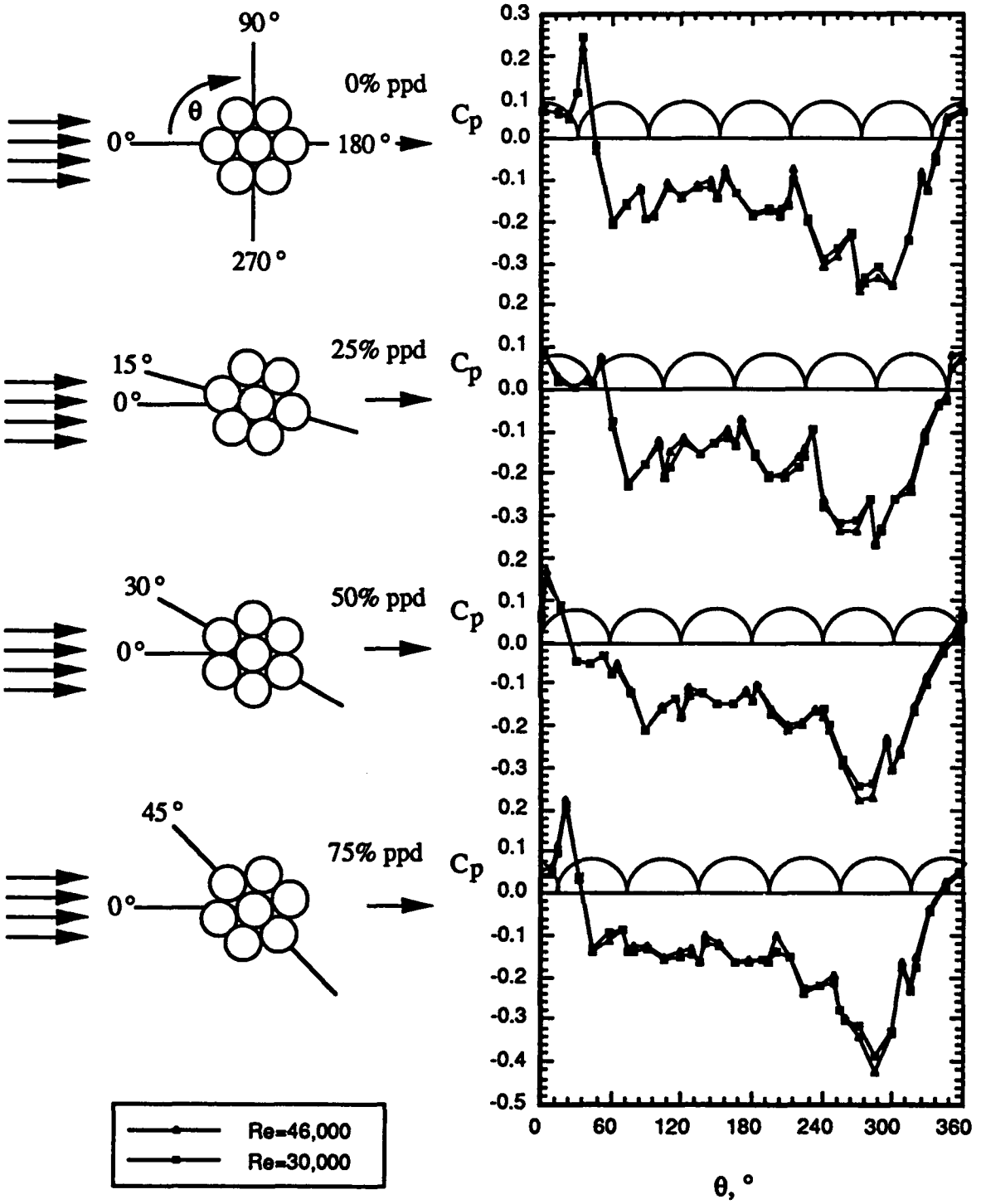


Figure 22. 7x1 cable, left lay, 20° cable angle

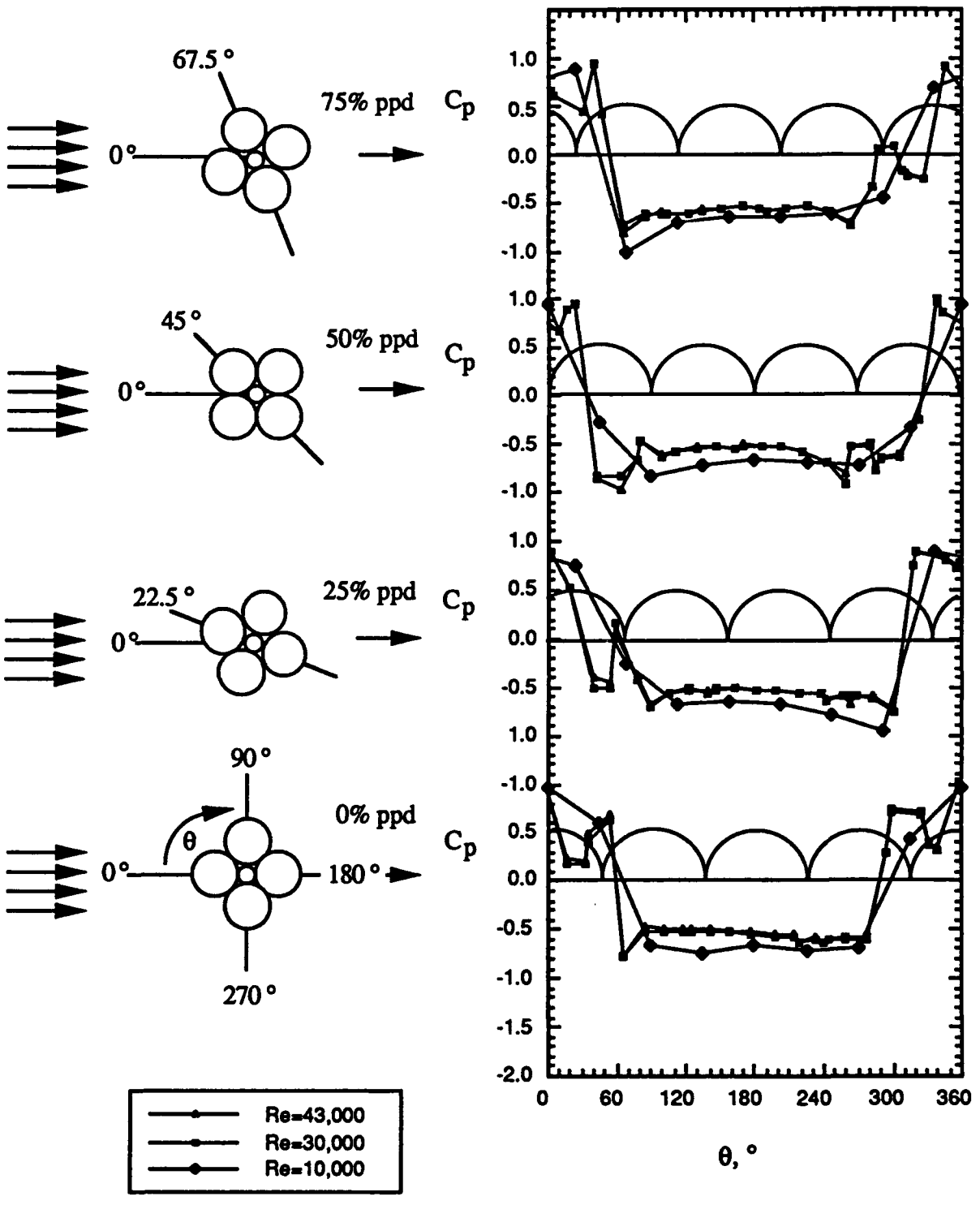


Figure 23. 4x7 cable, right lay, 90° Cable Angle

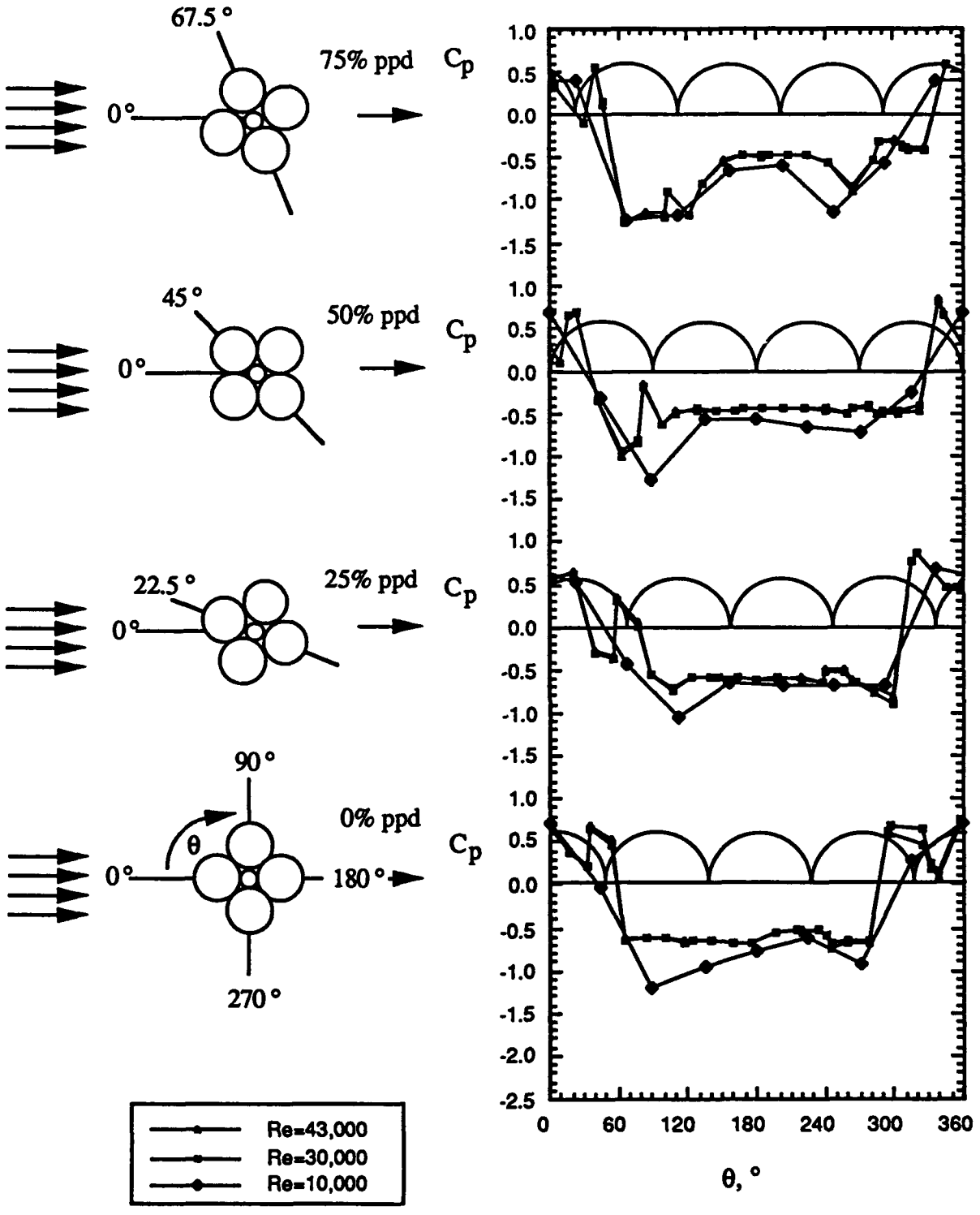


Figure 24. 4x7 cable, right lay, 60° Cable Angle

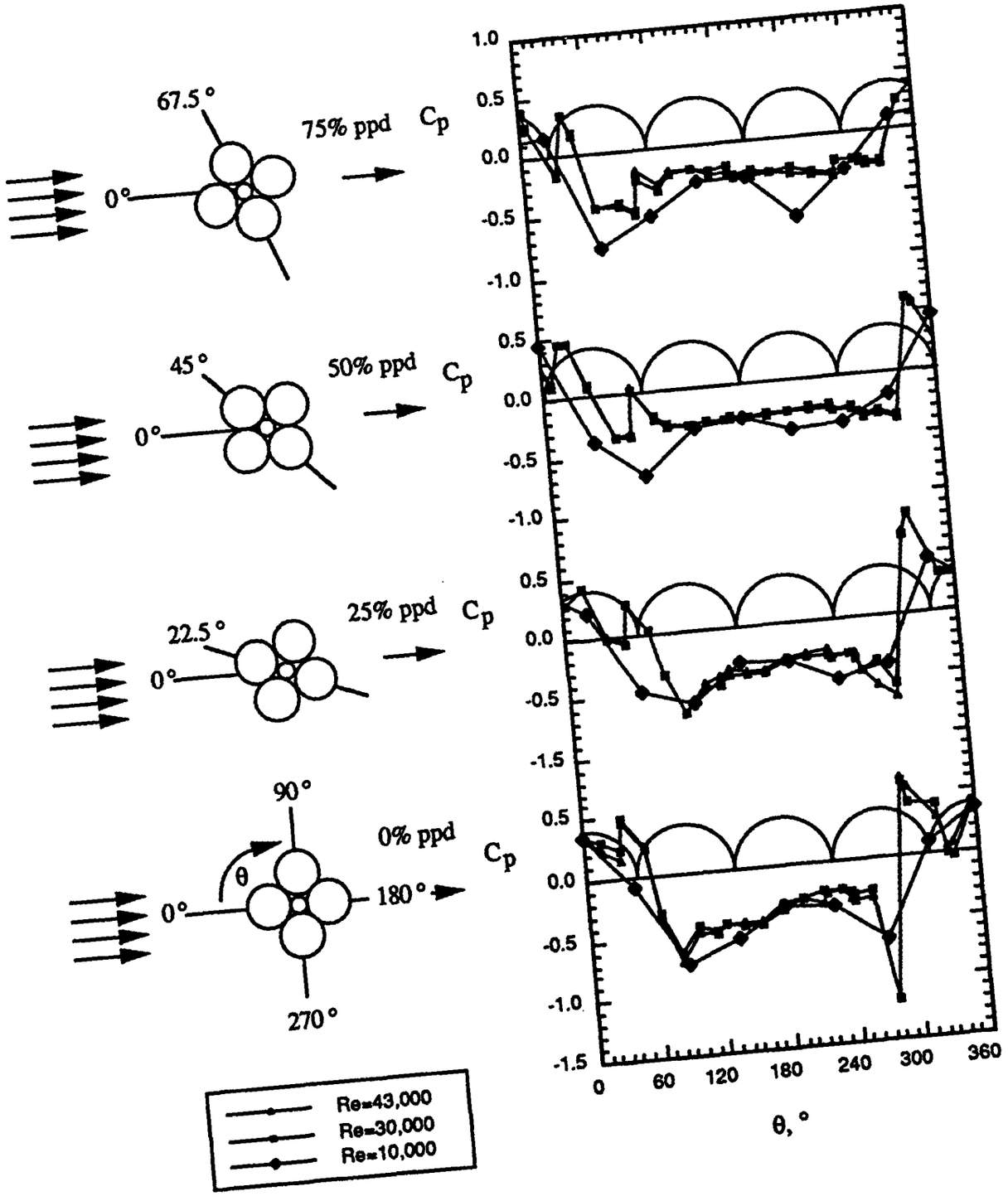


Figure 25. 4x7 cable, right lay, 40° Cable Angle

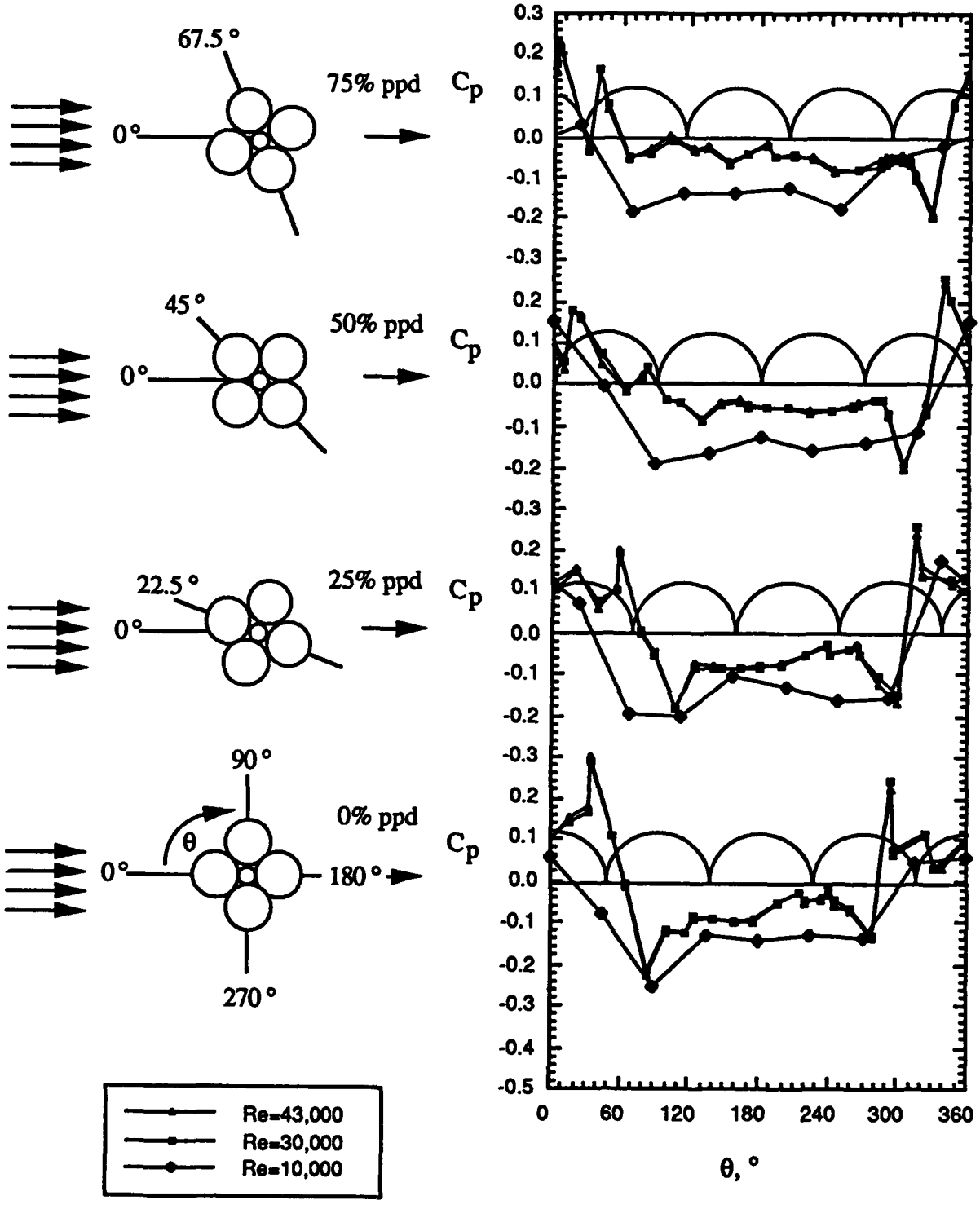


Figure 26. 4x7 cable, right lay, 20° Cable Angle

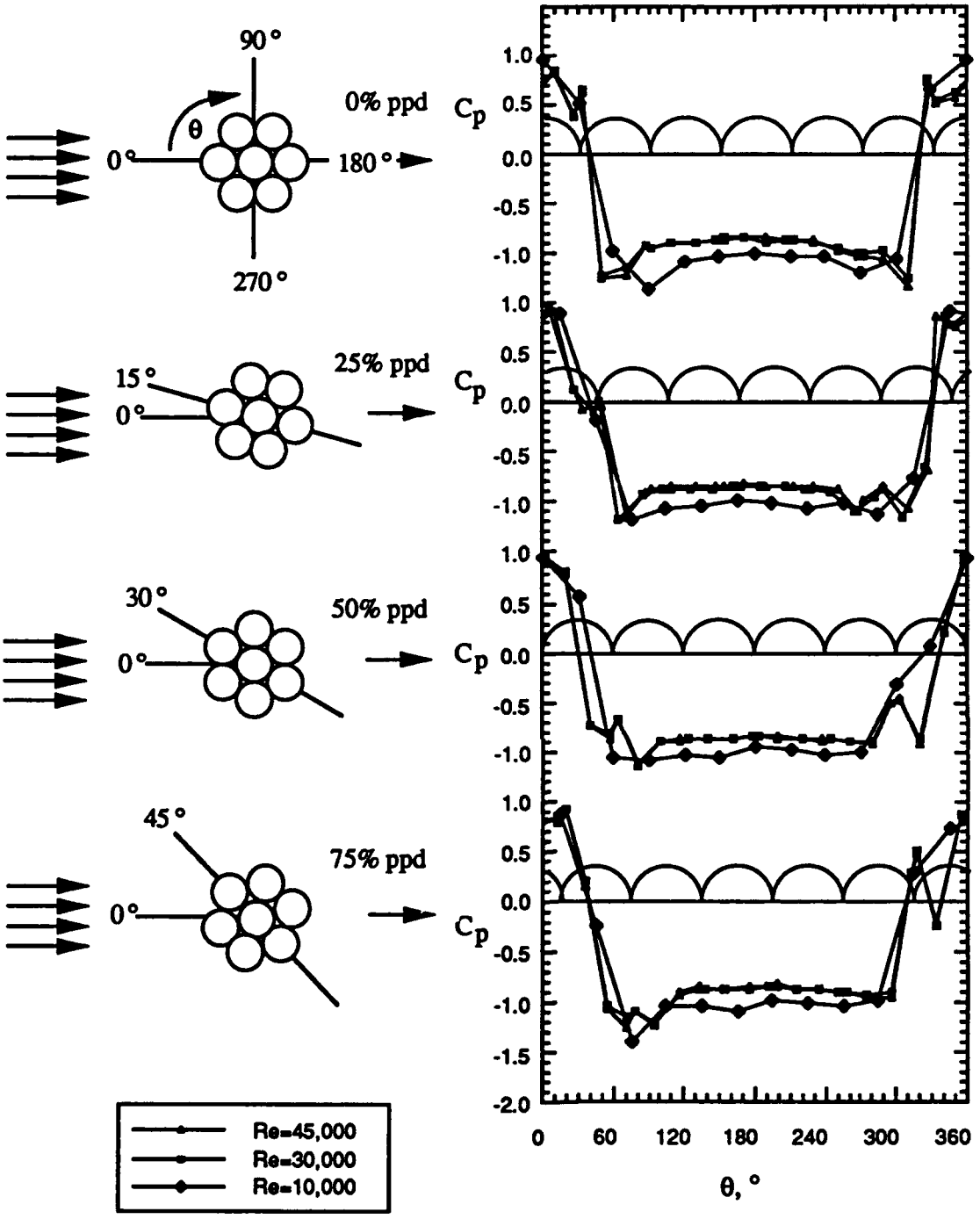


Figure 27. 7x7 cable, left lay, 90° cable angle

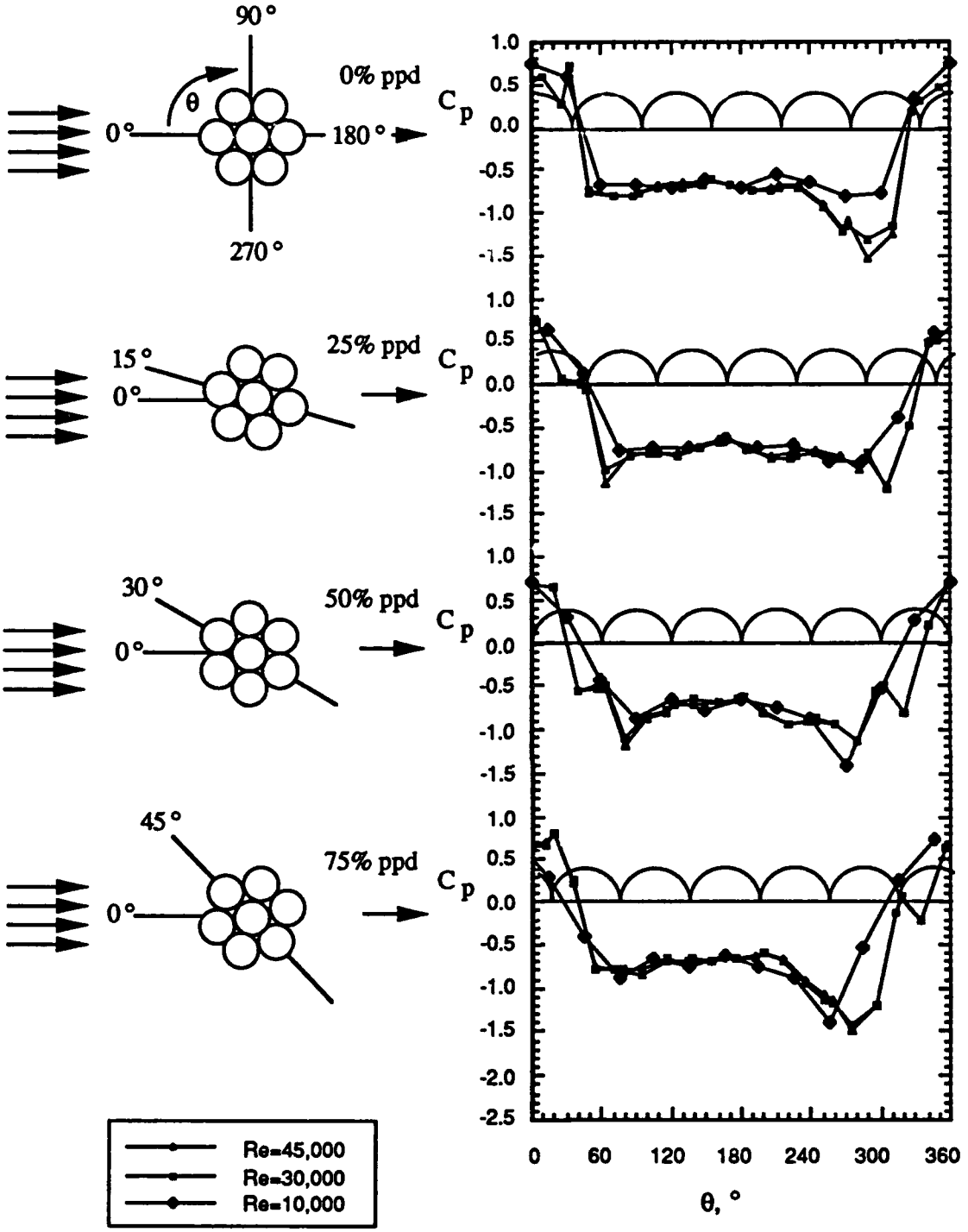


Figure 28. 7x7 cable, left lay, 60° cable angle

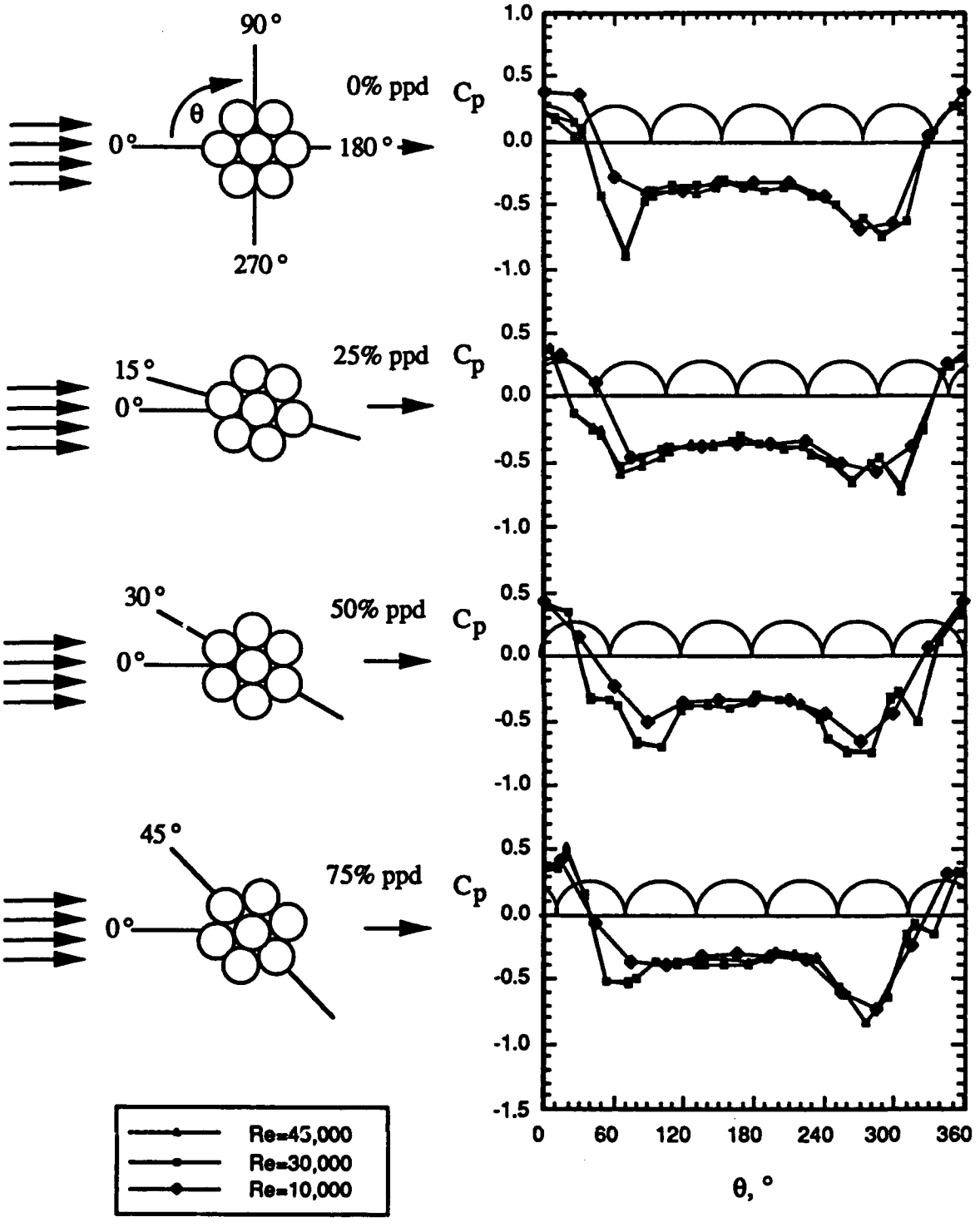


Figure 29. 7x7 cable, left lay, 40° cable angle

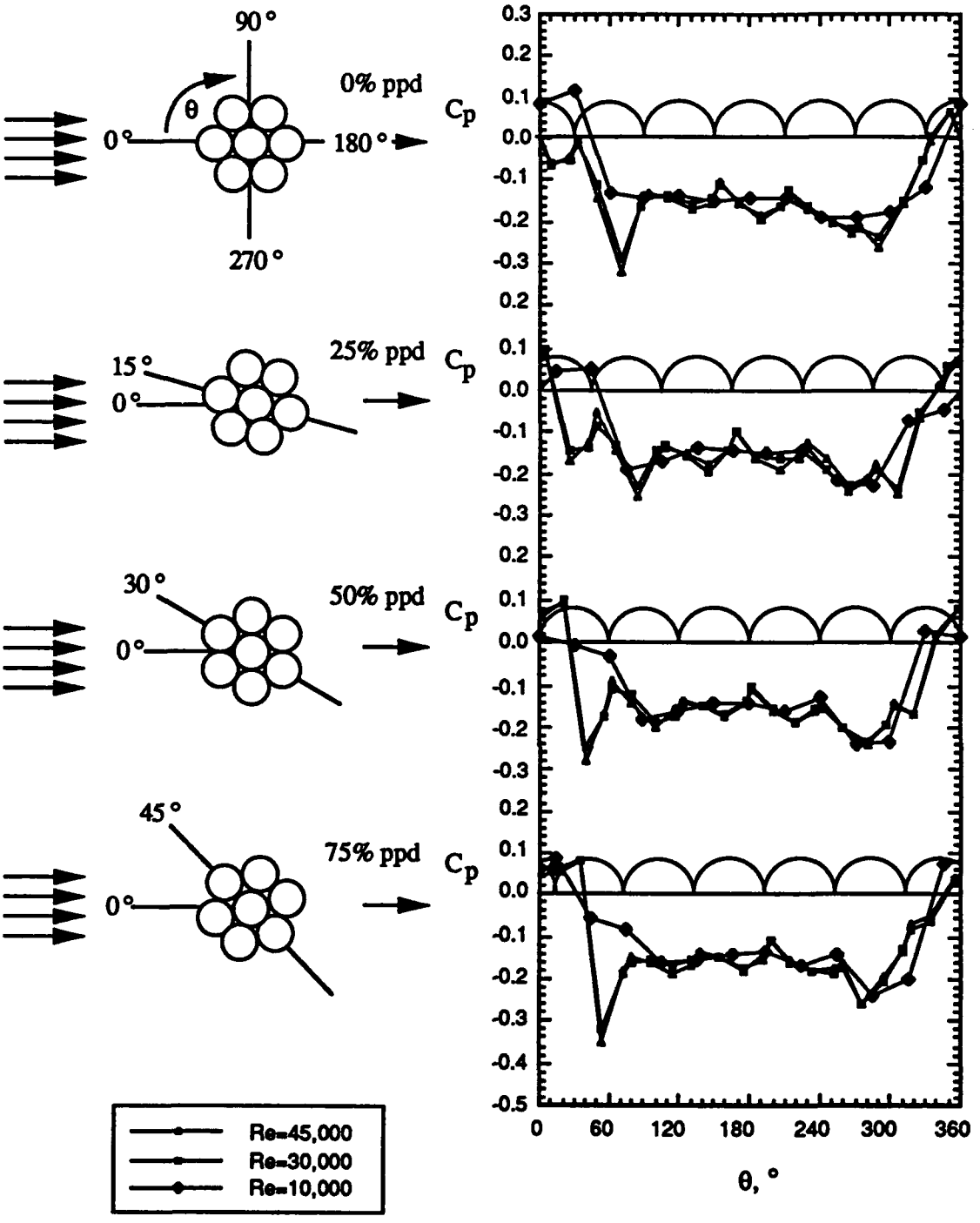


Figure 30. 7x7 cable, left lay, 20° cable angle

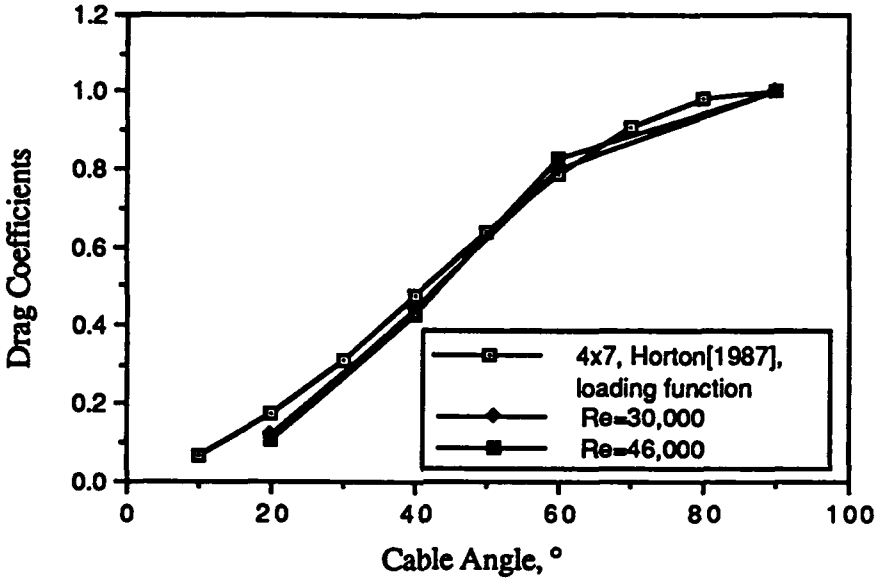


Figure 31
Integrated Drag Coefficients for the 4x1 Serrated Cable

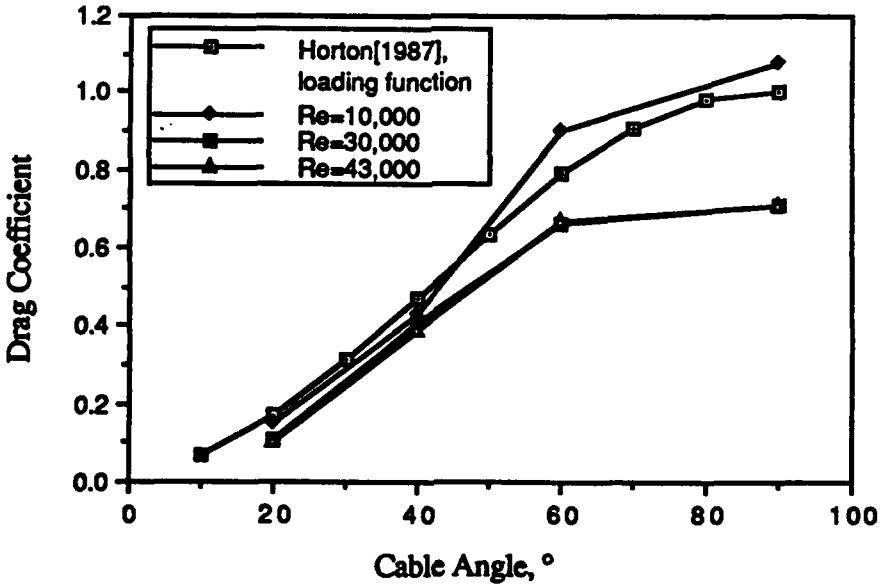


Figure 32
Integrated Drag Coefficients for the 4x7 Cable

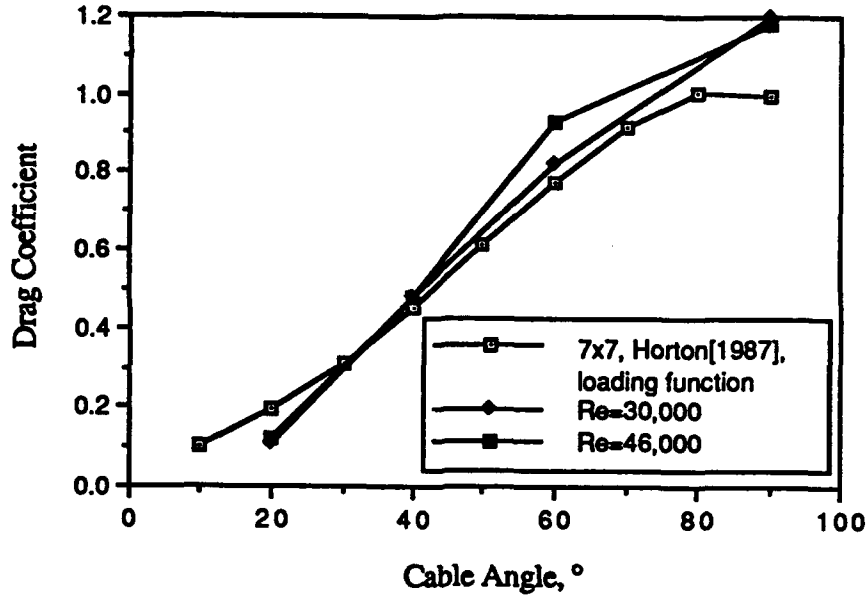


Figure 33
Integrated Drag Coefficients for the 7x1 Cable

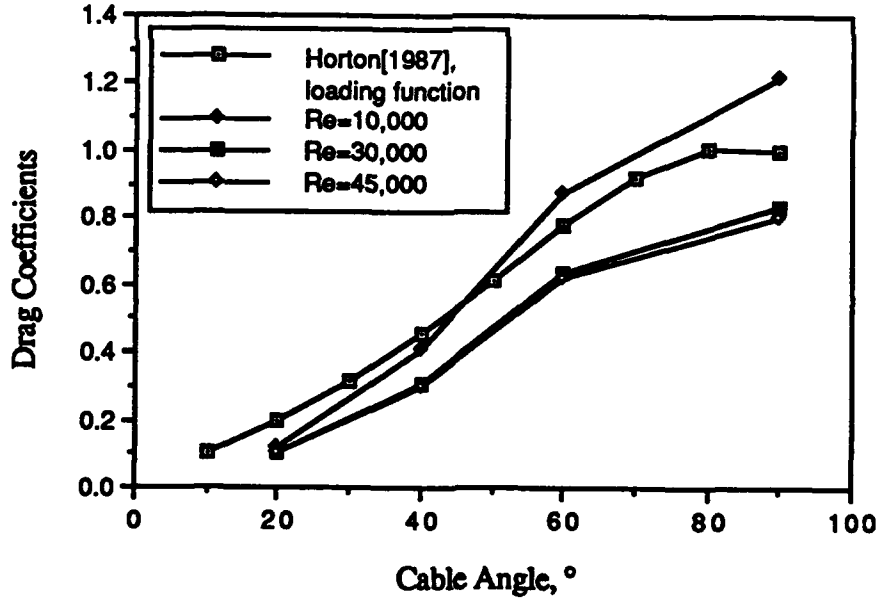


Figure 34
Integrated Drag Coefficients for the 7x7 Cable

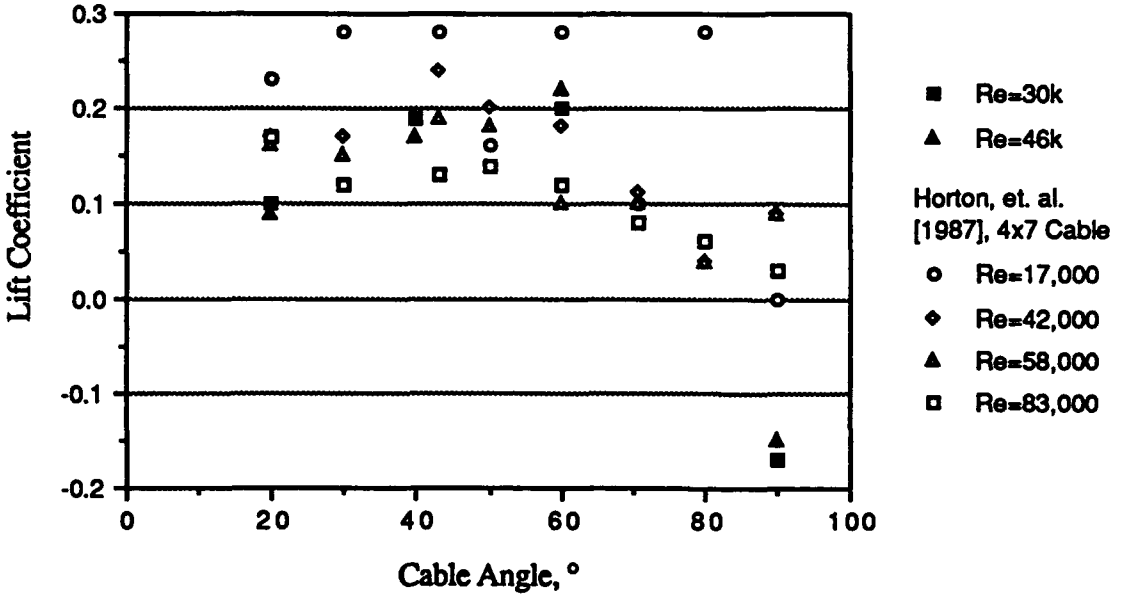


Figure 35
Integrated Lift Coefficients for the 4x1 Serrated Cable

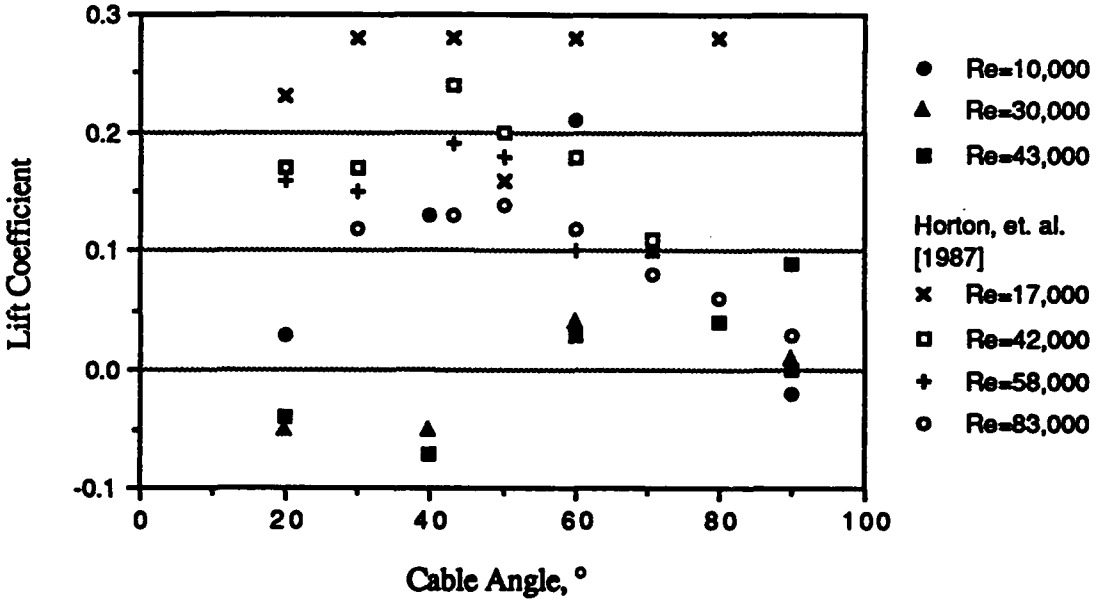


Figure 36
Integrated Lift Coefficients for the 4x7 Cable

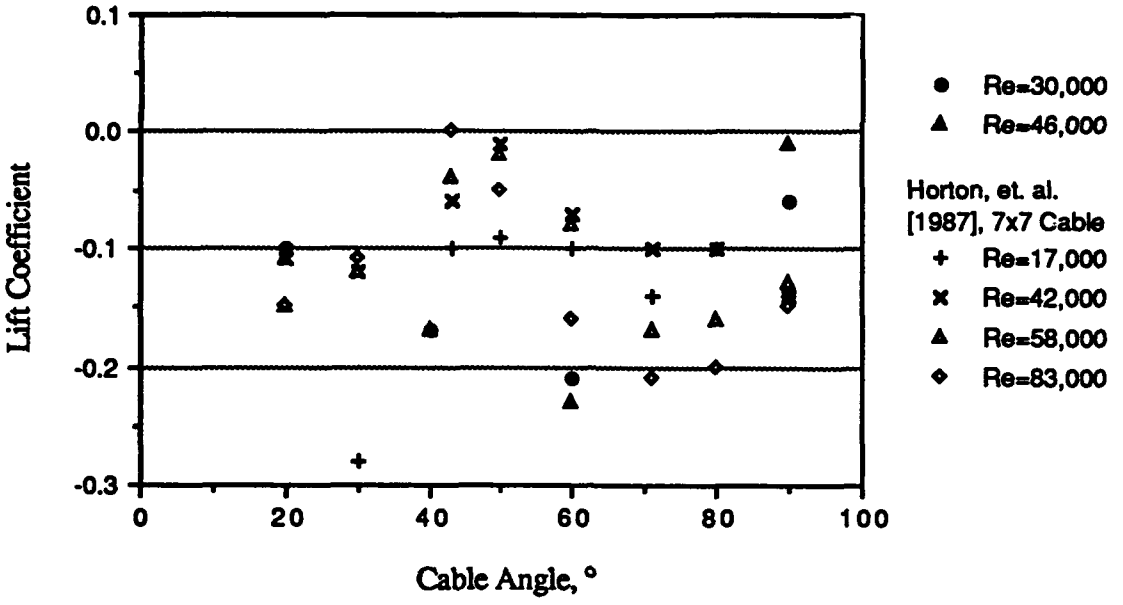


Figure 37
Integrated Lift Coefficients for the 7x1 Cable

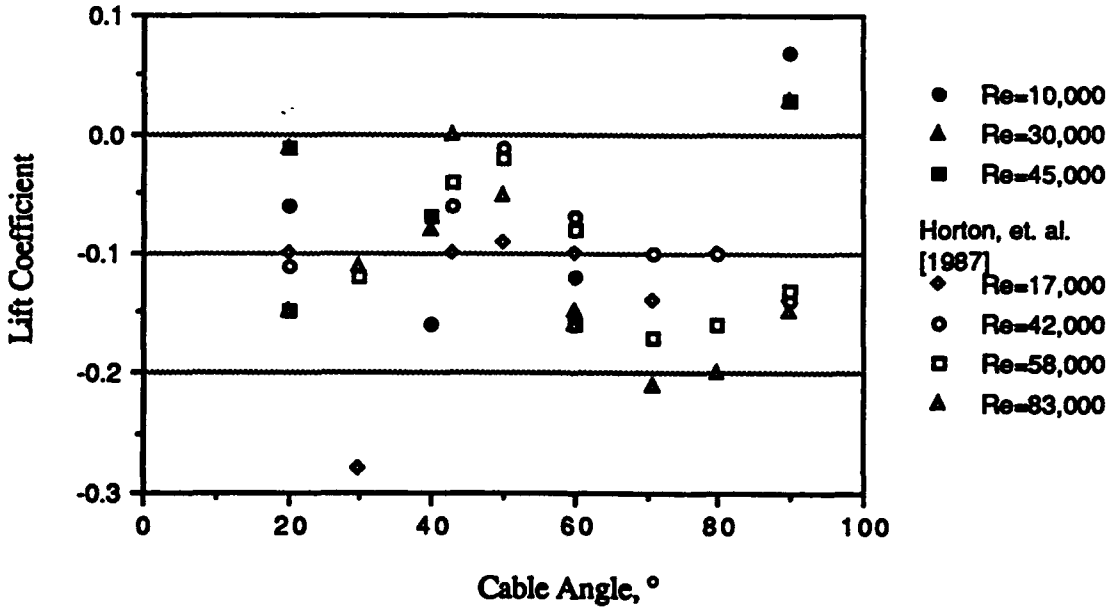


Figure 38
Integrated Lift Coefficients for the 7x7 Cable

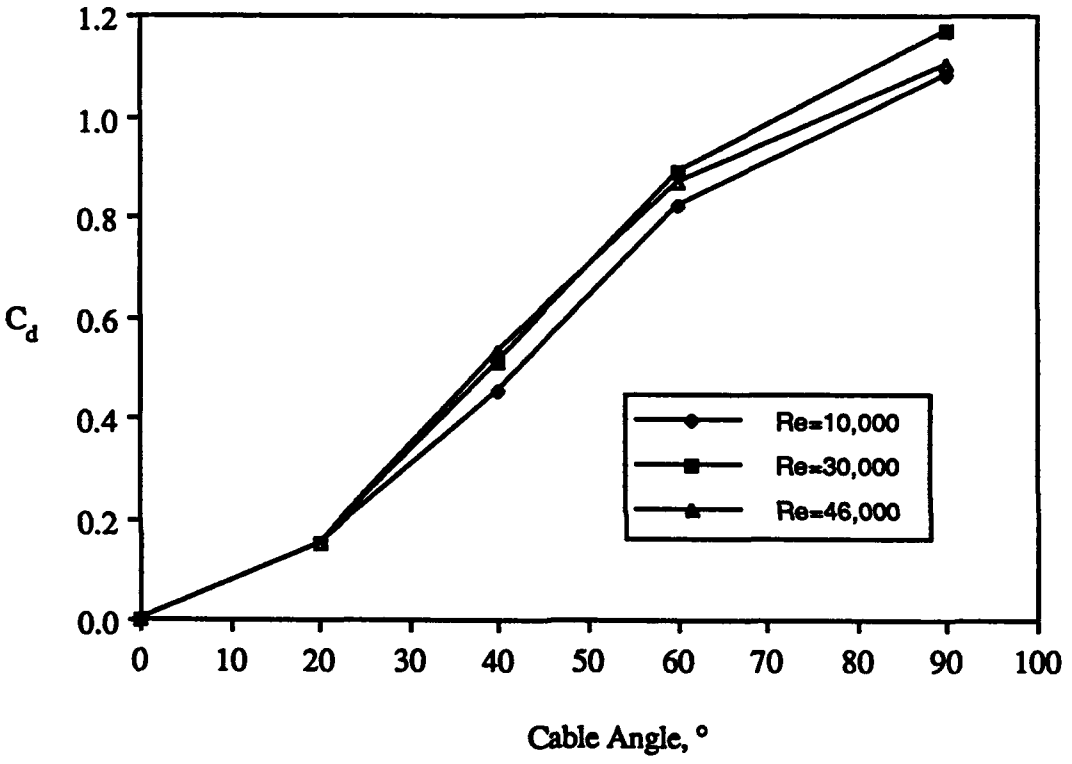


Figure 39

Drag Coefficients of the Circular Cylinder

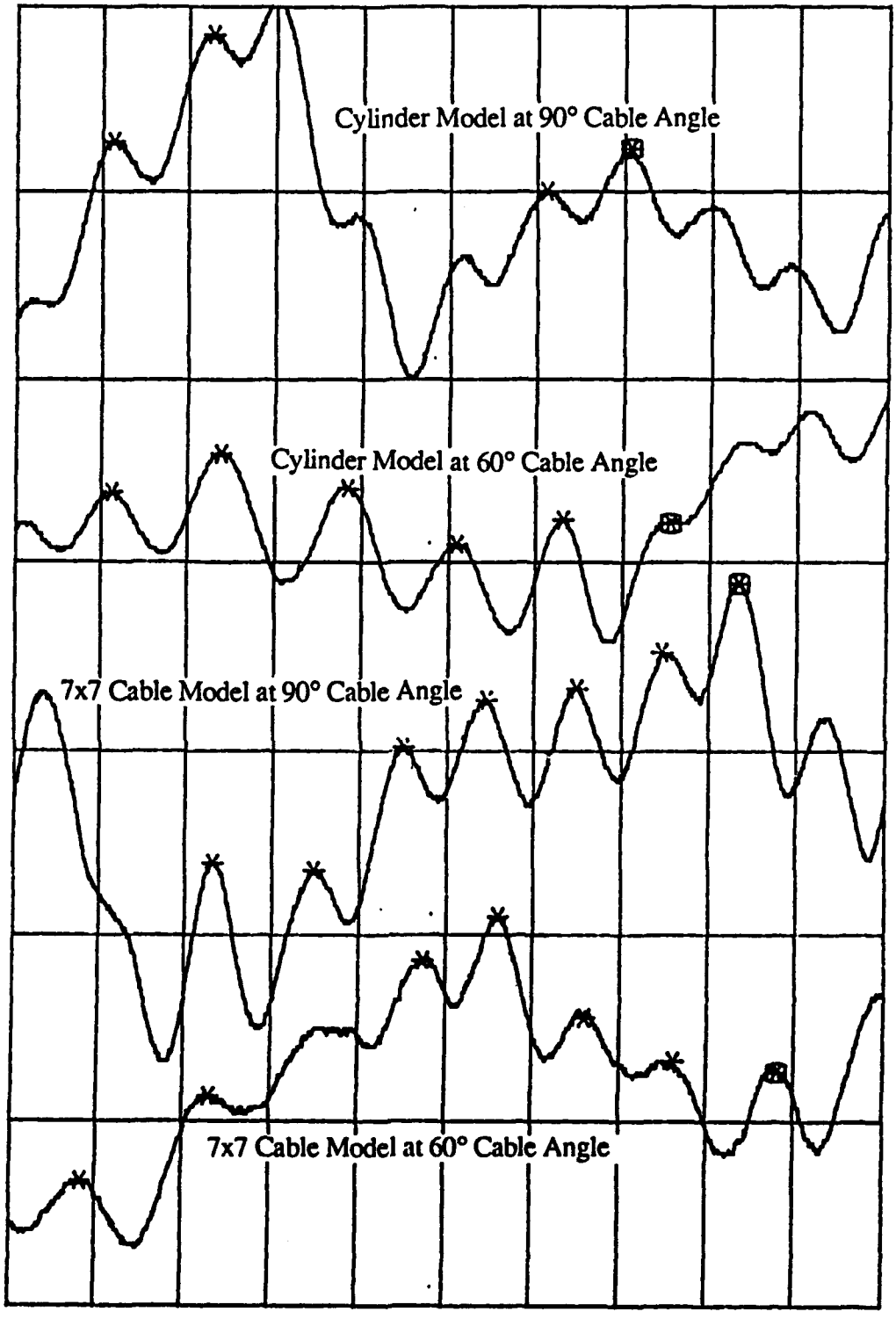


Figure 40. Time Domain Functions of Surface Pressure Fluctuations
Pressure tap located at 80° from stagnation point, Re=10,000

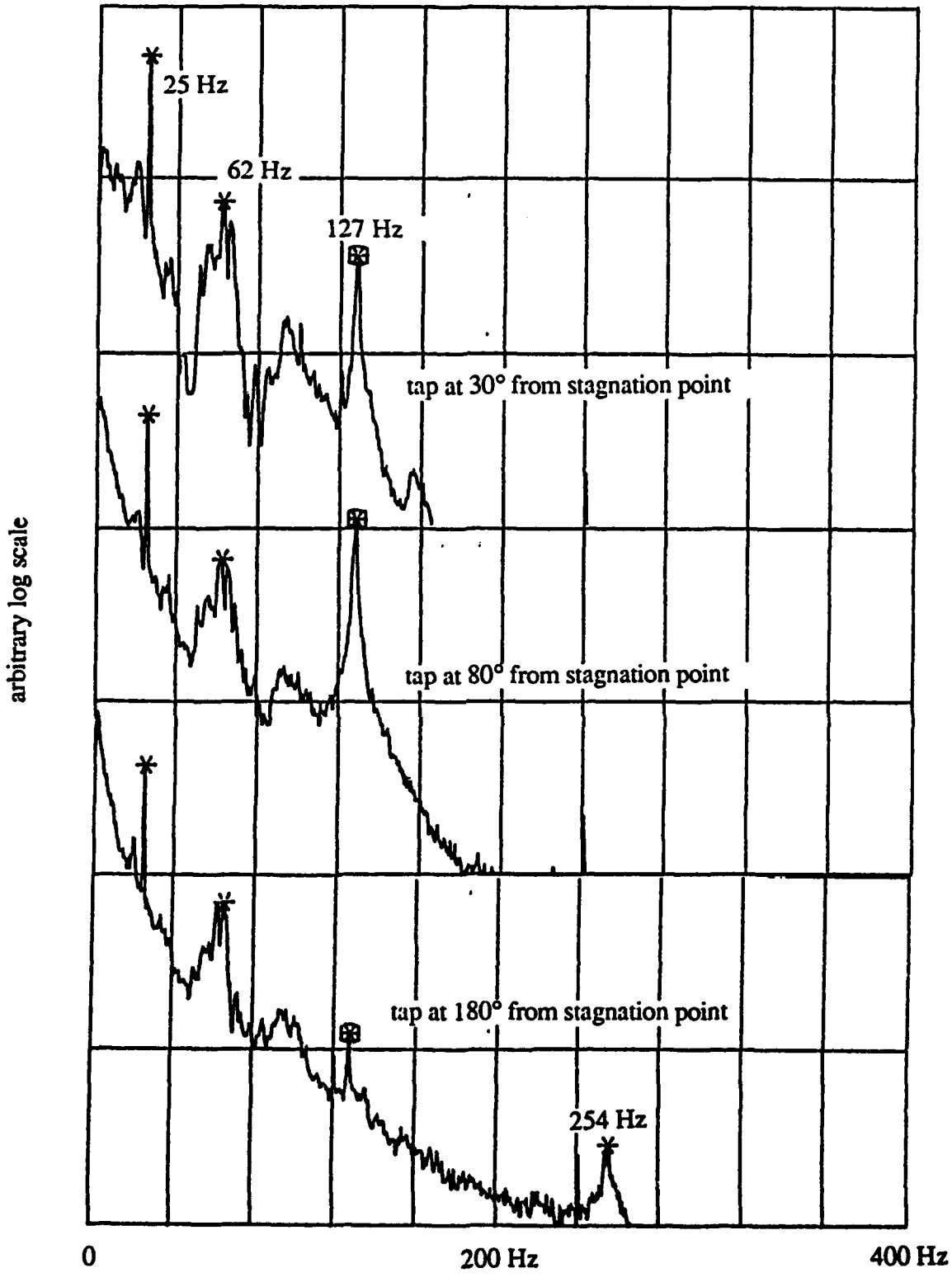


Figure 41. Spectra of Surface Pressure Fluctuations
Cylinder Model at 90° Cable Angle, Re=10,000

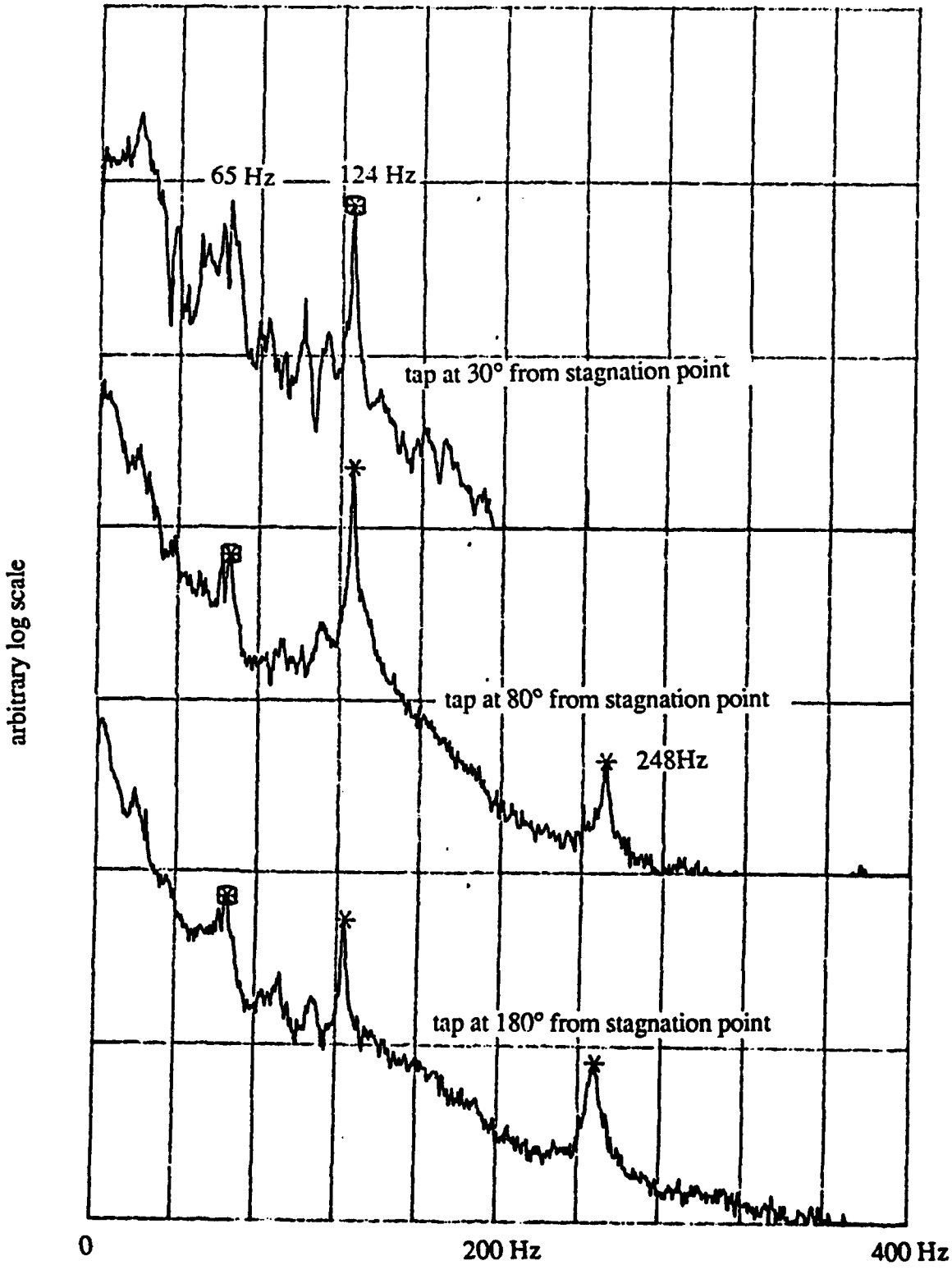


Figure 42. Spectra of Surface Pressure Fluctuations
7x7 Cable Model at 90° Cable Angle, Re=10,000

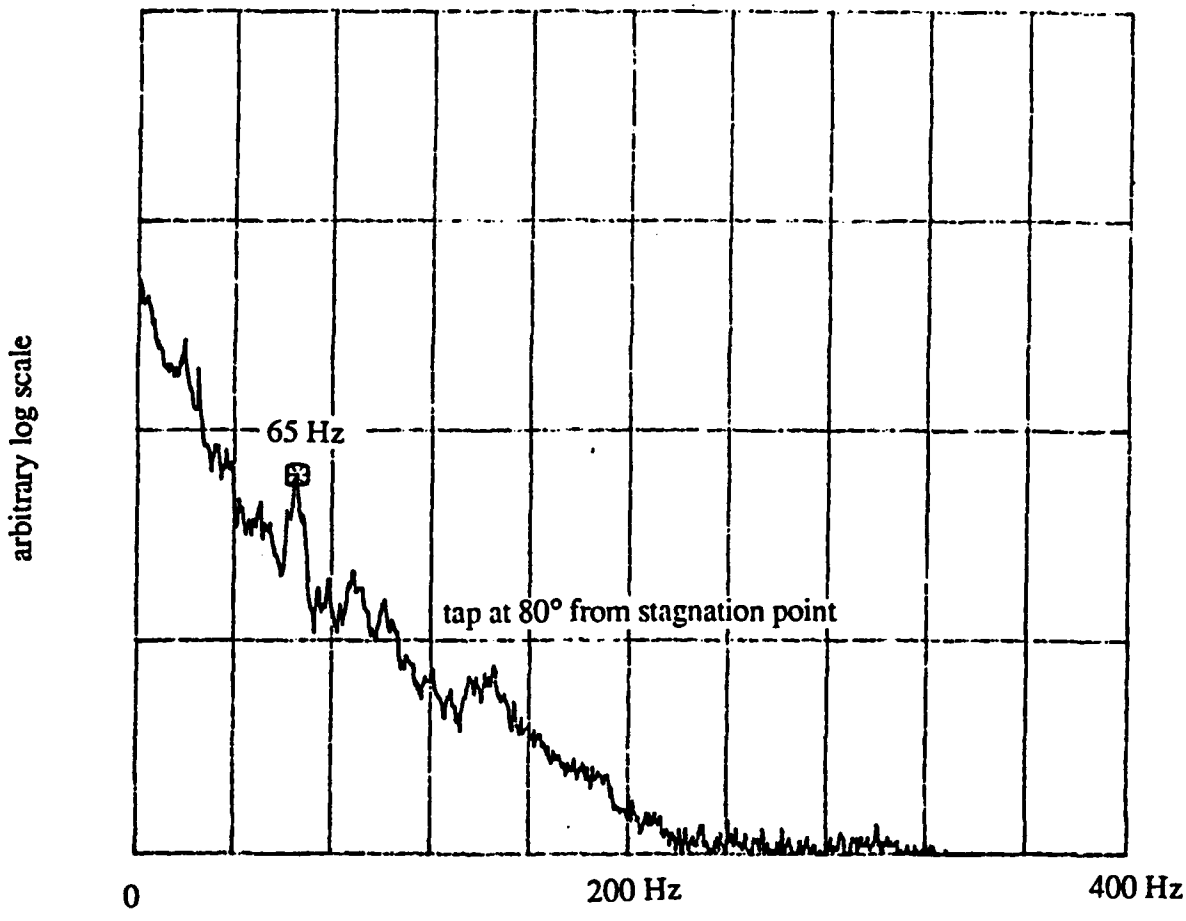


Figure 43. Spectrum of Surface Pressure Fluctuations
4x7 Serrated Cable Model at 90° Cable Angle, Re=10,000

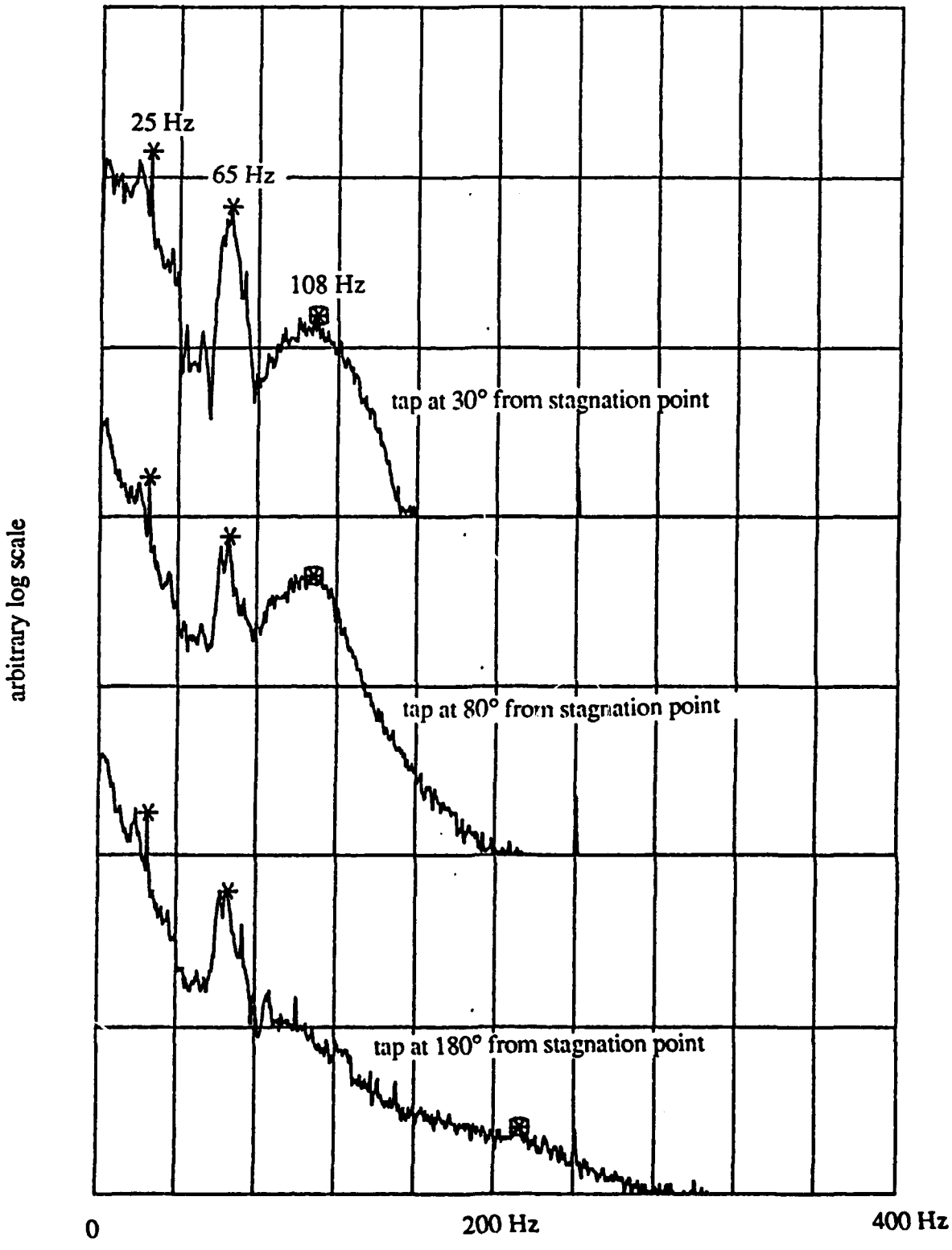


Figure 44. Spectra of Surface Pressure Fluctuations
Cylinder Model at 60° Cable Angle, Re=10,000

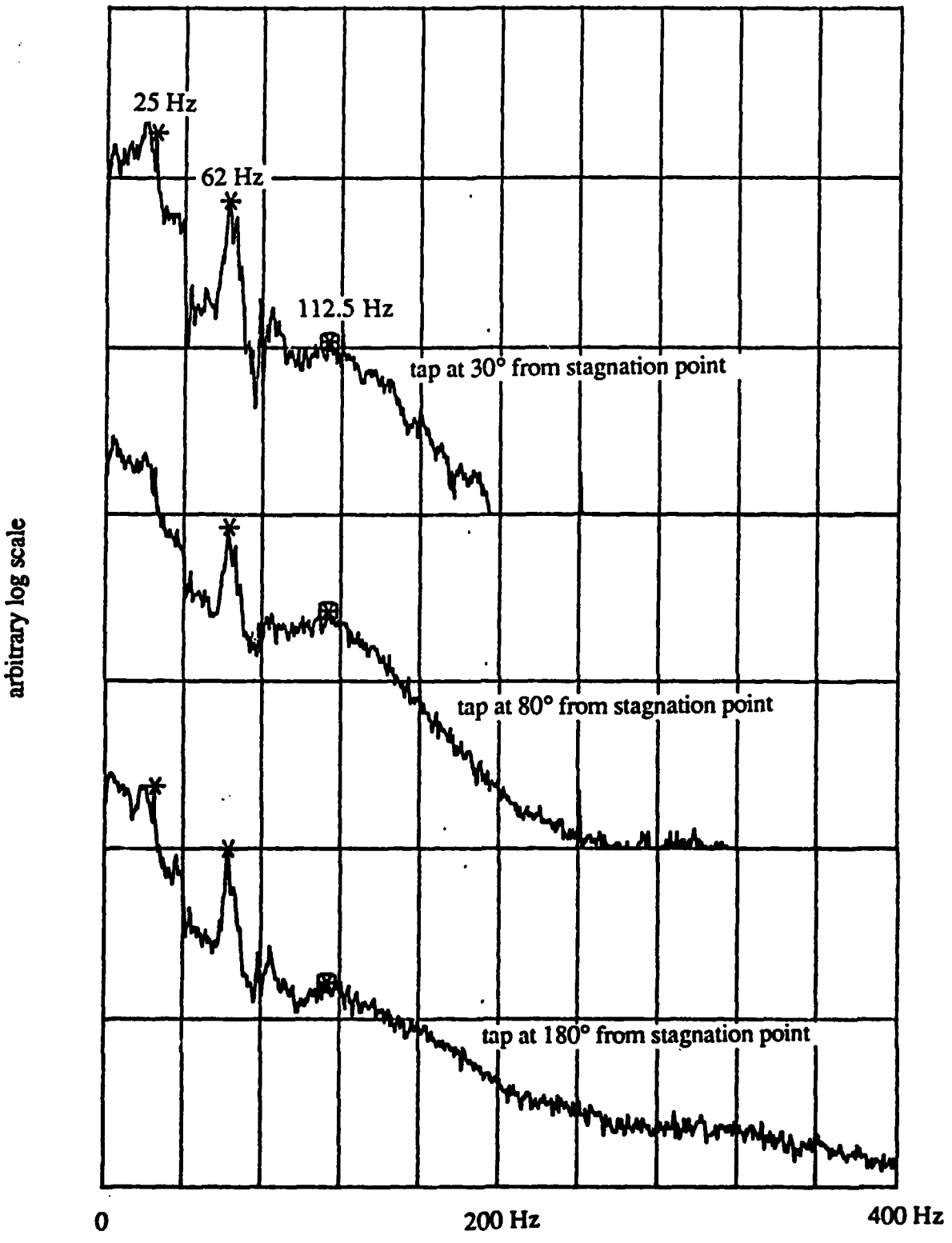


Figure 45. Spectra of Surface Pressure Fluctuations
7x7 Cable Model at 60° Cable Angle, Re=10,000

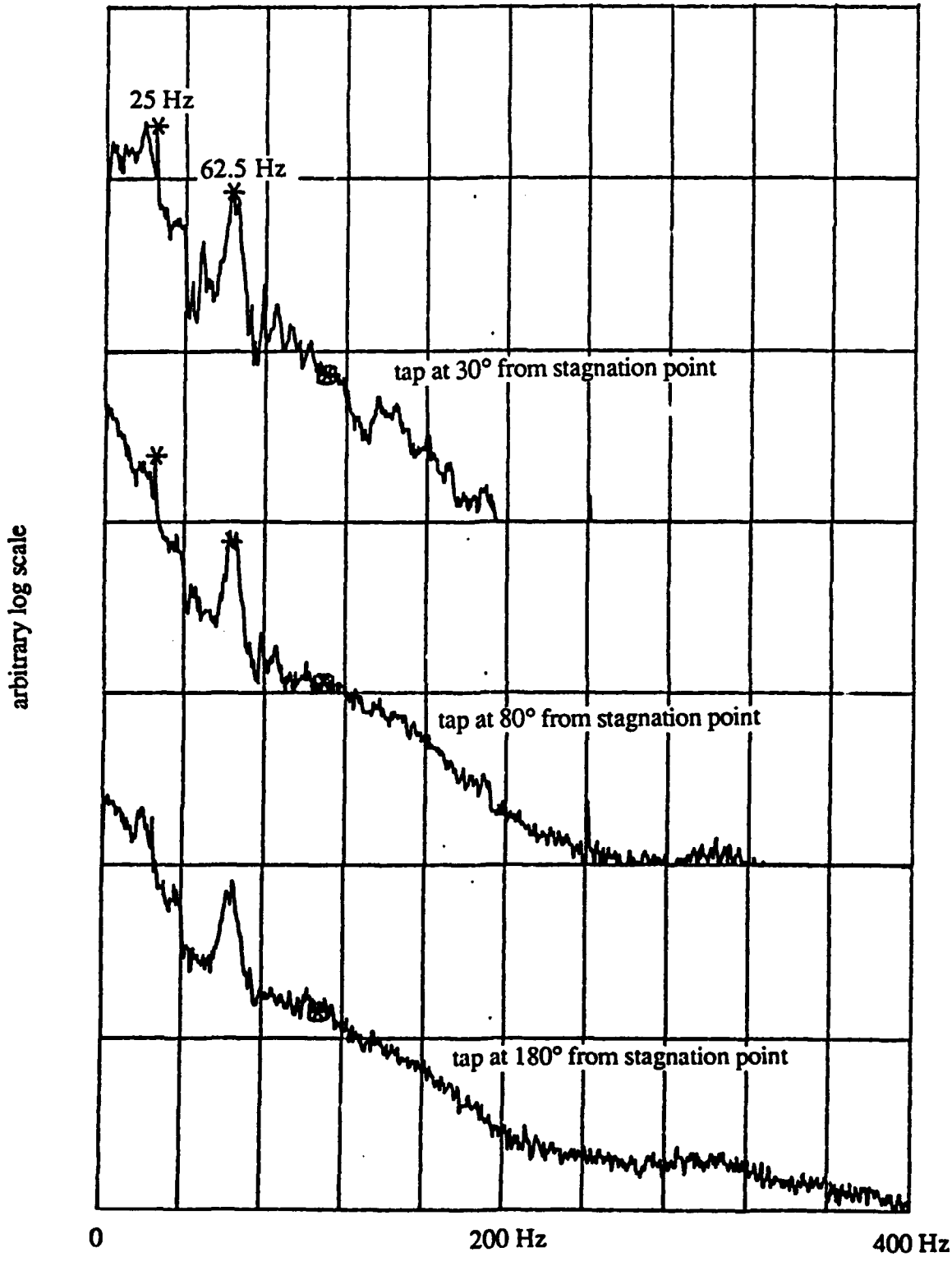


Figure 46. Spectra of Surface Pressure Fluctuations
4x7 Serrated Cable Model at 60° Cable Angle, Re=10,000

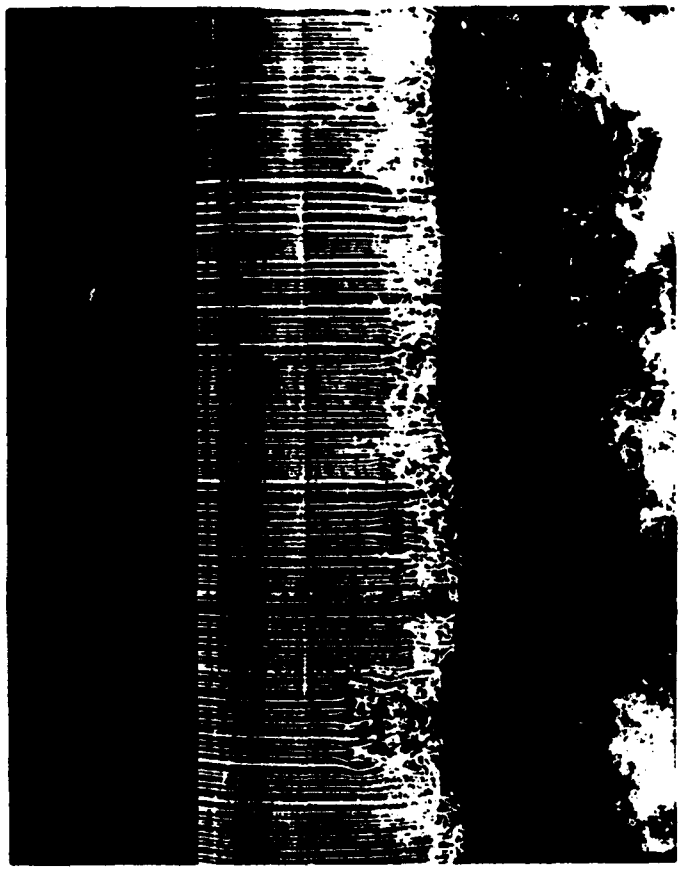

Cylinder Model

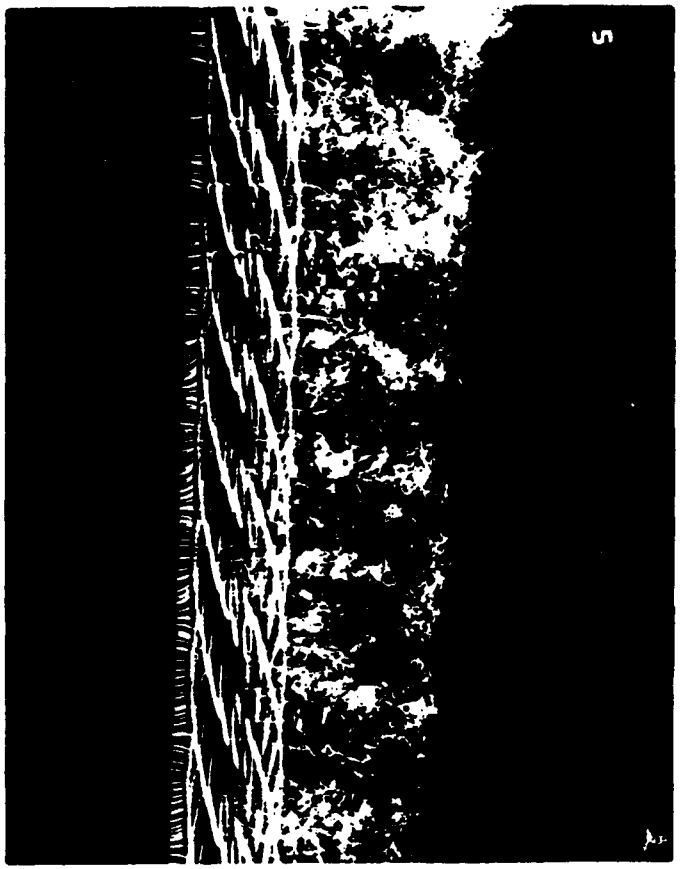

7x7 Cable Model

Figure 47. Comparison between Cylinder and 7x7 Cable Model
Re = 6,000 and $\beta = 90°$

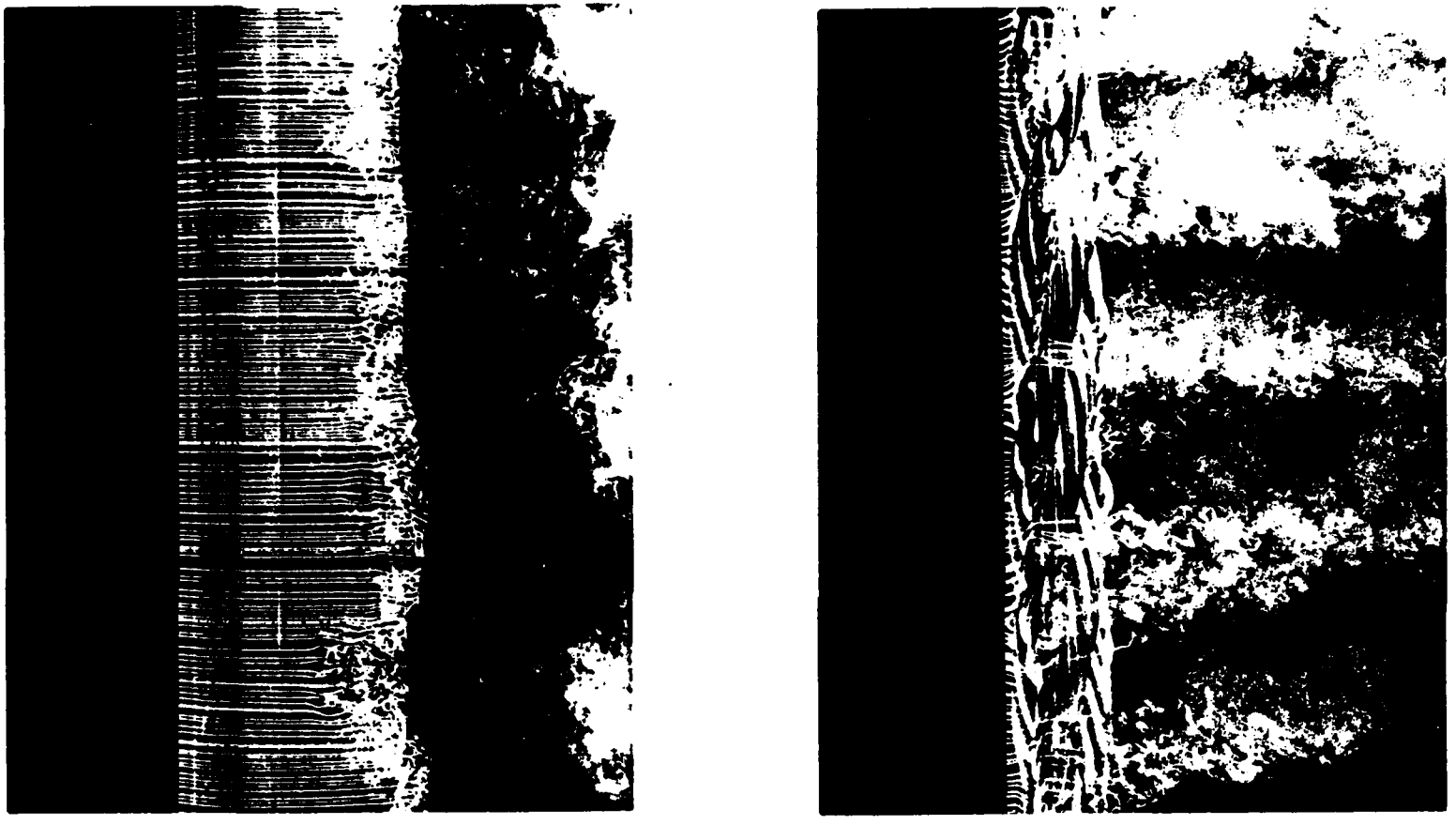

Cylinder Model

4x7 Serrated Cable Model

Figure 48. Comparison between Cylinder and 4x7 Cable Model
Re = 6,000 and $\beta = 90°$

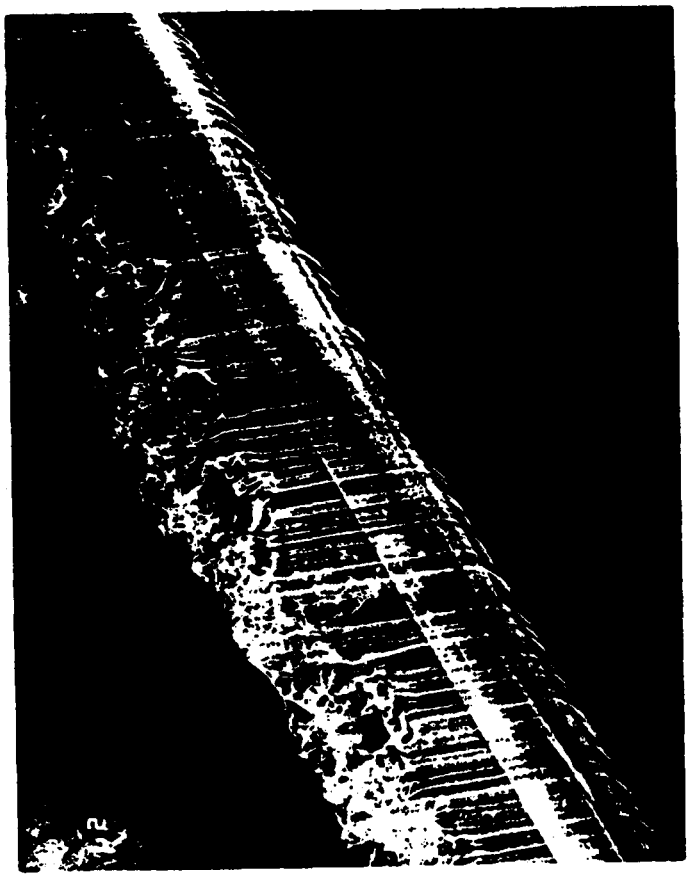

Flow Right to Left

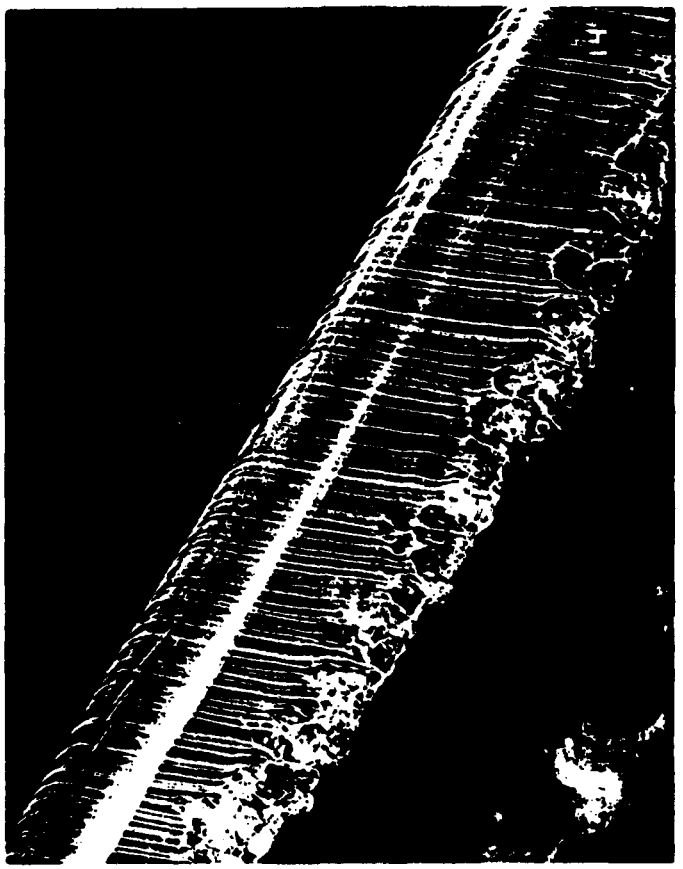

Flow Left to Right

Figure 49. Smoke Flow Visualization, Cylinder Model, Re=6,000, $\beta = 60°$

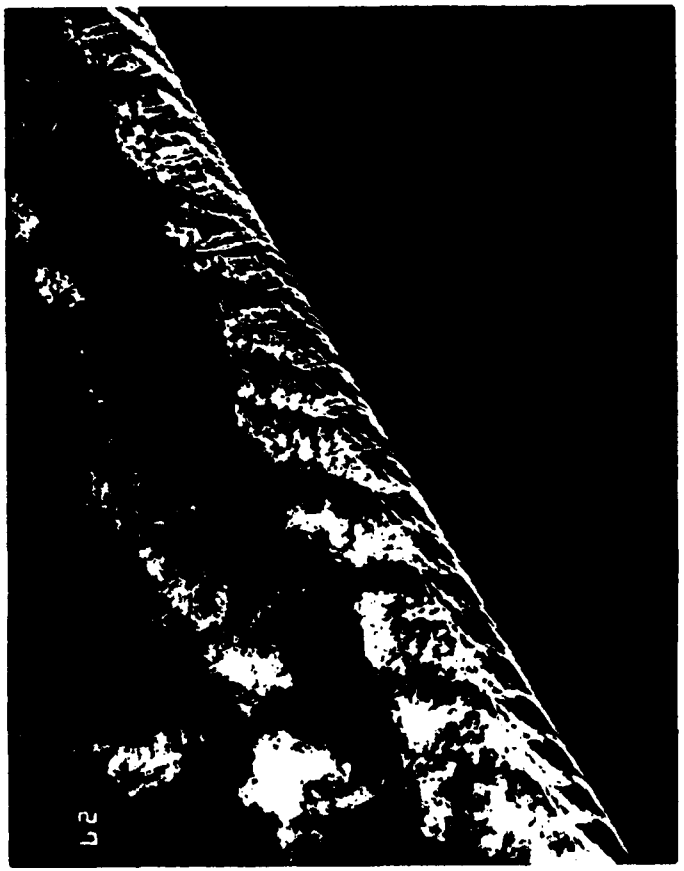

Flow Right to Left

Flow Left to Right

Figure 50. Smoke Flow Visualization, 7x7 Cable Model, Re=6,000, $\beta = 60°$

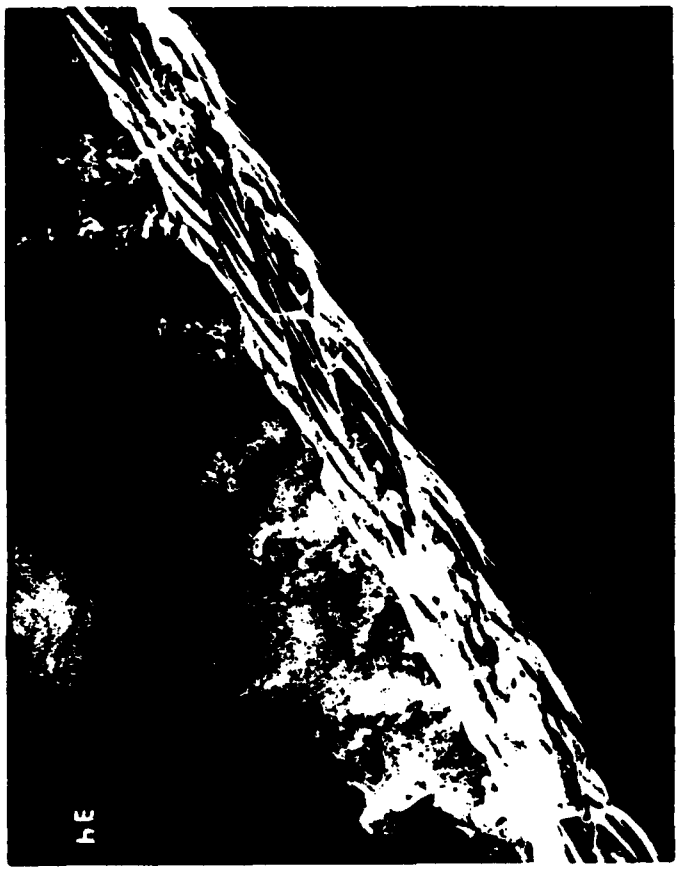

Flow Right to Left

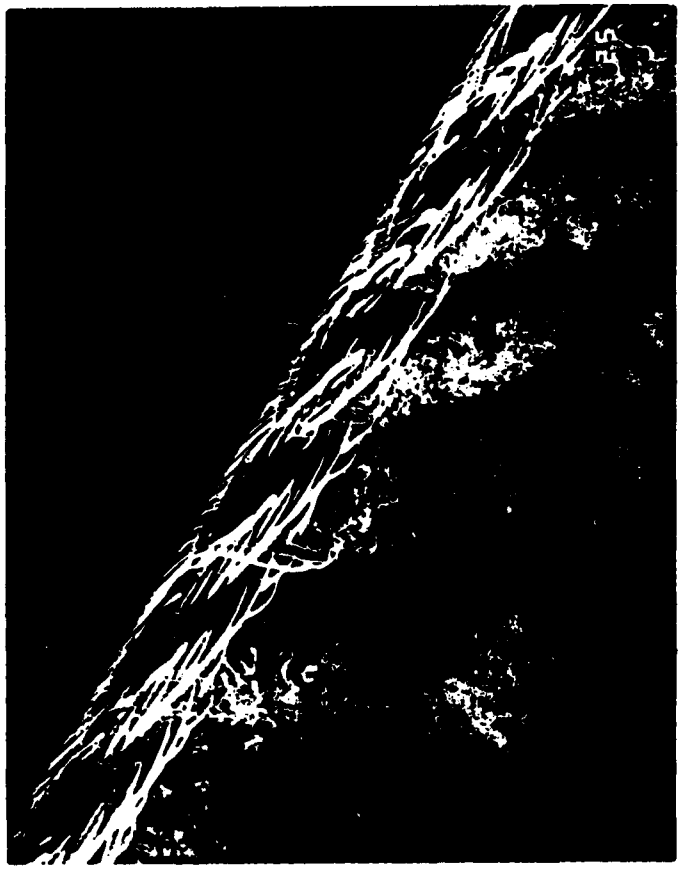

Flow Left to Right

Figure 51. Smoke Flow Visualization, 4x7 Cable Model, Re=6,000, $\beta = 60°$

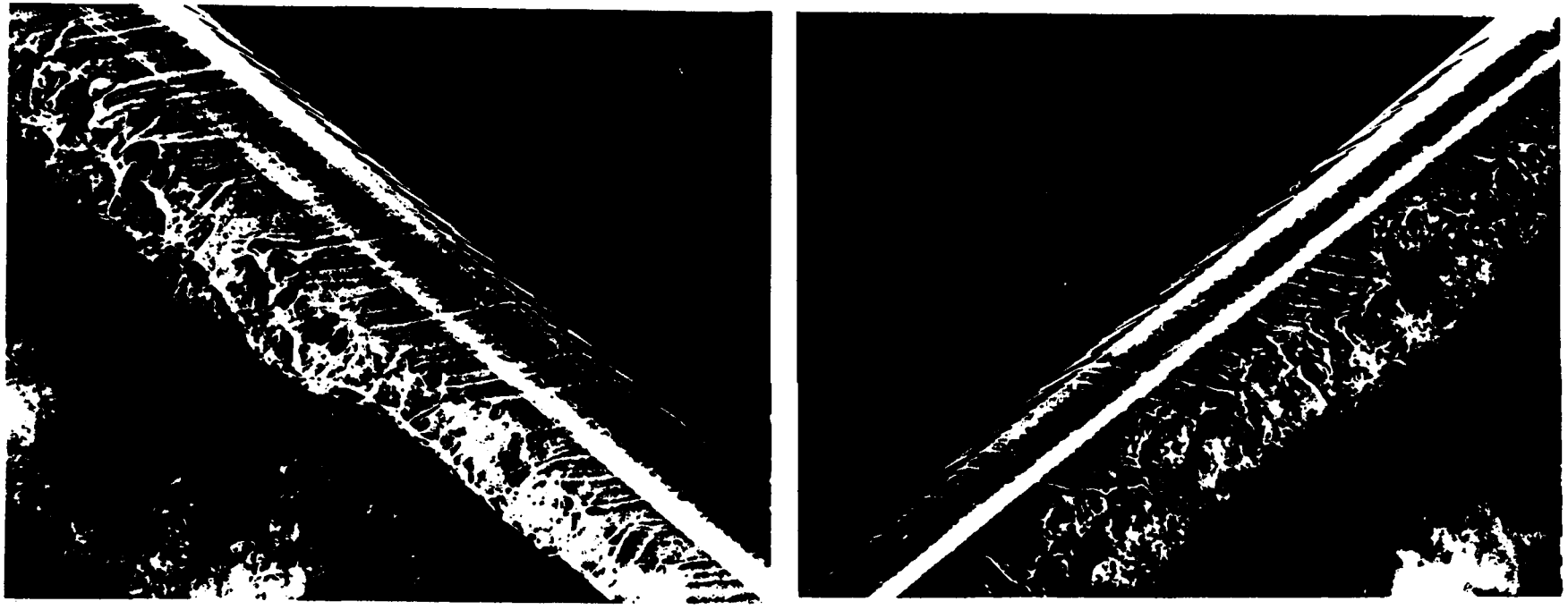

Flow Right to Left

Flow Left to Right

Figure 52. Smoke Flow Visualization, Cylinder Model, Re=6,000, $\beta = 40°$

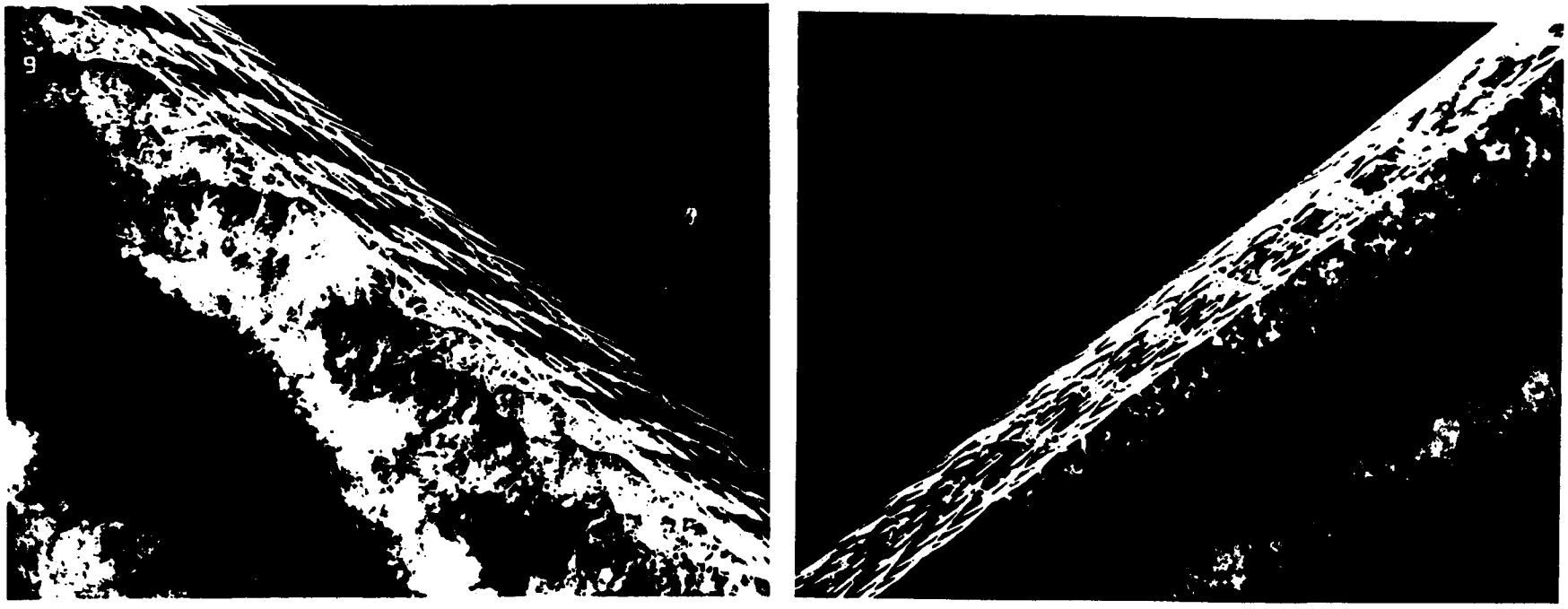

Flow Right to Left

Flow Left to Right

Figure 53. Smoke Flow Visualization, 7x7 Cable Model, Re=6,000, $\beta = 40°$

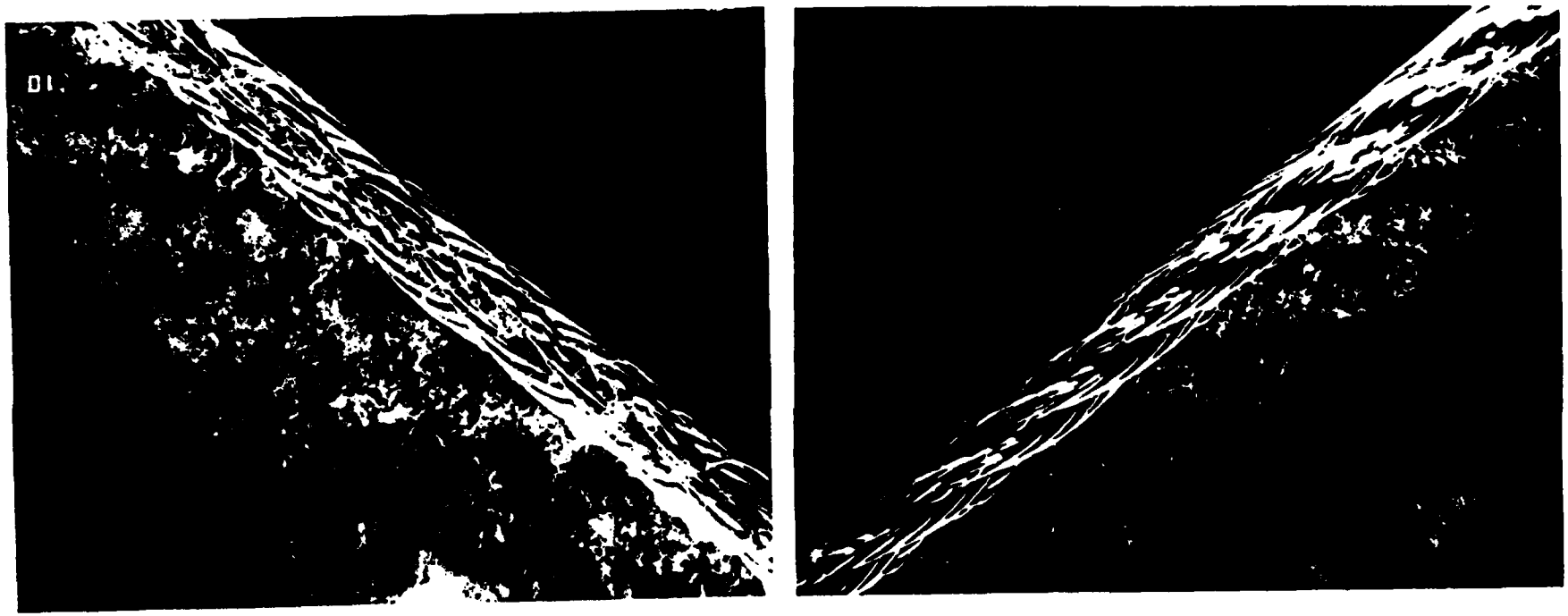

Flow Right to Left

Flow Left to Right

Figure 54. Smoke Flow Visualization, 4x7 Cable Model, Re=6,000, $\beta = 40°$

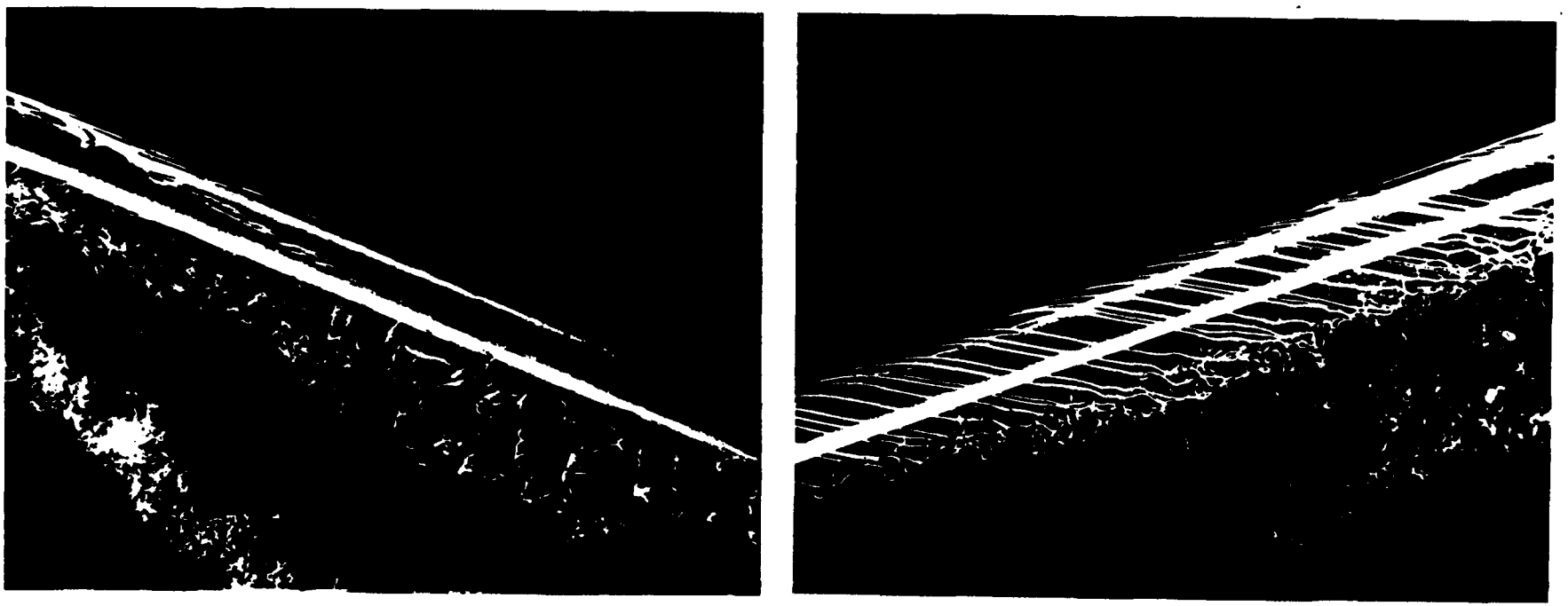

Flow Right to Left

Flow Left to Right

Figure 55. Smoke Flow Visualization, Cylinder Model, Re=6,000, $\beta = 20°$

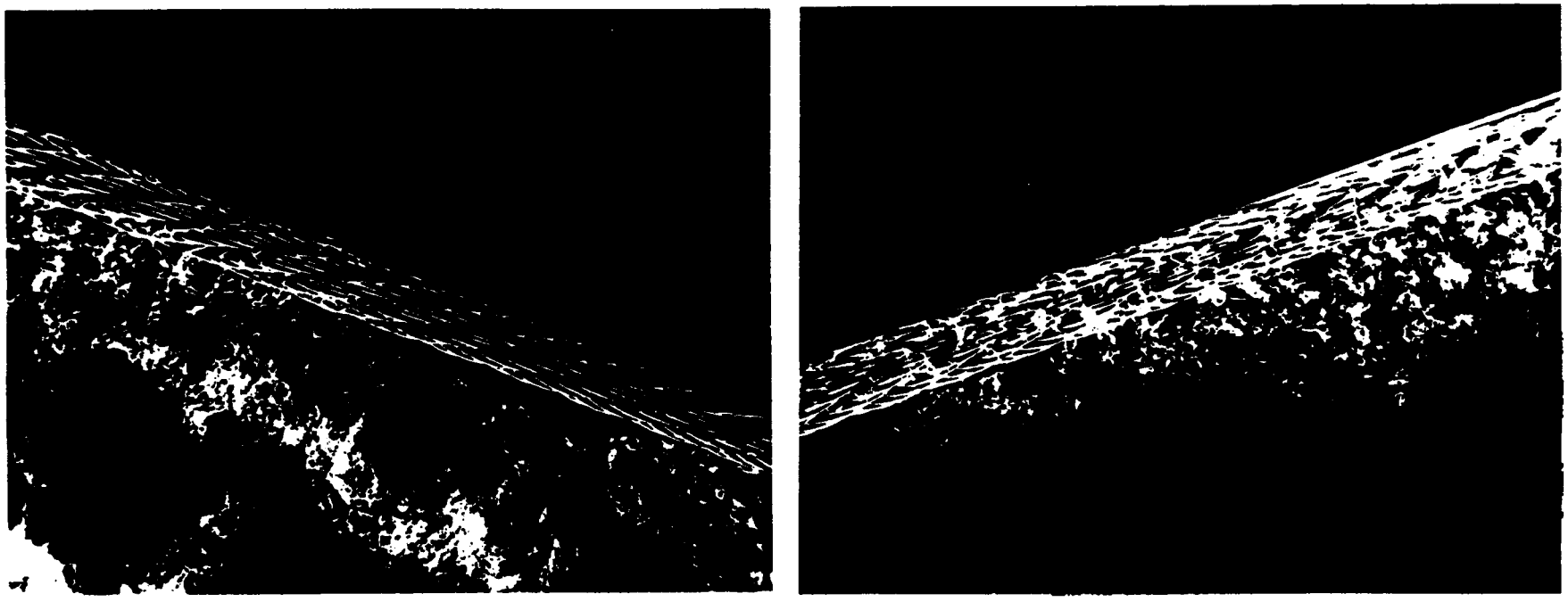

Flow Right to Left

Flow Left to Right

Figure 56. Smoke Flow Visualization, 7x7 Cable Model, Re=6,000, $\beta = 20°$

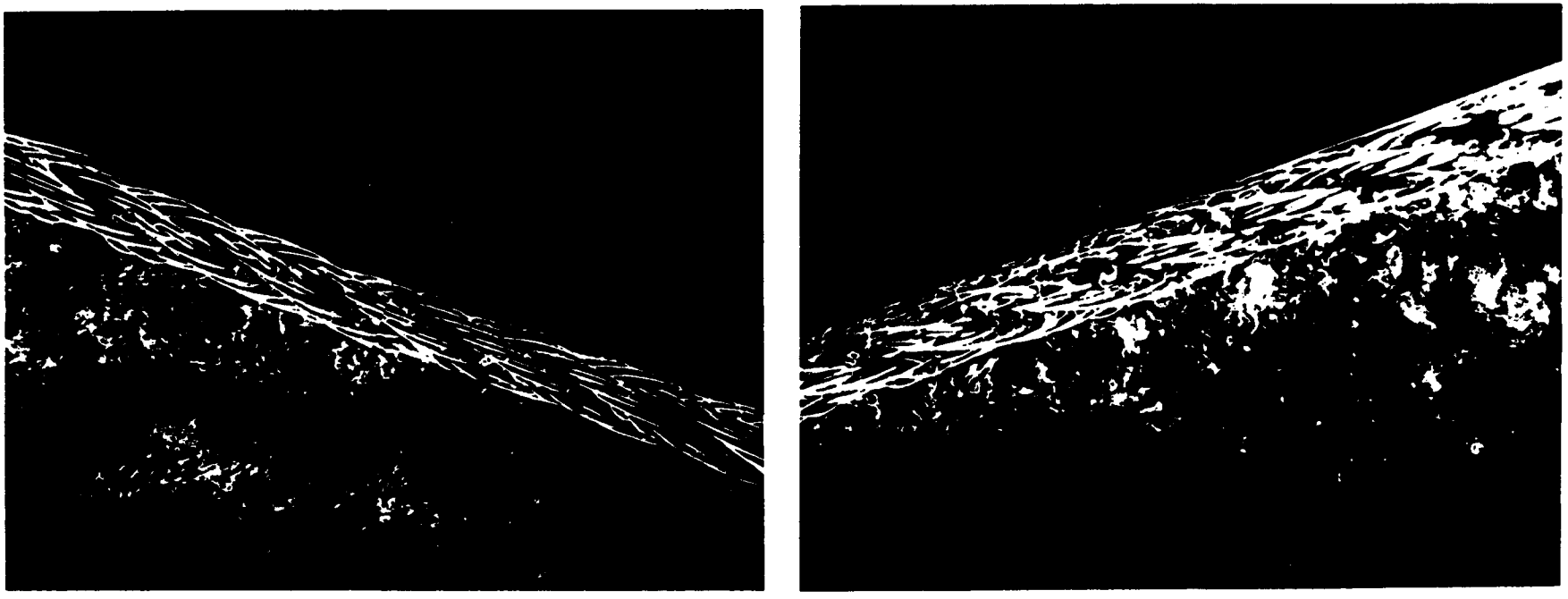

Flow Right to Left

Flow Left to Right

Figure 57. Smoke Flow Visualization, 4x7 Cable Model, Re=6,000, $\beta = 20°$

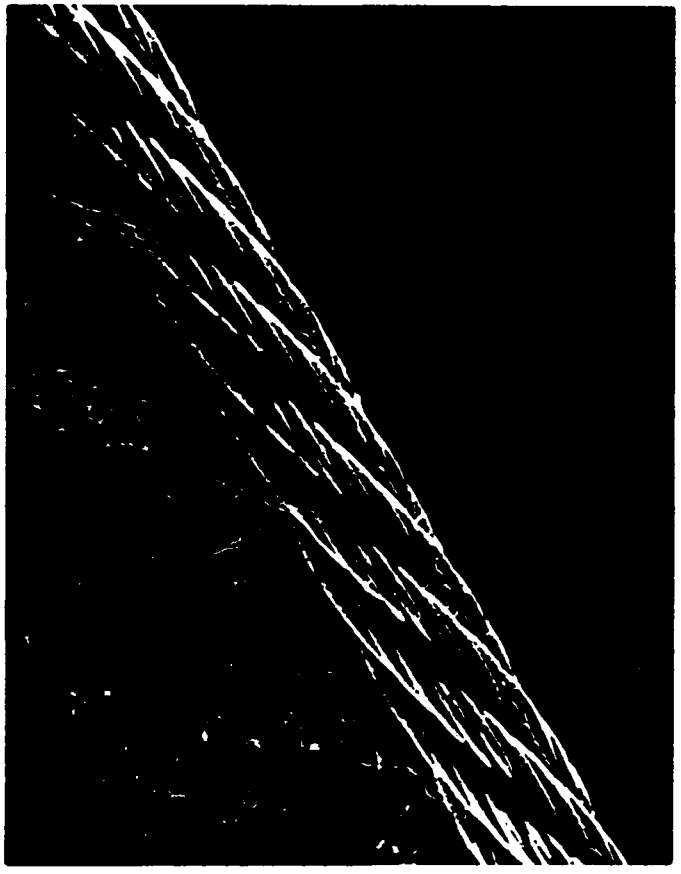

Flow Right to Left

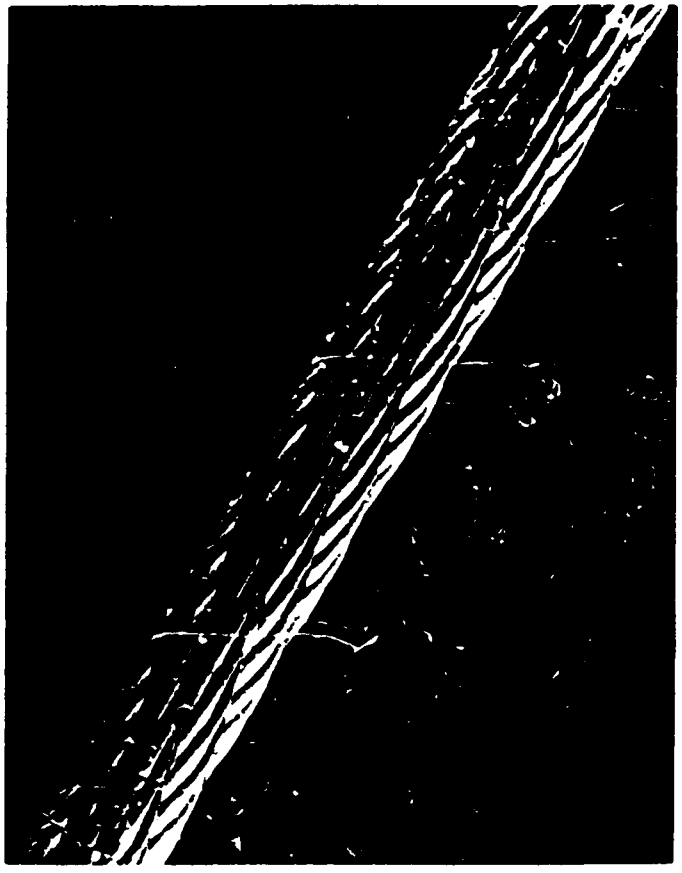

Flow Left to Right

Figure 58. Smoke Flow Visualization, 7x7 Cable Model, Re=6,000, $\beta = 60°, \theta = 45°$

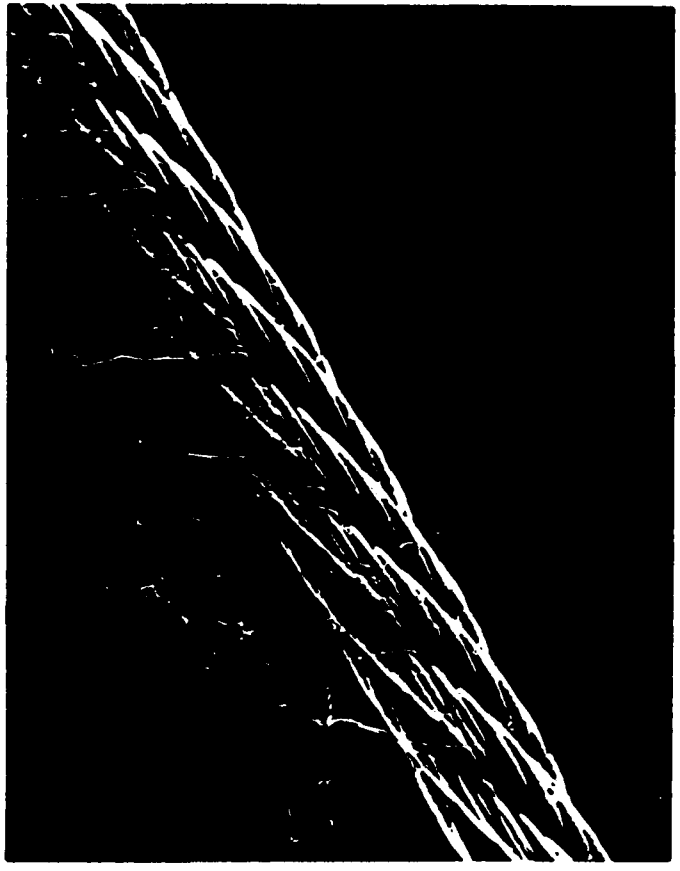

Flow Right to Left

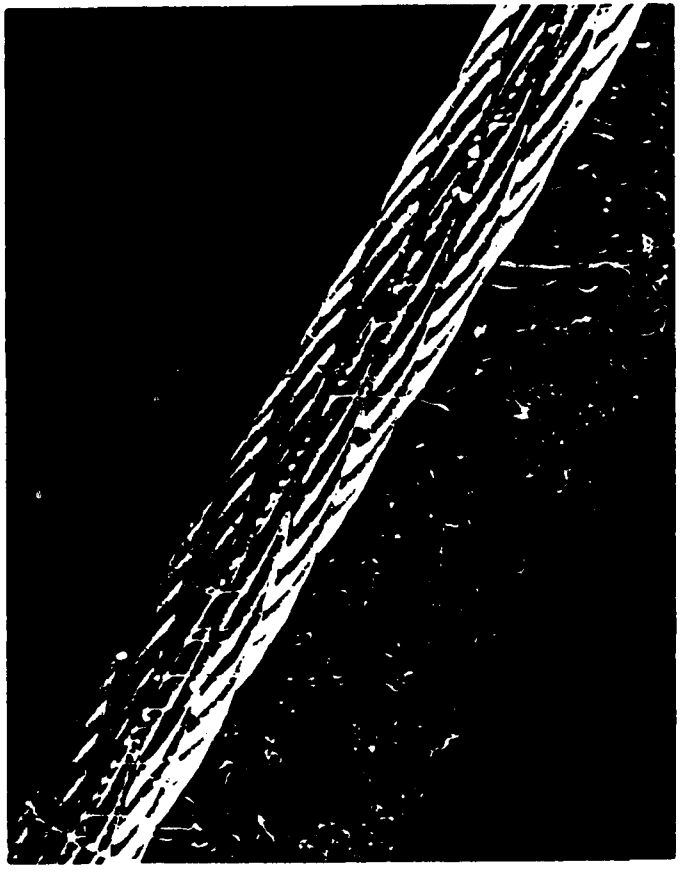

Flow Left to Right

Figure 59. Smoke Flow Visualization, 7x7 Cable Model, Re=6,000, $\beta = 60°, \theta = 90°$

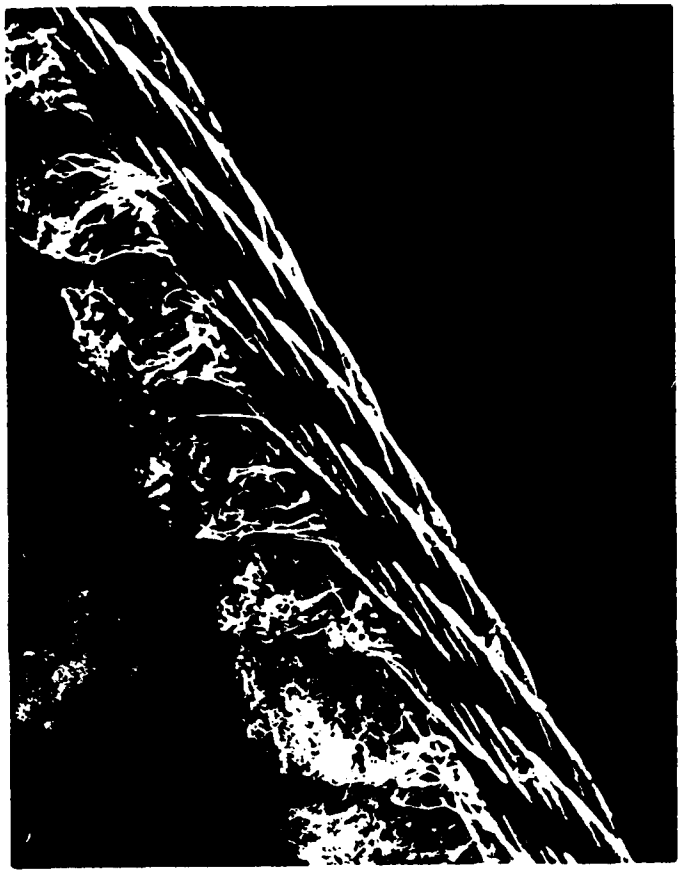

Flow Right to Left

Flow Left to Right

Figure 60. Smoke Flow Visualization, 7x7 Cable Model, Re=6,000, $\beta = 60°, \theta = 135°$

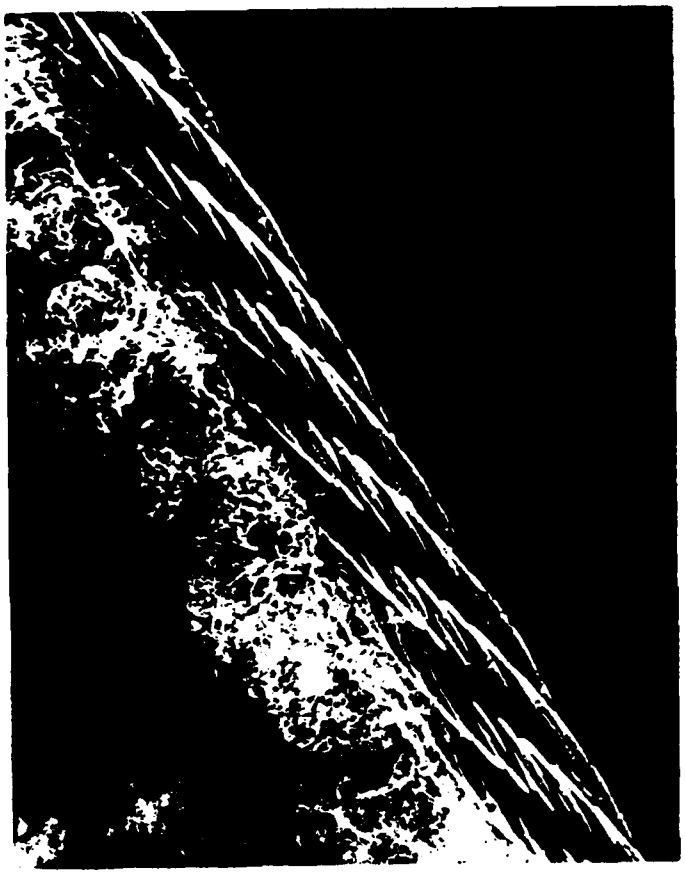

Flow Right to Left

Flow Left to Right

Figure 61. Smoke Flow Visualization, 7x7 Cable Model, Re=6,000, $\beta = 60°, \theta = 180°$

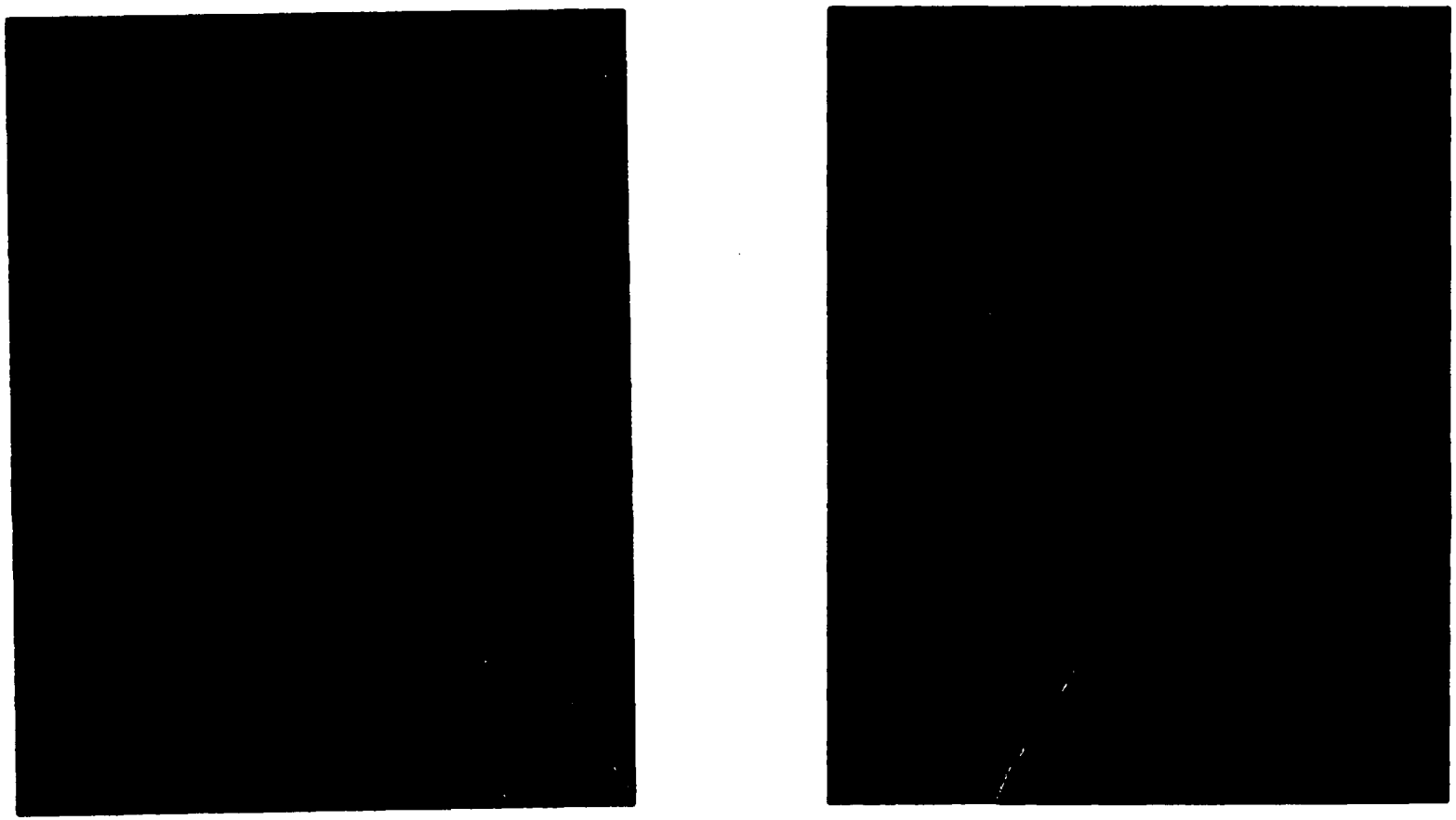

Flow Right to Left

Flow Left to Right

Figure 62. Surface Oil Flow Visualization, 7x1 Cable Model, $\beta = 60°$

Without End Plates

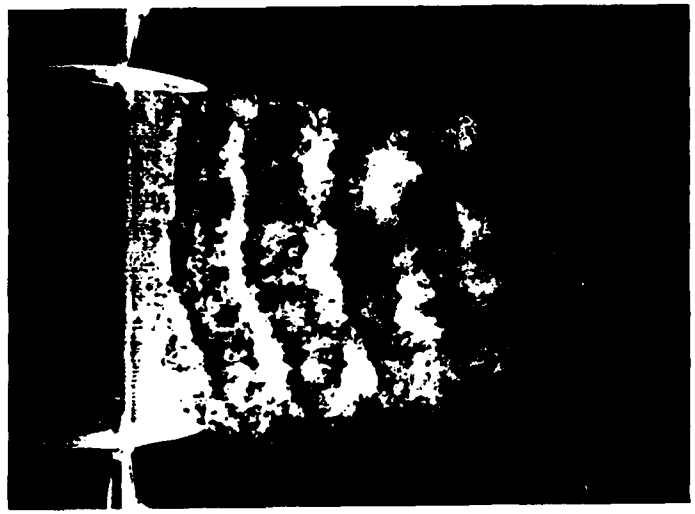

-5° End Plate Inclination

0° End Plate Inclination

+5° End Plate Inclination

Figure 63. End Plate Study, Cylinder Model, Re = 6,000, $\beta = 90°$
No end plate, -5°, 0° and =5° end plate inclinations

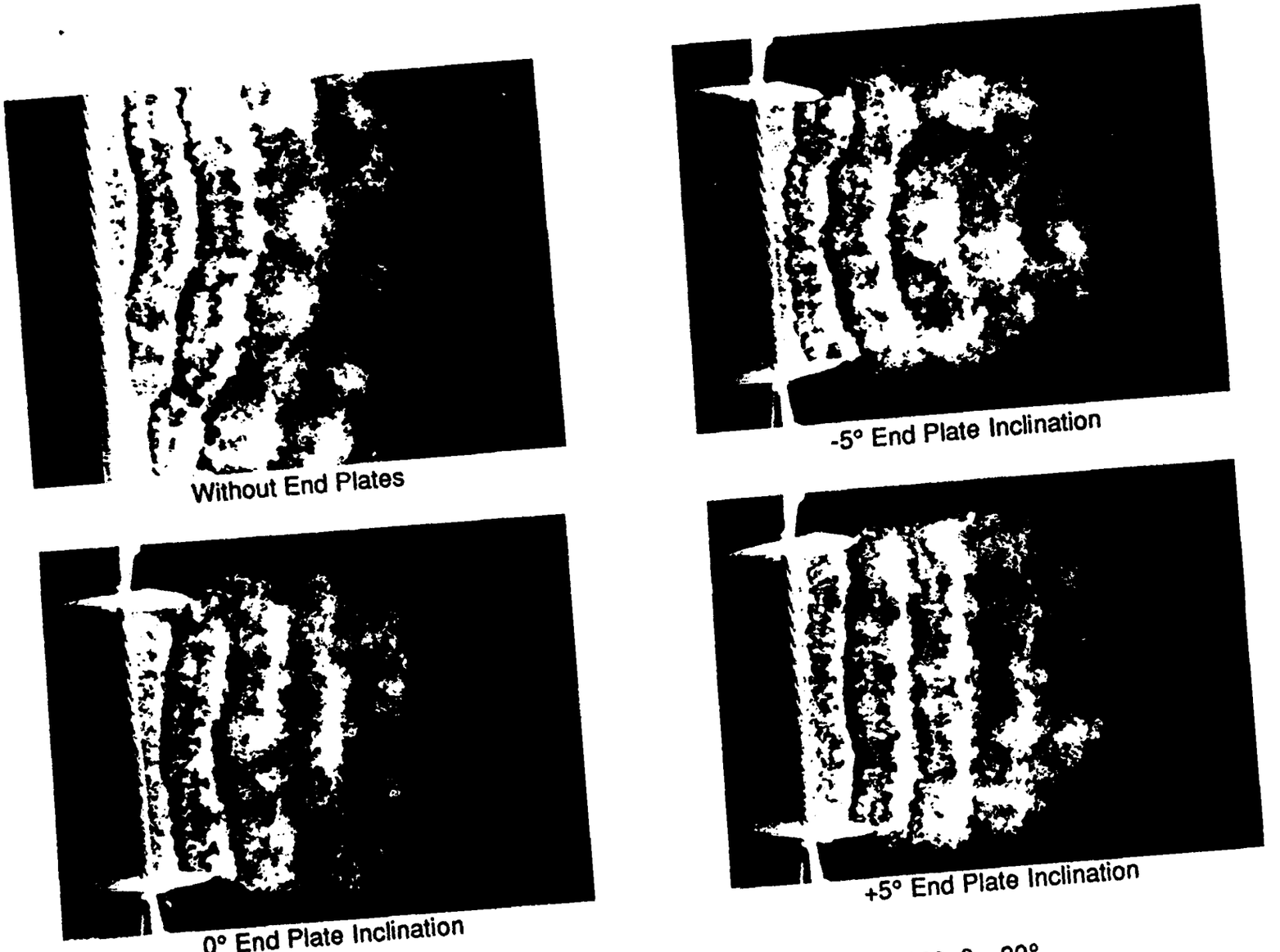


Figure 64. End Plate Study, 7x7 Cable Model, Re = 6,000, $\beta = 90°$
No end plate, -5°, 0° and =5° end plate inclinations

Without End Plates

-5° End Plate Inclination

0° End Plate Inclination

+5° End Plate Inclination

Figure 65. End Plate Study, 4x7 Cable Model, Re = 6,000, $\beta = 90°$
No end plate, -5°, 0° and =5° end plate inclinations

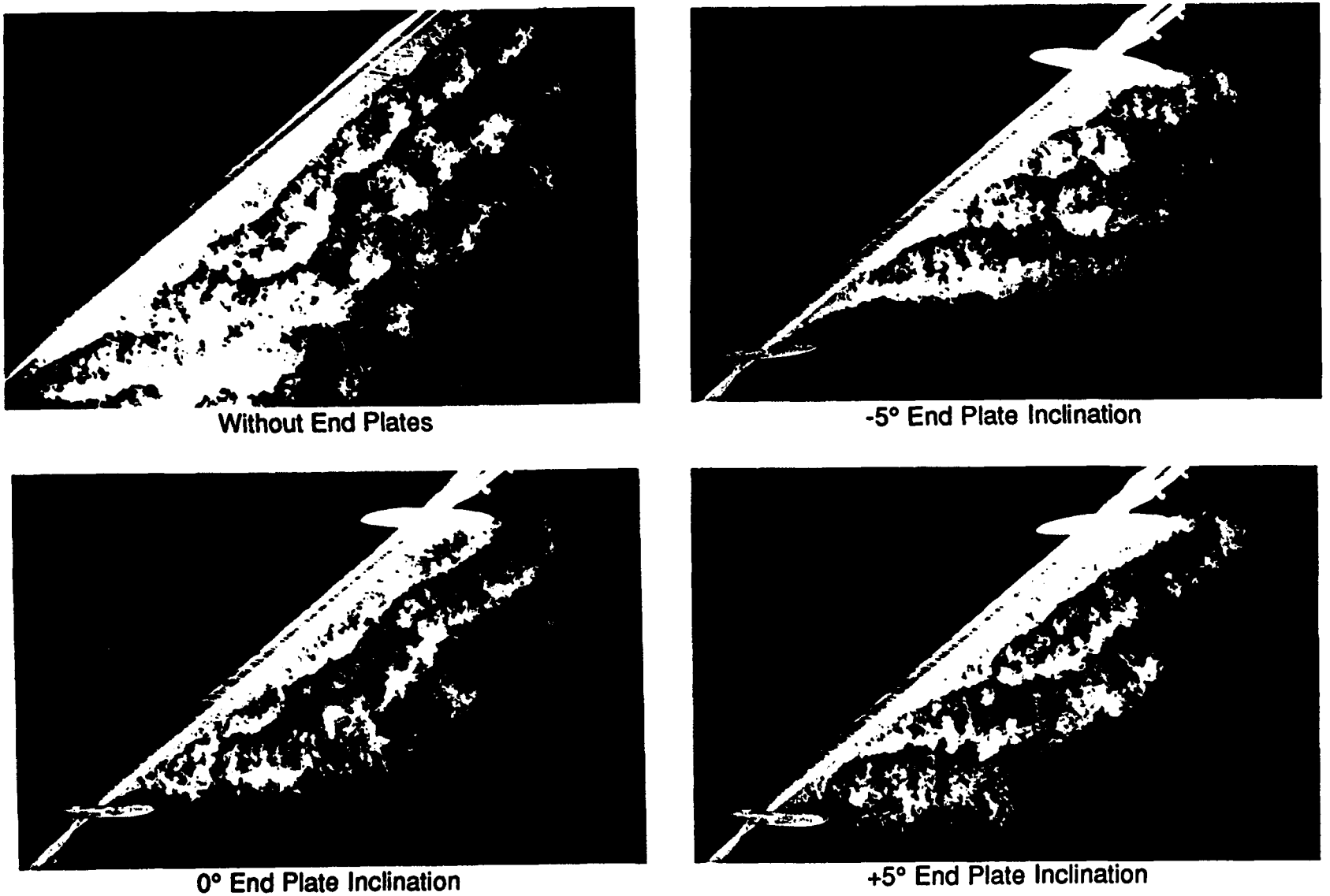


Figure 66. End Plate Study, Cylinder Model, Re = 6,000, $\beta = 40°$
No end plate, -5°, 0° and =5° end plate inclinations

Without End Plates

-5° End Plate Inclination

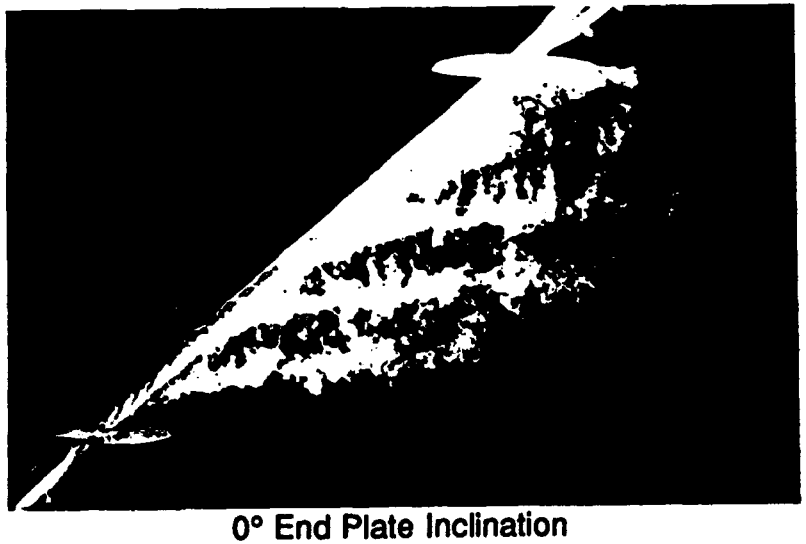

0° End Plate Inclination

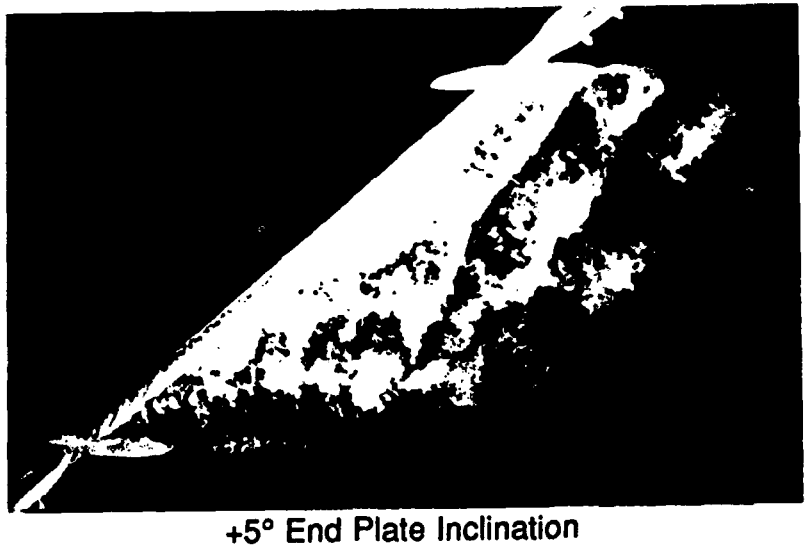

+5° End Plate Inclination

Figure 67. End Plate Study, 7x7 Cable Model, Re = 6,000, $\beta = 40°$
No end plate, -5°, 0° and =5° end plate inclinations

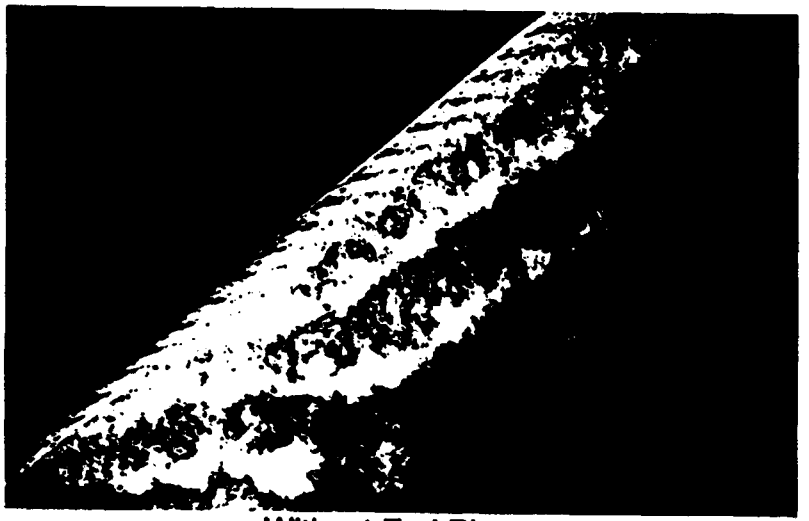

Without End Plates

-5° End Plate Inclination

0° End Plate Inclination

+5° End Plate Inclination

Figure 68. End Plate Study, 4x7 Cable Model, Re = 6,000, $\beta = 40°$
No end plate, -5°, 0° and =5° end plate inclinations

## DISTRIBUTION LIST

| | Copy No. |
|---|---|
| Chief of Naval Research<br>Office of Naval Technology<br>800 North Quincy St.<br>Arlington, VA 22217-5000 | |
| (Code 23, Dr. A. J. Faulstich) | 1 |
| (Code 235, Dr. W. Ching) | 2 |
| (Code 11210T, Dr. S. Ramberg) | 3 |
| (Code 1132F, Dr. S. Lekoudis) | 4 |
| Commander<br>Naval Air Systems Command<br>Naval Air Systems Headquarters<br>Washington, D.C. 20361-0001 | |
| (Library) | 5 |
| (PMA-210, B. Emshwiller) | 6 |
| (PMA-210, K. Haas) | 7 |
| Commanding Officer<br>Naval Civil Engineering Laboratory<br>Port Hueneme, CA 93043 | |
| (Library) | 8 |
| (Code L43, D. Meggit) | 9 |
| (Code L03C, J. Dummer) | 10 |
| (Code L44, Dr. W. Nordell) | 11 |
| Commanding Officer<br>Naval Research Laboratory<br>Washington, D.C. 20375-5000 | |
| (Library) | 12 |
| (Code 5841, Dr. R. Peltzer) | 13 |
| (Code 5841, Dr. O. M. Griffin) | 14 |
| Commander<br>Naval Sea Systems Command<br>Naval Sea Systems Headquarters<br>Washington, D.C. 23062-5101 | |
| (Library) | 15 |
| (PMS 407D, J. Grembi) | 16 |
| Commander<br>David Taylor Research Center<br>Bethesda, MD 20084-5000 | |
| (Library) | 17 |
| (Code 1541, D. Pickett) | 18 |
| (Code 1541, R. Rispin) | 19 |

| | Copy No. |
|---|---|
| Officer in Charge<br>Newport Laboratory<br>Naval Underwater Systems Center Detachment<br>Newport, RI 02841 | |
| (Library) | 20 |
| (Code 8333, S. Hassan) | 21 |
| Commander<br>Mine Warfare Command<br>Charleston, SC 29408-5500 | |
| (Library) | 22 |
| (Code N4A, G. Pollitt) | 23 |
| Director<br>Defense Technical Information Center<br>Cameron Station<br>Alexandria, VA 22304-6145 | 24-25 |
| University of Notre Dame<br>Department of Aerospace and Mechanical Engineering<br>Notre Dame, IN 47557 | 26-35 |